

PHOTOELECTRIC EMISSION  
FROM SODIUM, POTASSIUM AND Na-K ALLOYS

TH. G. J. VAN OIRSCHOT

Universiteit Leiden



2 016 597 8

Bibliotheek  
Gorlaeus Laboratoria  
Universiteit Leiden  
Postbus 9502  
NL-2300 RA LEIDEN

# PHOTOELECTRIC EMISSION FROM SODIUM, POTASSIUM AND Na-K ALLOYS

PHOTOELECTRIC EMISSION  
FROM SOLUBLE POTASSIUM AND NA-K ALLOY

BY  
S. S. CHEN AND  
R. H. BUNN  
Department of Chemistry,  
University of California,  
San Diego, California

PHOTOELECTRIC EMISSION  
FROM SODIUM, POTASSIUM AND Na-K ALLOYS

PROEFSCHRIFT

TER VERKRIJGING VAN DE GRAAD VAN DOCTOR IN  
DE WISKUNDE EN NATUURWETENSCHAPPEN AAN  
DE RIJKSUNIVERSITEIT TE LEIDEN, OP GEZAG VAN  
DE RECTOR MAGNIFICUS DR. J. GOSLINGS,  
HOGLERAAR IN DE FACULTEIT DER GENEESKUNDE  
TEN OVERSTAAN VAN EEN COMMISSIE UIT DE SENAAT  
TE VERDEDIGEN OP WOENSDAG 25 FEBRUARI 1970  
TE KLOKKE 16.15 UUR

DOOR

THEODORUS GERARDUS JACOBUS VAN OIRSCHOT

GEBOREN TE HAAREN IN 1943

1970

DRUKKERIJ BRONDER-OFFSET N.V.  
ROTTERDAM

PHOTOELECTRIC EMISSION  
FROM SODIUM POTASSIUM AND Na-K ALLOY

PROCEEDINGS

OF THE AMERICAN PHYSICAL SOCIETY

PROMOTOR: PROF. DR. W. M. H. SACHTLER

DEPARTMENT OF PHYSICS  
UNIVERSITY OF CALIFORNIA  
SAN DIEGO, CALIFORNIA

1952

PHYSICAL SOCIETY OF AMERICA

WASHINGTON, D. C.

PHYSICAL SOCIETY OF AMERICA  
WASHINGTON, D. C.

## STELLINGEN

### I

De door Lapp en Neumann geopperde mogelijkheid om fotoelektrische opbrengsten van kaliumfilms in het kortgolfige gebied in overeenstemming te brengen met de theoretische Fowler-curve is van twijfelachtige waarde.

O. Lapp en K. Neumann, *Z. Naturforsch.* 24a, 596 (1969).

### II

Bij de interpretatie van hun fotoelektrische meetresultaten aan natriumfilms gaan Garron et al. ten onrechte voorbij aan gegevens, die reeds gedurende ruim 40 jaar bekend waren.

R. Garron, L. Gaudart en R. Payan, *C.R. Acad. Sc. (Paris)* 268B, 266 (1969).

Zie bijv.: H.E. Ives en A.L. Johnsrud, *Astrophys. J.* 60, 231 (1924).

A.L. Hughes en L.A. DuBridge, "Photoelectric Phenomena", McGraw-Hill Book Company, Inc., New-York, 1932, p. 141.

H. Simon en R. Suhrmann, "Der lichtelektrische Effekt und seine Anwendungen", Springer-Verlag, Berlijn, 1958, p. 69.

### III

De term "surface potential" is, voor zover gebruikt in samenhang met het begrip uittree-arbeid, in de literatuur niet eenduidig gedefinieerd en kan dientengevolge aanleiding geven tot verwarring.

R.V. Culver en F.C. Tompkins, *Advan. Catalysis* 11, 67 (1959).

J.R. Smith, *Phys. Rev.* 181, 522 (1969).

### IV

In de afleiding, die Gundry en Tompkins geven voor de adsorptiewarmte bij de vorming van een "charge-transfer no-bond" complex, komt een onjuiste vergelijking voor.

P.M. Gundry en F.C. Tompkins, *Trans. Faraday Soc.* 56, 846 (1960).

### V

Yamashita meent ten onrechte optisch zuiver (+)-2-butanol te hebben verkregen door een asymmetrische Meerwein-Ponndorf-Verley reductie.

S. Yamashita, *J. Organometal. Chem.* 11, 337 (1968).

## VI

Het toepassen van metingen van het kern-Overhauser-effekt bij  $N_1$ - en  $N_3$ -gesubstitueerde 2,4-dioxo-1,2,3,4-tetrahydropyrimidines kan extra aanwijzingen geven over de aanhechting van de substituenten.

A. J. H. Nolle, G. J. Koomen, W. F. A. Grose en U. K. Pandit, *Tetrahedron Letters* 1969, 4607.

## VII

De door Klute opgegeven waarde voor het eerste absorptiemaximum in het zichtbare spectraalgebied van het carboniumion, dat ontstaat bij de oxydatie van 1,1-dianisyl-2,2,2-tribroomethaan, is onjuist.

H. Klute, Thesis, Basel, 1964.

S. J. Oldenburg, Thesis, Leiden, 1969.

## VIII

Uit de experimenten van Abon volgt niet, dat een verhoging van de uittree-arbeid van 0,7 eV kenmerkend is voor het systeem stikstof-molybdeen.

M. Abon, Thèse, Lyon, 1969.

## IX

De veronderstelling van Holt, dat platina-goud legeringen een continue serie vaste oplossingen vormen bij kamertemperatuur, is onjuist.

E. L. Holt, *Nature* 857 (1964).

A. S. Darling, R. A. Mintern en J. C. Chaston, *J. Inst. Metals* 81, 125 (1952).

## X

Thorner et al. geven een foutieve beschrijving van de ordening van vacatures in het fluorietrooster voor  $Zr_3Sc_4O_{12}$ .

M. R. Thorner, D. J. M. Bevan en J. Graham, *Acta Cryst.* B24, 1183 (1968).

*International Tables for X-ray Crystallography I*, (1952).

## XI

Ten onrechte stellen Lang en Löber, dat Feichtmayr en Schlag van mening zijn dat metachromasie in verschillende oplosmiddelen geheel op basis van ionenpaarvorming verklaard kan worden.

H. Lang en G. Löber, *Z. phys. Chem. N.F.* 66, 69 (1969).

F. Feichtmayr en J. Schlag, *Ber. Bunsenges. phys. Chem.* 68, 95 (1964).

*Aan Elly*

*Aan mijn moeder*

*Aan de nagedachtenis van mijn vader*

## CONTENTS

		page
Chapter I	INTRODUCTION	9
	1. Electron emission from alloys	9
	2. Outline of the present study	13
Chapter II	EXPERIMENTAL	16
	1. Ultra-high vacuum technique	16
	2. Photoelectric apparatus and measurements	19
Chapter III	PRINCIPLES AND TECHNIQUES OF PHOTOELECTRIC MEASUREMENTS	22
	1. Fowler's theory on photoelectric emission	22
	2. The photocells	26
Chapter IV	PURIFICATION OF ALKALI METALS AND <i>IN SITU</i> DETERMINATION OF ALLOY FILM COMPOSITION BY MEANS OF SURFACE IONIZATION	31
	1. Purification of alkali metals	31
	2. Determination of film thickness and alloy composition from surface ionization experiments	33
Chapter V	PHOTOELECTRIC PROPERTIES OF POTASSIUM AND SODIUM	48
	1. Introduction	48
	2. The photoelectric properties of potassium films	49

	page
1. Photoelectric yield as a function of layer thickness	49
2. Photoelectric spectral distribution curves	54
3. Sintering phenomena	56
4. Changes in reflectivity	57
5. Photoelectric parameters of potassium films	60
6. Conclusion	66
3. The photoelectric properties of sodium films	67
1. Photoelectric yield as a function of layer thickness	67
2. Photoelectric spectral distribution curves	69
3. Sintering phenomena	72
4. Photoelectric parameters of sodium films	73
5. Conclusion	77
 Chapter VI	
PHOTOELECTRIC PROPERTIES OF SODIUM-POTASSIUM ALLOYS	79
1. Photoelectric yield during deposition of alloy films	81
1. Successive deposition	81
2. Simultaneous deposition	83
2. Photoelectric distribution curves of vapour quenched alloy films	85
3. Sintering phenomena	87
4. Photoelectric distribution curves of presintered alloy films	92
1. At room temperature	92
2. After cooling to 80°K	93
5. Photoelectric parameters of sodium-potassium alloys	95
1. Films prepared by means of vapour quenching at 80°K	95
2. Films after sintering at room temperature	97
3. Films cooled to 80°K after presintering	98
4. Position of spectral maxima at various stages of an annealing cycle	99
 Chapter VII	
GENERAL DISCUSSION - WORK FUNCTION AND PHOTOELECTRIC EFFECT	102
1. Work functions	102

	page
1. Thermodynamic definition of the work function	102
2. Discussion of the work function data	107
a. Pure metals	107
b. Alloys	108
3. Conclusion	110
2. Photoelectric sensitivities and spectral distribution curves	111
1. Factors governing the photoemission process	111
a. Photoexcitation	112
b. Scattering processes	113
c. Escape	114
2. "Volume" versus "surface" photoeffect	117
3. "Escape depths"	118
4. Influence of the film structure	119
5. Spectral maxima	124
6. Conclusion	125
 Chapter VIII	
PHYSICAL ADSORPTION OF XENON ON POTASSIUM	127
1. Introduction	127
2. Experimental	128
3. Results	131
4. Discussion	134
 REFERENCES	139
 SUMMARY	143
 SAMENVATTING	146

## CHAPTER I

### INTRODUCTION

#### I.1 ELECTRON EMISSION FROM ALLOYS

The electron emission of alkali metals has been investigated by means of various techniques, including photoemission, more effectively and more repeatedly than of any other class of metals. As the conduction band is formed essentially by *s*-electrons a comparison of experimental results with theoretical models is easier for alkali than for other metals. As a consequence of the low work function of alkali metals their photoemissive properties can be investigated in the easily accessible region of visible light.

In recent years a growing interest can be noticed for electron emission by metal alloys. Application of electron emission has considerably contributed to a better understanding of several peculiar properties of alloys.<sup>9, 21, 34, 35, 49, 69, 100, 103, 118</sup> On the other hand, new questions have arisen regarding the interpretation of some unexpected results, for example, the occurrence of minima in the work function-versus-alloy-composition plots.<sup>69, 100</sup>

Unfortunately, a theory of the work functions of alloys does not exist; even theoretical starting points are lacking. Also for pure metals the theory of the electron work functions is highly unsatisfactory and far from capable of making quantitative predictions.

Progress in the field of electron emission by alloys is retarded both by theoretical problems and by an almost total lack of reliable experimental data. In view of the simple electronic structure of sodium-potassium alloys the present investigation of their photoelectric properties was undertaken because it might be hoped that for these alloys a theoretical interpretation of experimental

data will be attempted once these data are available.

In studying alloys it appears inevitable to use the constituent pure metals as references. However, when surveying the vast amount of literature concerning the photoelectric behaviour of pure alkali metals, it appears that different investigators report different photoelectric data on sodium and on potassium and that theories of photoemission are conflicting. Also artifacts imposed by the adopted experimental techniques can complicate the interpretation of the obtained results. Since additional complications must be expected for the investigation of photoemission from alloys, it is not surprising that the thorny field of photoemission by alkali metal alloys was hitherto avoided by scholars. Another consequence is that an investigation of alloys must create its own reference standards, i. e. it must include an investigation of the constituent metals under exactly the same experimental conditions.

In this introductory chapter we shall first briefly consider some topics, which are of interest in connection with the present investigation. With that background information the objectives of this study will be outlined.

Two major uncertainties in our knowledge are: 1) where are the photoelectrons excited by interaction with a light quantum, and 2) how is the momentum conserved if a "quasi-free" electron receives energy  $h\nu$  from the radiation field? For many years, when electrons inside a metal were visualized to be free as in Sommerfeld's model, it was postulated that the potential variation at the surface of the metal supplies both the impulse mechanism and the locality for the excitation of those electrons that have energies near the Fermi level and that contribute to photoemission near the long wave limit (*surface photoeffect*<sup>113</sup>). In particular, photoemission from alkali metals was treated as a surface effect over the whole spectral region accessible to measurement.<sup>24, 42, 43, 56, 72, 84, 113</sup> The opposite proposal that the required interaction to conserve momentum can be provided by the lattice field of the metal, with other words that photoexcitation of metal electrons is a *volume photoeffect*<sup>113</sup> received little more than passing attention<sup>40</sup> until a few years ago, when evidence in its favour became available<sup>76, 89, 115</sup> (see also below). For example, the energy distribution of photoemitted electrons from metals was shown to reflect the electronic band structure (i. e. the density of occupied states in the conduction valence band) of these metals.<sup>10, 106</sup>

In the older concept<sup>113</sup> the existence of a volume effect in addition to a surface effect was not denied, but different thresholds were assigned to the two

kinds of photoeffect; this view has continuously been supported by authors<sup>5, 45</sup> who found a second onset of photoemission at some distance from the long wave threshold. According to more recent concepts<sup>76</sup> the threshold for the volume effect is just the work function of the metal, in absence of selection rules prohibiting photon excitation of electrons from the Fermi level to the vacuum level. According to this view, a second onset of emission would be due to other driving forces or to artifacts.

Certain phenomena which were formerly ascribed to the surface effect (e. g. the maximum in the spectral distribution curve and the selective vectorial effect of alkali metals) have recently found a theoretical explanation in terms of a volume effect,<sup>20</sup> provided that sufficient account is taken of the optical properties which are often complex.

Even the well-known fact that small changes in the surface (e. g. due to adsorption) produce drastic changes in work function and, hence, in photoemission is easily reconciled with the idea that the photoexcitation proper is a volume effect. The strong dependence of photoemission on the structure and composition of the surface of the emitter makes it an extremely sensitive detector of various types of adsorption.<sup>12, 30, 37</sup> The physical adsorption of xenon on potassium was included in the present investigation because the experimental set-up for measuring photoemission of extremely pure alkali metals could easily be used to characterize this interesting example of gas-solid interactions. The system potassium-xenon is an example of considerable importance for understanding physical adsorption of gases on metal substrates in general.

The assumption that the photoelectric effect of alkali metals is primarily a volume effect and that emitted electrons have travelled over considerable distances (a few hundred angstroms) through the metal before escaping implies that the observed spectral distribution curve also depends on the nature of the subsurface region of the metal.

Several pieces of evidence can be found in the recent literature<sup>9, 16</sup> demonstrating that the photoelectric sensitivity depends on the degree of ordering: pure metal films prepared by so-called *vapour quenching* (or *quenching condensation*) show an enhanced sensitivity with respect to ordered films, although the work function is not changed accordingly. The enhanced sensitivity is attributed to the occurrence of many lattice defects in these films. For vapour quenched *alloy* films only one result is known:<sup>9</sup> a film of the Sn-10 at. % Cu alloy prepared by vapour quenching at 8°K is reported to have a liquid-like amorphous structure and to show a much lower photoyield than pure Sn-films.

One of the objectives of the present investigation is the examination of the effect of vapour quenching (i. e. the introduction of numerous lattice defects or even the formation of a liquid-like structure) on the photoelectric behaviour of sodium-potassium alloy films as well as of pure sodium and potassium films. These structure defects are investigated here by recording photoelectric emission during and after slow warming of the films deposited at very low temperature. By subsequently cooling a sintered film and heating it again, reversible and irreversible effects can be distinguished. The sodium-potassium system, the phase diagram of which shows the existence of an incongruent compound  $\text{Na}_2\text{K}$  melting at  $6.9^\circ\text{C}$  and the presence of an eutectic point at  $-12.5^\circ\text{C}$ , offers ample opportunity to study ordering phenomena in alloys such as order-disorder transitions, precipitation of components or intermetallic compounds and ordering with phase separations. The hope appears justified that experimental data on alloys of this kind might also be helpful in clarifying the mechanism of the photoelectric effect of pure metals.

An important advantage of alkali metals and alloys for the present purpose is that they are known to possess a low work function; consequently, the photoelectric response can be investigated over a much broader range of frequencies of the incident light than is possible for most other alloys (e. g.  $\text{Cu-Ni}^{100}$ ) with the same classical techniques. Since for these non-alkali alloys the region between the long wave limit and the short wave end of the quartz-ultraviolet is very narrow the measured data on those alloys are just sufficient for an exact evaluation of the work function. For alkali metals the photoelectric data cover a wide frequency region and are, therefore, more informative. Whereas the work function is extremely sensitive to surface conditions, the spectral region far from the threshold frequency with the spectral maximum is likely to provide information on the subsurface region, if the volume effect is dominant.

As was alluded to before, the sodium-potassium system having a relatively simple electronic structure seems to be an interesting object for study of work functions. In the photoelectric investigation of sintered copper-nickel alloy films a peculiar result was obtained:<sup>100</sup> the work function of the surface-phase (the copper-rich phase) (4.61 eV) appeared to be slightly lower than that of the pure components (for Cu: 4.66 eV; for Ni:  $> 5.20$  eV). With various experimental techniques similar minima of the work function were found for the alloy systems Au-Pt,<sup>17</sup> W-Mo,<sup>34</sup> W-Ta,<sup>34</sup> Ti-Re,<sup>35</sup> W-Hf,<sup>49</sup> Cs-Hg,<sup>69</sup> whereas such minima were not observed for the alloys Ta-Nb,<sup>35</sup> W-Re (0-25% Re),<sup>57</sup>

Al-92 at. % Ni.<sup>21</sup>

Sometimes, at temperatures near the melting point, the minima have been ascribed to the influence of adsorption of one component on the surface of the alloy<sup>34, 69</sup> (as in adsorption of an alkali metal on the surface of a refractory metal); for the other cases no explanation does exist up to date.

Another important peculiarity of sodium-potassium alloys in this connection is that they form a liquid phase at room temperature. In a number of reports on liquid amalgams of alkali metals<sup>32, 68, 69</sup> a correlation was found between the surface tension and the photoelectric work function. As the work function is a characteristic property of the surface the results indicated properly a preferential enrichment of the alkali constituent at the surface. From surface tension measurements of liquid binary alloys it follows that the surface atomic layers almost totally consist of the component with the lower surface tension.<sup>28</sup> An analogous effect may be expected for the Na-K alloys.

Several of the topics mentioned above pertain directly to the nature of the photoelectric emission process. One of the most-quoted experimental proofs of the preponderance of the volume photoeffect was furnished some years ago by results on potassium and sodium.<sup>89, 115</sup> Since the conflicting opinions differ mainly with respect to the place in the metal from where the excited photoelectrons originate, measurements of the photocurrent as a function of film thickness are of crucial importance. Such experiments have been performed by Thomas, Mayer and Piepenbring,<sup>76, 89, 115</sup> who could show for potassium and sodium that photoelectrons are excited up to several hundred angstroms below the surface the precise escape depth depending on the light frequency. Unfortunately, their measurements were limited to quenched films far from equilibrium. As the escape depth is, essentially, characteristic for the three-dimensional metallic state and as other parameters of this metallic state are known to differ drastically for quenched and annealed metals, it appeared highly desirable to investigate further the layer thickness dependence of the photocurrent for alkali films and for films of their alloys. Such measurements have, therefore, been incorporated in the program of the present thesis.

## I. 2 OUTLINE OF THE PRESENT STUDY

From the foregoing it appears that an investigation of the photoelectric properties of alkali metal alloy films after and during preparation by means of

vapour quenching, subsequent sintering and cooling may provide insights in controversial questions on the physical nature of metals and alloys.

We already indicated the possibility of studying: the influence of the various degrees of disorder by means of the photoelectric properties, the correlation between photoeffect and phase compositions, the problem whether work function versus composition diagrams have intriguing extrema. The form of the spectral sensitivity curves at different annealing stages furnishes information about the origin of spectral maxima. Further, information might be obtained pertaining to the nature of the photoelectric emission process.

For these purposes it appeared necessary to start with a detailed and varied investigation of pure sodium and potassium films as a proper reference for the alloy work: results on the pure metals found in the literature are either incomplete with regard to deposition conditions, temperature influences and shape of spectral distribution curves, or they are unreliable owing to suspect vacuum conditions. Besides, it appears that the uncertainty of the work functions reported in the literature for one and the same alkali metal is larger than the difference between the most reliable values of the two metals (Na: 2.47 eV; K: 2.25 eV<sup>51, 104</sup>).

For explaining the bonds formed in physical adsorption on substrates of very low work function, we studied the adsorption of xenon on potassium by means of the photoelectric technique. A more comprehensive motivation for this choice will be given in the introduction to Chapter VIII.

The present investigation is described in the following chapters. Chapter II deals with part of the apparatus and experimental methods, which were of general interest. These include the ultra-high vacuum equipment and certain measuring devices.

Chapter III describes the principles of photoelectric measurements and evaluation of work functions. Furthermore it includes a description of the photocells, designed and constructed for this work.

Chapter IV deals with the purification of alkali metals and the determination of film thickness and alloy composition, respectively.

Special attention was paid to the method applied by us for controlling and determining the alloy compositions *in situ* by counting the atoms during deposition. In chapter V experimental results of sodium and potassium films are reported and discussed. They are compared with literature data.

Chapter VI deals with results of simultaneously deposited sodium-potassium alloy films.

Chapter VII contains a general discussion of work functions and photoemission where an attempt is made to interpret the most important results of the investigation described in this thesis. Suggestions are made for further studies.

In chapter VIII experiments on xenon adsorption on alkali metals are described. The results are discussed in connection with their bearing on current theories of the nature of the binding forces involved in physical adsorption. This chapter forms an individual entity.

## CHAPTER II

### EXPERIMENTAL

#### II. 1 ULTRA-HIGH VACUUM TECHNIQUE

The use of an ultra-high vacuum with partial pressures of all reactive gases in the order of  $10^{-10}$  Torr\* or less is necessary to gain reliable work function data. From simple gas kinetics it follows that at a stationary pressure of  $10^{-6}$  Torr a metal surface is covered in a few seconds with a monolayer of adsorbate when the gas has a high sticking probability; in an ultra-high vacuum system as given above, several hours are available for unsuspected measurements. Especially when dealing with alkali metals good vacuum conditions are important as these metals react strongly with several atmospheric gases even at liquid nitrogen temperature.<sup>3, 78</sup>

The attainment of ultra-high vacuum has become a routine procedure.<sup>91, 97</sup> The principal requirement for it is a preliminary bake-out of the whole vacuum system at the highest temperatures possible (for our Pyrex glass system about  $400^{\circ}\text{C}$ ), which has its consequences for the choice of materials to be used for the construction.

In our photoelectric measurements and the adsorption studies of xenon as well as during purifying alkali metals the vacuum apparatus shown in fig. II, 1 was used. It consists of three main parts: a fore-vacuum line, a high-vacuum line and an ultra-high vacuum compartment. The last part is almost entirely above the table-top T, made of Sindanyo board, a heat-resistant material, and comprises as an important unit the ion getter VacIon pump V (Varian). The

\* 1 Torr (abbreviation of "Torricelli") is equal to 133.3224 Newtons/sq. m.

ultra-high vacuum part is separated from the high-vacuum line by a bakeable all-metal Granville Phillips valve 6. The high-vacuum ( $10^{-5}$  Torr) is achieved by the operation of an oil-diffusion pump D (Edwards 10 l/sec). The cold trap C, cooled by liquid nitrogen, protects the system against back-diffusion of oil. In this part of the system, a xenon storage flask X, a potassium getter bulb G

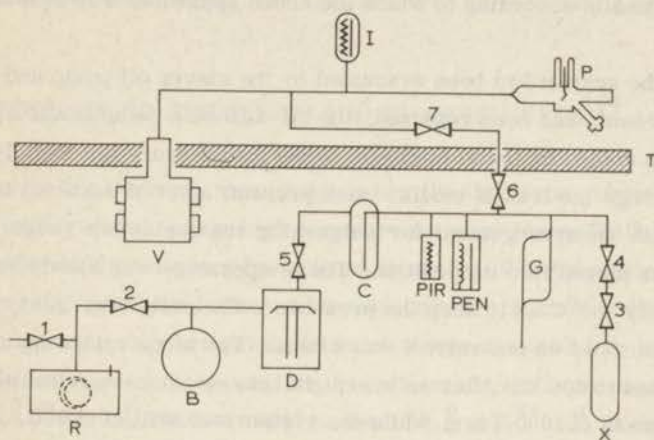


Fig. II.1. Schematic representation of vacuum apparatus.

B	buffer flask	T	working table
C	cold trap	V	Vaclon pump (Varian, 50 l/s)
D	oil-diffusion pump (10 l/s, Edwards)	X	xenon flask (L'Air Liquide)
G	getter bulb with potassium	1, 2, 3, 4	greased stopcocks
I	ionization gauge (Philips)	5	baffle valve (Edwards)
PIR	Pirani gauge (Edwards)	6	bakeable UHV valve (Granville Phillips type C)
PEN	Penning gauge (Edwards)	7	magnetically operated ball-joint valve
P	photoelectric cell		
R	rotary oil pump (35 l/s, Edwards)		

and two manometers were also connected to the vacuum line. B is a 2-litre buffer flask allowing a non-continuous operation of the rotary oil pump R, when backing the oil-diffusion pump D. Xenon could be introduced via the dosing valves 3 and 4 (greased stopcocks); 1 and 2 are also greased stopcocks.

The system above the table-top can be baked out at  $400^{\circ}\text{C}$  by enclosing it in portable ovens (Balzers). A ball-joint valve 7, which is magnetically operated, could be used as a second separation valve of the ultra-high vacuum part. Pressures down to  $10^{-10}$  Torr could be measured with a Bayard-Alpert type ionization gauge I (Philips). In the drawing P represents the photoelectric cell; sometimes the cell was replaced by a distillation apparatus for sodium and potassium. In order to utilize as much as possible the high pumping capacity of the

VacIon pump, especially of interest during distillation of alkali, wide diameter tubing was used for the ultra-high vacuum line (28 mm diameter) and no further valve was incorporated, e. g. for closing the ion getter pump before breaking the vacuum.

The schedule according to which the above apparatus was evacuated was as follows.

After the system had been evacuated by the rotary oil pump and major leaks, if present, had been repaired, the oil-diffusion pump D was switched on, the cold trap cooled by liquid nitrogen. When the pressure fell rapidly to the  $10^{-5}$  Torr range (no leak of medium size present) a set of bake-out ovens often provided with an arrangement for outgassing the ionization gauge during bake-out was placed into its position. The temperature was slowly raised to approximately  $250^{\circ}\text{C}$  as to keep the pressure sufficiently low. Next, the VacIon pump was switched on and valve 6 was closed. The temperature inside the oven was increased to  $400^{\circ}\text{C}$ . After an overnight bake-out pressure had normally dropped to about  $5 \cdot 10^{-8}$  Torr, while the system was still at  $400^{\circ}\text{C}$ . After removal of the ovens all metal parts of the system, that had to be heated during the measurements were outgassed for a prolonged period. After a second overnight (or week-end) bake-out and cooling to room temperature, a pressure lower than  $10^{-9}$  Torr was reached in a leak-free system. If at this stage a small leak was detected, air was let in into the whole apparatus via valve 1 and after repair the whole procedure was repeated.

As during the actual measurements many metal films could be investigated in the same photocell, the vacuum usually remained intact for several months.

In the xenon adsorption studies, the fore-vacuum line was also used to remove the major part of the xenon after the adsorption had been measured. Though in some cases contamination of the alkali film by back-flow of gases into the ultra-high vacuum part of the system has been observed the desired vacuum conditions appeared to be easily recovered after closing valve 6.

The xenon used in this study was of high purity. It was supplied from a 1-litre flask at atmospheric pressure provided with a greased stopcock. According to the specifications, the impurity content was less than 0.001%. When admitted to the system condensable impurities were frozen out (together with most of the xenon itself) in the cold trap of the high-vacuum line (background pressure:  $10^{-6}$  Torr). In some experiments a potassium film, deposited freshly

on the walls of a glass cylinder, which was inserted into the junction between the flask and the Granville Phillips dosing valve 6, was used as a getter. The film adsorbed contaminating gases such as oxygen, hydrogen and water vapour. The potassium film was evaporated from an ampulla, filled with ultra-pure potassium and broken by means of an iron ball held in a glass envelope, which could be moved magnetically.

## II. 2 PHOTOELECTRIC APPARATUS AND MEASUREMENTS<sup>104</sup>

Photoelectric currents were produced by the light from a horizontally mounted, water-cooled, super-high pressure mercury lamp (Philips, 500 Watt) with a considerable continuous background intensity. Via a planar and a concave mirror (fig. II, 2) the light was focused onto the entrance slit of a double Van Cittert quartz monochromator, in which it was resolved into light of high purity\*. The wave-length spread for the slit-width employed was approximately  $10 \text{ \AA}$  at  $3000 \text{ \AA}$  and increased to about  $40 \text{ \AA}$  at  $5000 \text{ \AA}$ . It can be shown that the error in the determination of work functions caused by using the mean wave-length is roughly  $0.002 \text{ eV}$  which is considered negligible.

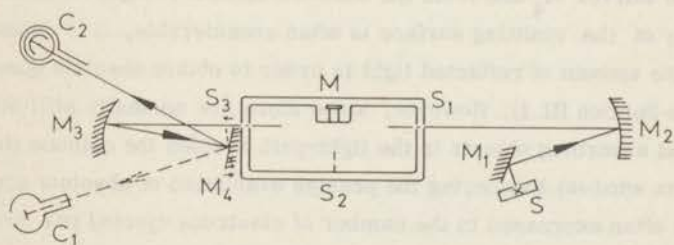


Fig. II. 2. Schematic diagram of the optical train.

S	light source	M	Van Cittert's double monochromator (Kipp)
M <sub>1</sub>	planar mirror, cooled	S <sub>1-3</sub>	slits
M <sub>2</sub>	concave mirror	C <sub>1</sub>	alkali photoelectric cell
M <sub>3</sub>	concave mirror	C <sub>2</sub>	reference photoelectric cell (RCA)
M <sub>4</sub>	planar mirror with two possible positions		

Coming from the exit slit provided with a photographic shutter with wire-release, the monochromatic light passed first onto a concavely curved mirror

\* During the initial stage of this investigation all mirrors of the instrument had been replaced by new ones and the wave-length drum was recalibrated by means of a low pressure mercury arc.

and next onto a planar mirror, which could be brought into one of two accurately adjustable locked positions. In one position the image of the exit slit was focused onto the cathode of a reference cell (RCA 936, resp. 935) calibrated in energy-units by means of a thermopile; in the other position the image was focused onto the alkali film surface. The reference cell was operated with an applied potential of 200 V, the alkali cell with 100 V unless otherwise stated. The voltages were obtained from regulated stabilized low-voltage supplies (Van der Heem, type 8619).

The photoelectric currents, like the ion currents in surface ionization experiments (see chapter IV) were measured on a highly sensitive vibrating reed electrometer (Vibron 33B, E. I. L.) the output of which could be displayed on a recorder (Philips). Shielded cables were used for the electrical connections. In general, photocurrents exceeded  $10^{-11}$  A; under favourable conditions photocurrents down to  $10^{-13}$  A could be detected. The accuracy of the current measurements was accordingly estimated to be  $\pm 2\%$  for the greater part of the investigated wave-length region.

Obviously, the error limits of the quantum yield given by the ratio of the photoelectric current to the amount of light absorbed are farther apart, owing to additional errors which result from slight deviations from the desired positions of the mirror  $M_4$  and from the unknown amount of light reflected. As the reflectivity of the emitting surface is often considerable, it is necessary to measure the amount of reflected light in order to obtain absolute quantum yields (see Section III. 1). However, since there are normally still other reflective and absorbing objects in the light-path besides the cathode (for example a quartz window) hampering the precise evaluation of absolute photoyields, yields are often expressed in the number of electrons ejected per *incident* photon.

In view of the major objective of this investigation - comparison of the photoelectric properties of alkali metals with those of alloys - absolute quantum yields are not of prime interest; throughout this work they are given in electrons per incident photon.

Nevertheless, a number of measurements of the amount of light reflected by the cathode has been carried out by means of a second reference cell (RCA 935) situated behind the Pyrex window of the photocell in the path of the reflected light. With this arrangement reliable determinations of the changes in reflectivity were possible, provided that the measurements were done continuously, e. g. by monitoring during deposition or sintering a film.

The estimated accuracy of yield determinations between 280 and 500 nm was  $\pm 5\%$ , below 280 nm the error limits were approximately  $\pm 20\%$  or even more owing to the weakness of the incident radiation; also in the threshold region errors were large, of course, especially at low temperatures.

## CHAPTER III

### PRINCIPLES AND TECHNIQUES OF PHOTOELECTRIC MEASUREMENTS

#### III. 1 FOWLER'S THEORY ON PHOTOELECTRIC EMISSION

Since the classical experiments of Heinrich Hertz in 1887 it has been known that light may be able to liberate electrons from a metal. For that purpose light must possess a frequency exceeding a certain minimum, corresponding with the long wave-length limit  $\lambda_0$ .

According to Einstein's equation (1905) the threshold frequency  $\nu_0$  may be associated with energy-quanta  $h\nu_0$  where  $h$  is Planck's constant. The photoelectric work function  $\phi$  (in eV) is now given by

$$\phi = h\nu_0 \quad (1)$$

For higher frequencies  $\nu$ , the difference  $h\nu - h\nu_0$  equals the kinetic energy  $\frac{1}{2}mv^2 = \frac{p^2}{2m}$  of the fastest emitted electrons, wherein  $m$ ,  $v$  and  $p$  represent the electronic mass, velocity and momentum, respectively. Einstein's equation then becomes

$$h\nu = \frac{mv^2}{2} + \phi \quad (2)$$

Experimentally, the work function may be obtained from the threshold frequency. This is, however, very inaccurate. There is a more refined treatment of photoelectric emission and work function determination, based on the spectral distribution of the photoelectric yield\*.

\* Henceforth abbreviated with SDC (= Spectral yield, or sensitivity, Distribution Curve).

In the theory of the free-electron gas due to Sommerfeld and based on Fermi-Dirac statistics, the work function equals the amount of work required to remove an electron from the top-most filled energy level to charge-free infinity\*. The distribution function in Fermi-Dirac statistics has the form

$$f(\epsilon) = \frac{1}{\exp \{ (\epsilon - \epsilon_F)/kT \} + 1}$$

which gives the probability that a state at energy  $\epsilon$  will be occupied in an ideal electron gas in thermal equilibrium.

Here  $\epsilon_F = \frac{\hbar^2}{2m} (3\pi^2 N/V)^{2/3}$  = Fermi energy: the energy of the top-most filled level at  $T = 0^\circ\text{K}$ .

$N$  = number of electrons;  $V$  = volume;  $\hbar$  = Dirac's constant;  $k$  and  $T$  have their usual meaning.

The work function at a temperature  $T$  ( $T \neq 0^\circ\text{K}$ ) will be given by the energy of the electrons in the tail of the Fermi distribution function. For the photoelectric yield  $I$ , i. e. the number of electrons emitted per photon absorbed, Fowler<sup>42</sup> succeeded in 1931 to evaluate the influence of the temperature and of the frequency of the incident light by using Sommerfeld's model. He developed a graphical method to determine the work function at  $0^\circ\text{K}$  from experimental data at any given temperature.

At  $T = 0^\circ\text{K}$  electrons with energy  $\epsilon_F$  can just leave the metal after excitation with light-quanta of frequency  $\nu = \nu_0 = \hbar/h$ ; for frequencies  $\nu > \nu_0$  electrons from lower energy levels may also be able to leave the metal. At higher temperatures, according to Fermi statistics, electrons of energy  $\epsilon > \epsilon_F$  exist, that may be enabled to surmount the energy barrier at the surface by light-quanta with  $\nu < \nu_0$ .

Fowler<sup>42</sup> obtained the following expressions for the distinct frequency regions:

$$\text{a) } x \equiv \frac{h(\nu - \nu_0)}{kT} \leq 0 \quad h\nu \leq \hbar$$

$$I = \frac{\alpha 4 \pi e m k^2 T^2}{h^3} \left\{ e^x - \frac{e^{2x}}{2^2} + \frac{e^{3x}}{3^2} - \dots \right\} \quad (3)$$

where  $\alpha.e$  equals the probability that an electron with energy  $\epsilon > \epsilon_0$  takes up a quantum of light.

\* However, in practice, there are some reasons why we define the work function as the amount of work for removing the electron up to the distance of  $10^{-4}$  cm from the surface (see chapter VII).

b)

$x \geq 0$

$h\nu \geq \bar{\phi}$

$$I = \frac{\alpha 4 \pi e m k^2 T^2}{h^3} \left\{ \frac{\pi^2}{6} + \frac{x^2}{2} - \left( e^{-x} - \frac{e^{-2x}}{2^2} + \frac{e^{-3x}}{3^2} - \dots \right) \right\} \quad (4)$$

By means of these equations, especially equation (4), it is possible to determine the work function  $\bar{\phi}$  from the measured photocurrent, the wave-length, the temperature and the radiation energy. These quantities must be known in order to fit photoelectric data to Fowler's theoretical SDC, which obviously has the same form for all metals. The more important equation (4) is, therefore, transformed to

$$\frac{I}{T^2} = \alpha A k^2 \exp \{ F(x) \}$$

where  $A = \frac{4\pi em}{h^3}$  and  $F(x)$  follows from (4).

The photoyield  $I_M$  for the metal under study is obtained by measuring the photoelectric currents from this metal and that of a reference cell with known photoelectric yield for the same light quantity. Obviously, the photoelectric yield of the metal under study is then given by

$$I_M = \frac{i_M}{i_{Ref}} \cdot I_{Ref} \frac{\text{electrons}}{\text{photon}} \quad (5)$$

where  $I_M$  = photoelectric yield of the metal under study in electrons per incident photon

$i_M$  = photoelectric current from the metal under study in A

$i_{Ref}$  = photoelectric current from the reference photocell in A

$I_{Ref}$  = photoelectric yield of the reference photocell calibrated in electrons per incident photon.

When we put  $\alpha A k^2 = M =$  emission constant we may write\*:

$$\log \frac{I}{T^2} = F(x) + \log M \quad (6)$$

The function  $F(x)$  is tabulated for different values of  $x$  (see e. g. ref. 104, p. 27). For a graphical evaluation it is useful to draw  $F(x)$  on transparent graph paper; the measured  $\log(I/T^2)$  data are plotted in another graph in the same

\* Throughout this work  $\log x$  means  $^{10}\log x$ ;  $\ln x$  means  $^e \log x$ .

units as a function of  $h\nu/kT$ . After a proper horizontal and vertical shift the experimental curve is superimposed upon Fowler's theoretical curve. From the horizontal shift the work function  $\phi$  is determined; the vertical shift yields the emission constant  $M$  in electrons  $\times$  (photons  $\times$  deg.<sup>2</sup>)<sup>-1</sup>. If the wave-length  $\lambda$  is given in nm,  $T$  in <sup>o</sup>K, the dimensionless quantity  $h\nu/kT$  is given by  $\frac{h\nu}{kT} = \frac{14.385 \times 10^6}{\lambda T}$ .

The assumptions present in Fowler's theory seem to restrict its applicability to free-electron like metals in the vicinity of the threshold. However, it has been found that Fowler's method can be successfully applied not only to a wide variety of pure metals (e. g. Au, Pt, Ag, W), but also to metals with contaminated surfaces. On the other hand, many reliable experimental results on alkali metals cannot be fitted to the theoretical curve, not even in the range near the threshold where the approximations involved in the theory should be valid.<sup>67, 73, 109</sup> Also at higher frequencies deviations occur (see below).

For data, lying not too close to the threshold frequency an approximation of Fowler's theoretical equation may be derived, which is easier to handle.

When  $x \gg 1$  equation (4) may be written as:

$$I^{\frac{1}{2}} = \left(\frac{\alpha A}{2}\right)^{\frac{1}{2}} kT \left(\frac{\pi^2}{3} + x^2\right)^{\frac{1}{2}}$$

The other terms of the series are negligible.

Then

$$I^{\frac{1}{2}} = \left(\frac{\alpha A}{2}\right)^{\frac{1}{2}} kTx \left(1 + \frac{\pi^2}{3x^2}\right)^{\frac{1}{2}}$$

Expanding the last factor in a series and neglecting all terms except the first one ( $x \gg 1$ ), we obtain

$$I^{\frac{1}{2}} = \left(\frac{\alpha A}{2}\right)^{\frac{1}{2}} (h\nu - \phi) \quad (7)$$

A plot of  $I^{\frac{1}{2}}$  versus photon energy (in electronvolts) yields a straight line in the case of ideal behaviour. The intercept gives the work function and from the slope  $\left(\frac{\alpha A}{2}\right)^{\frac{1}{2}}$  the emission constant  $M$  may be calculated as:

$$M = \alpha Ak^2 = 2k^2 (\text{slope})^2 \quad (8)$$

The slope is expressed in [electrons  $\times$  (photons  $\times$  eV<sup>2</sup>)<sup>-1</sup>]<sup>1/2</sup>.

Evaluation of photoelectric data by the method of the linear Fowler equation is in common use nowadays and has been employed for a number of metals, for example, Ni,<sup>4, 10</sup> Cu,<sup>10</sup> Pb,<sup>9</sup> Sn,<sup>9</sup> Cr,<sup>66</sup> Au.<sup>101</sup>

As will be shown in chapter V, also for alkali metals and alloys this method yields the same values for the photoelectric parameters  $\phi$  and  $M$  as the original Fowler theory does, but the same systematic divergences are observed as well. The data in the vicinity of the long wave-length limit deviate from the straight line, producing a "tail" on the long wave-length side of the SDC, which is not only a consequence of the approximation used in the derivation of equation (7). At high frequencies a different sort of deviation from the straight line is observed, particularly for alkali metals, due to the presence of a selective maximum in the SDC\*. As a rule, the points situated in between these two anomalies could be satisfactorily fitted to a straight line. Still, a determination of work functions and emission constants along these lines has some consequences: the extrapolated photoelectric work function, in general, will not coincide with the threshold energy (even at very low temperatures); the position and height of the maximum in the SDC influence the emission constant.

We conclude, therefore, that in order to describe the particular photoelectric behaviour of alkali metals and alloys the parameters  $\phi$  and  $M$  of the Fowler theory are insufficient as far as more information about the spectral maximum is needed. Furthermore, it remains useful to evaluate work functions not only from the linearized SDC, but also, when comparing work functions of alloys with those of the pure components, from the long wave-length limit.

### III. 2 THE PHOTOCELLS

The photoelectric measurements were carried out in different photocells constructed for the investigation of pure alkali metals or alloys, respectively. In designing a photocell for this work we have to take into account the following points:

\* This type of selective maxima are also known to exist for other, refractory, metals, but then they are situated in the vacuum U. V. region ( $< 2000 \text{ \AA}$ ), outside the range used normally for work function determinations.

1. In order to obtain clean surfaces the alloys have to be prepared by evaporating under ultra-high vacuum.
2. All required measurements on one film have to be performed within a short period of time to warrant absence of contamination of the film by residual gases at a pressure below  $10^{-9}$  Torr.
3. As much time is consumed in achieving ultra-high vacuum it will be preferable to study several films in succession without breaking the vacuum. This will also contribute to better mutual correspondence between the experimental results of different films.
4. To determine crucial parameters like layer thickness and composition of alloys, rates of deposition must be ascertained *in situ*.
5. To prevent alkali atoms from returning into the vapour phase during deposition on the substrate, this substrate must be cooled to low temperature. On the other hand, the possibility of heating the substrate would permit easy removal of an old deposit (cf. point 3).
6. To obtain the photoelectric yield in absolute units the amount of light reflected must be known.

From equation (5): 
$$I_{\text{abs}}(\nu) = \frac{I(\nu)}{1 - r(\nu)} \quad (9)$$

where  $I_{\text{abs}}$  = photoelectric sensitivity of the metal under study in electrons per absorbed photon\*.

$I$  = photoelectric sensitivity of the metal under study in electrons per incident photon.

$r$  = reflective power of the metal under study.

Although the exact measurement of the reflectivity is usually impracticable (see section II. 2), it may be of great importance to have an indication of the quantity of light reflected by the alkali film.

In the course of the present study four photocells were used. The first one was only suited for the study of pure alkali metals; the second one, like the third one, was also suited for the study of sodium-potassium alloys. The fourth cell used for the xenon experiments will be described separately in chapter VIII.

As the third photocell satisfied all requirements stated above and as its design was based on the experiences gained with its two predecessors, we will confine ourselves here to a description of this particular photocell, with

\* The definition of the absolute yield given by Lapp and Neumann<sup>67</sup> is artificial and incorrect.

which the majority of the data described in this thesis were determined.

This cell was made of Pyrex glass and is shown in fig. III, 1.

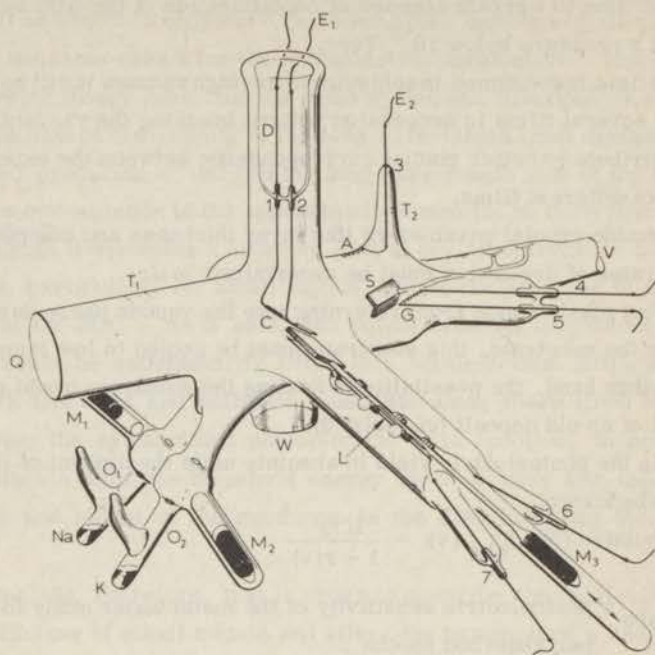


Fig. III, 1. The photoelectric cell used in the study of Na-K alloys.

In the centre of the cell the cathode C is mounted, consisting of a molybdenum foil (22 x 7 x 0.025 mm) spot-welded on two tungsten rods 1 and 2 (2 mm diameter), which emerge outside the cell. The emitting surface was obtained by covering the cathode C with an alkali metal layer evaporated from the atomic beam ovens  $O_1$  and  $O_2$ . C is thermally connected with the Dewar vessel part D of the cell, which can be filled e. g. with liquid nitrogen. Alternatively, C can be outgassed or cleaned from alkali's in vacuo by prolonged resistance heating and occasional flashing.  $E_1$  is the electrical cathode lead. A gold film deposited on the inner walls of the cell served as a collecting anode. To assure good internal contact with the anode lead  $E_2$  the platinum wire at A was covered by Aquadag. The tungsten rod 3 was molten in quartz rather than in glass to avoid leak currents outside the photocell between  $E_1$  and  $E_2$ . The gold beads could be degassed and evaporated by means of the tungsten coil at G supported by the tungsten rods 4 and 5. The glass shield S protected the quartz window Q and

the cathode C against being covered by gold. Through Q monochromatic light could be shed on a portion of the cathode at a fixed angle of incidence ( $45^\circ$ ).

$T_1$  and  $T_2$  are quartz-Pyrex glass graded seal transitions. Through the plane glass window W the reflected visible light could leave the cell.

The alkali metals were evaporated from the sodium and potassium reservoirs indicated in fig. III, 1. For each of the metals two diaphragms controlled the atomic beams directed to the cathode C. The intensity of the beams was regulated by varying the temperature of the reservoirs. For sodium evaporation the temperature range of  $260 - 320^\circ\text{C}$  was chosen, for potassium it was  $160 - 220^\circ\text{C}$ . The beam shutters  $M_1$  and  $M_2$  containing an iron bar in a glass envelope were operated magnetically. Before and during the evaporation, part of the already deposited alkali film acted as a getter. At L a movable assembly for so-called Saha-Langmuir ionization measurements was mounted to determine atomic beam intensities and alloy compositions *in situ*. This is described in more detail in section IV. 2. The tungsten rods 6 and 7 provided the electrical connections of the surface ionization filament to the exterior of the cell.

In a separate apparatus, the dimensions of which agreed with those of the Dewar part of the photocell, we measured the temperature-difference between the cathode cooled by conduction from D and liquid nitrogen ( $77^\circ\text{K}$ ) by means of a chromel-aluminel thermocouple. At a pressure of  $10^{-5}$  Torr we found that the cathode was warmer than the coolant by approximately  $6^\circ\text{K}$  owing to radiation and convection. At the equilibrium pressure of xenon at liquid nitrogen temperature ( $1.8 \times 10^{-3}$  Torr) this difference had increased to about  $15^\circ\text{K}$ , which is of relevance to the xenon adsorption measurements. Since, however, during the actual photoelectric experiments in vacuum the conditions were somewhat more favourable to the attainment of a low cathode temperature (due to better vacuum and the presence of a metal film as radiation shield) a temperature-difference between C and D of  $3^\circ\text{K}$  has been assumed, when a numerical value was needed (e. g. in Fowler plots). This is still more than the value of  $2^\circ\text{K}$  as reported by Ehrlich<sup>38</sup> for a similar experiment in a field emission apparatus.

In the same auxiliary apparatus the course of the temperature as a function of the time passed after evaporation of all liquid nitrogen from D was determined by repeated calibration with the thermocouple.

In the third cell the molybdenum foil was mounted as shown in fig. III, 2. Another way of mounting, used initially, is shown in fig. III, 3. The foil is spot-welded on thick platinum wires instead of on tungsten rods and it is folded, permitting a thorough annealing of the part exposed to the alkali beams. With this arrangement it was difficult, however, to get the foil tightly stretched and well located, at the same time. This rendered measurements of the reflected light very cumbersome.

After installation of the photocell the molybdenum foil was cleaned by annealing and flashing in a reducing atmosphere of hydrogen. Just within the limits of accuracy of our equipment (the monochromator being suited to measurements at wave-lengths where alkali metals produce high currents) we could show that the work function of a cleaned molybdenum foil was equal to 4.30 eV, in agreement with literature data.<sup>51</sup> Once alkali metal had been introduced into the photocell the foil got slowly covered by vagabonding alkali metal atoms as could be readily seen from an increase of the photocurrent. Flashing then led only to a temporarily clean molybdenum substrate.

The photoelectric cell was connected to the ultra-high vacuum line at V (fig. III, 1) and during operation pressure was maintained at a few times  $10^{-10}$  Torr.

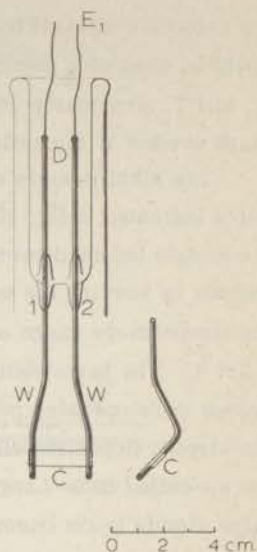


Fig. III, 2. Dewar and cathode part of the photocell.

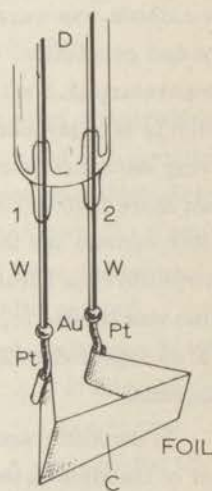


Fig. III, 3. Molybdenum cathode mounted in a favourable way for outgassing.

## CHAPTER IV

### PURIFICATION OF ALKALI METALS AND *IN SITU* DETERMINATION OF ALLOY FILM COMPOSITION BY MEANS OF SURFACE IONIZATION

#### IV.1 PURIFICATION OF ALKALI METALS

Much care was taken to prepare ultra-pure alkali metals. The main step of the purification procedure was a fractional distillation in ultra-high vacuum.

The basic materials for most of the samples used were from the same stock: Sodium, Merck, *Pro Analyti* (0.01% K) Potassium, Alfa Inorganics, Inc. (K-101, 0.05% Na, furnished in vacuum ampulla).

After having been washed in petroleum ether several times, a piece of sodium was cut into small pieces and dried between filter paper. A number of these small pieces, or a broken ampulla in the case of potassium, was introduced into a vacuum apparatus shown schematically in fig. IV, 1.

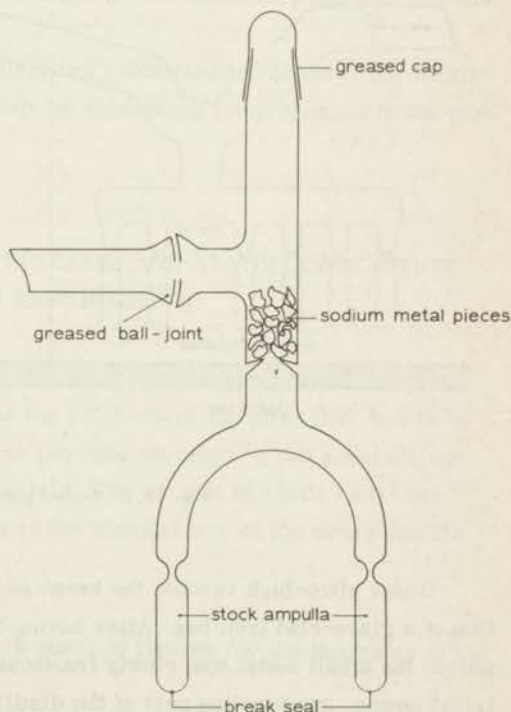


Fig. IV, 1. First purification step.

When by action of the oil diffusion pump a pressure of  $10^{-5}$  Torr was reached the metal was slowly warmed up, without melting. The metal, especially sodium, released gases, such as hydrogen and hydrocarbons. After pumping for about an hour pressure had diminished sufficiently ( $< 10^{-4}$  Torr) to melt the alkali metal out of its oxide-crust. It ran down into the stock ampullae provided with break seals; these ampullae were then melted off.

Thereupon, such a stock ampulla filled with alkali metal was put into a Pyrex distillation apparatus, connected to the ultra-high vacuum line on the same place where the photocell was attached in the photoelectric measurements. In fig. IV, 2 the distillation apparatus and the position of the table-top are represented. As shown, in this equipment the ampullae were not exposed to high bake-out temperatures, because these alkali metals heavily attack glass above  $300^{\circ}\text{C}$ .

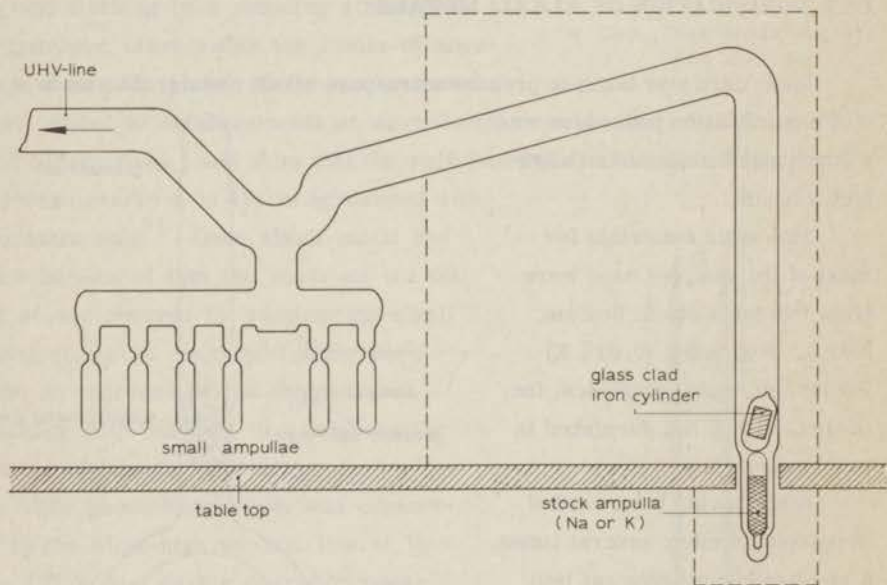


Fig. IV, 2. Second purification step.

Under ultra-high vacuum the break seal was smashed by magnetic operation of a glass-clad iron bar. After having been degassed for a rather long period the alkali metal was slowly fractionally distilled by means of two electrical ovens, surrounding part of the distillation equipment (indicated by the dashed lines in fig. IV, 2) at a pressure below  $10^{-7}$  Torr. Subsequently, part

of the metal was distributed, again by distillation with a flame, over a number of smaller ampullae with break seals. The large diameter of the main pumping line (28 mm) is important to maintain a low pressure during the first distillation step; when melting off the small ampullae the pressure was always lower than  $10^{-8}$  Torr. As the vapour pressure is smaller for sodium than for potassium<sup>22</sup> a higher temperature (about 325°C) was applied for distilling sodium as compared with potassium (about 275°C). Remarkable, but in agreement with the literature,<sup>62</sup> was the fact that sodium caused a pronounced change in colour of the glass (to brown), more than potassium did (to pale yellow).

When preparing a series of measurements, one of the sample holders obtained in this way was put again into an auxiliary distillation equipment connected to the photocell, in this case the alkali reservoirs. Thus, before final deposition the alkali metals were distilled once more under ultra-high vacuum.

The alkali films prepared in this way are of extremely high purity. By means of flame photometric analysis no potassium could be detected in a sodium film and *vice versa*; i. e., each alkali metal contained less than 0.01% of the other. (About 0.001 mg Na per litre can be detected in a potassium solution of 10 mg per litre.)

During the photoelectric investigations contamination of the films by ambient residual gases could immediately be recognized from changes in the photoelectric distribution curve.

#### IV. 2 DETERMINATION OF FILM THICKNESS AND ALLOY COMPOSITION FROM SURFACE IONIZATION EXPERIMENTS

One of the essential features of this work was the use of two molecular beams of alkali atoms intersecting at the point where the alloy film had to be formed. The atoms were ejected from pin-hole openings in two separate reservoirs, containing the two alkali metals. The amount of alkali metal deposited could be controlled by means of the temperature of the ovens and the evaporation time.

There are several ways to obtain absolute figures for the thickness of the deposited layer.

From the kinetic theory of gases under low pressure a theoretical relation may be derived between the current of matter from the atomic beam oven and

the vapour pressure within. Under favourable conditions of geometry the effusion-flow of matter  $I$  through an orifice of known area  $A_o$  from an oven with known vapour pressure  $p$  of the substance in the vessel is given by

$$I = \gamma A_o p / (2 \pi m k T)^{\frac{1}{2}} \quad (1)$$

where  $m$  is the mass of a vapour molecule,

$k$  and  $T$  have their usual meaning, and

$\gamma$  is a parameter depending on the geometry and the nature of the material of the oven.

Recently, Winterbottom<sup>119</sup> introduced some refinements into the model which changed the significance of the parameter  $\gamma$  and made it sensitive to several other factors as well.

In order to get a rough estimate of layer thickness in our first experiments carried out in photocells into which no provisions for surface ionization determinations were inserted, we applied a formula originally due to Stern<sup>107</sup> and used by Brady<sup>18</sup> in his study of alkali metals. This semi-empirical equation is essentially the same as equation (1) and has the form

$$I = 5.83 \times 10^{-2} A_o p / (M T)^{\frac{1}{2}} \quad (2)$$

where  $I$  represents the number of moles ejected from the pin-hole in one second;  $M$  is the atomic weight of the alkali metal;  $T$  its absolute temperature;  $p$  its vapour pressure, in Torr, at temperature  $T$ ;  $A_o$  again the area of the orifice in  $\text{cm}^2$ .

The number of atoms striking one square centimeter of a surface at a distance  $r$  (in cm) from the orifice in one second is then given by the equation

$$N = 6.02 \times 10^{23} I / (\pi r^2) \quad (3)$$

It is inconvenient, referring to the film thickness, to state the number of atoms deposited. Instead, a definition for a molecular layer, or monolayer, will be given and this expression used in reference to the thickness. A molecular layer equals the number of atoms per  $\text{cm}^2$  in a solid mass of metal when the layer has the thickness of a unit cell axis of the bcc lattice. This number can be easily calculated from the density and the lattice constant. It will be

understood, however, that in forming a thin film, the spacing may be somewhat different from that in a solid mass of the metal. Throughout this work we used the following data:<sup>29</sup> 1 monolayer of sodium contains  $1.09 \times 10^{15}$  atoms/cm<sup>2</sup>

and has a thickness of 4.29 Å;

1 monolayer of potassium contains  $6.88 \times 10^{14}$  atoms/cm<sup>2</sup>

and has a thickness of 5.25 Å.

Inserting in equations (2) and (3) measured values for  $A_0$  and  $r$  and using recent vapour pressure data:<sup>22</sup>

$$\log p_K = 7.56 - 4587/T \quad (4)$$

$$\log p_{Na} = 8.08 - 5479/T \quad (p \text{ in Torr})$$

we obtained results on film thicknesses. In a few cases, at the end of a series of measurements when the vacuum was broken, we analyzed by means of flame photometry the total amount of a thick alkali metal film deposited just before air was led into the system. Thus, we were able to compare results predicted by the Stern formula quantitatively with analysis data. Reminding that the Stern formula might not be applicable under the particular conditions of our experiments (for example, other numerical factor required), we got the following results:

Photocell 1: Evaporation of sodium during 50 min. at 323°C.

Stern formula:  $2.8 \times 10^3$  monolayers;

Flame photometric:  $1.3 \times 10^3$  monolayers.

Photocell 2: Evaporation of potassium during 60 min. at 219°C.

Stern formula:  $15.3 \times 10^3$  monolayers;

Flame photometric:  $6.0 \times 10^3$  monolayers.

The poor agreement could be improved by correcting for the difference between the experimentally measured temperature inside the electrical oven and the real temperature of the alkali metal inside the vessel (see fig. IV, 3). But, still, the calculated thickness ( $1.5 \times 10^3$  and  $11.4 \times 10^3$  monolayers, respectively) deviated markedly from the results determined by flame photometry.

Besides, there is a more serious drawback of this method, which became apparent in the course of this investigation. The theoretical equation does not provide information about mutual geometry of the beams and the spatial distribution of the flow from the ovens, but yields only a value averaged over the

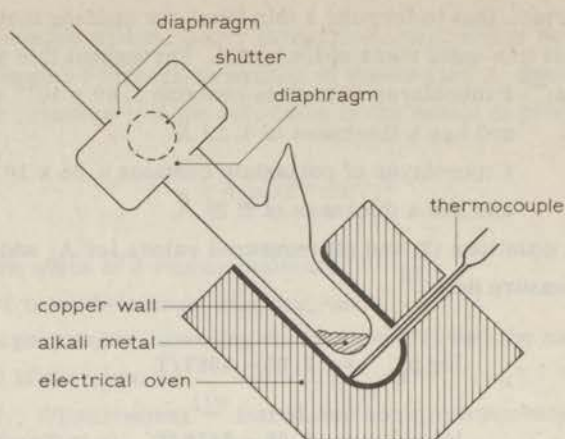


Fig. IV, 3. Cross-section of atomic beam oven, connected to the photocell.

whole substrate surface, whereas only a small part of the deposit was studied photoelectrically. The same drawback is valid for the flame photometric results.

Another way of detection and measurement of density of molecular beams that receives growing technical and scientific interest is based on surface ionization, i. e. the re-emission as positive ions of metal atoms impinging on a hot metal surface. The ionization of alkali atoms at metal surfaces, particularly tungsten, has been extensively studied since the pioneering researches of Langmuir *c. s.*<sup>65, 114</sup> The basic equation underlying the phenomenon of surface ionization is the Saha-Langmuir (= S. L.) equation.<sup>27, 65, 85</sup>

The ratio of the number of emitted ions  $n_+$  to the number of atoms  $n_a$  evaporating from a surface with work function  $\phi$  is, under equilibrium conditions, given by the S. L. equation

$$\frac{n_+}{n_a} = \left( \frac{1 - r_+}{1 - r_a} \right) \frac{\omega_+}{\omega_a} \exp \left( \frac{\phi - eI}{kT} \right) \quad (5)$$

where  $r_a$  and  $r_+$  are reflection coefficients for atoms and ions respectively.  
 $\frac{\omega_+}{\omega_a}$  = ratio of statistical weights which is equal to  $\frac{1}{2}$  for alkali atoms;

$I$  = ionization potential of the atom;

$\phi$  = work function of the metal surface (in eV);

$e$  = electronic charge.

This equation holds if we assume that any incident atom reaches thermal

equilibrium with the surface. In the present study, however, the situation is not necessarily equivalent to the equilibrium situation envisaged in equation (5).

The probability of an incident atom reaching equilibrium with the filament in vacuum may be taken into account by the insertion of a reflection coefficient  $r_i$  for the incident atom.<sup>31</sup> This is not necessarily identical with  $r_a$  because the beam atoms are not at filament temperature.

If the thermal accommodation coefficient differs from unity, the probability that an incident atom leaves the surface as an ion (i. e. the ionization efficiency  $\beta$ ) is given by

$$\beta = \frac{n_+}{n_i} = \frac{n_+}{n_+ + n_a} = (1 - r_i) \left\{ 1 + \frac{\omega_a}{\omega_+} \left( \frac{1 - r_a}{1 - r_+} \right) \exp \left( \frac{-\phi + eI}{kT} \right) \right\}^{-1} \quad (6)$$

where  $n_i$  is the number of incident atoms;

$r_i$  is the reflection coefficient of an incident atom.

The validity of the S. L. equation (5) or (6) (modified) was investigated more recently by several workers for the system K on Pt, which also is of interest for this work. The reflection coefficients  $r_+$  and  $r_a$  are usually neglected, which seems reasonable as the strong electrostatic image forces cause  $r_+$  to be zero and as departure of  $r_a$  from zero would produce an enhanced ionization efficiency, whereas discrepancies always consist in too low efficiencies. Besides, both of these are multiplied by the exponential term which is small for K on Pt. Discrepancies do exist, however, with regard to the reflection coefficient  $r_i$ .

Datz and Taylor<sup>31</sup> measured the ionization efficiency of K on Pt in the range between 1200 and 2000°K, where according to equation (5), it should be equal to 100% over the whole range ( $I_K = 4,34$  V,  $\phi_{Pt} = 5,50$  eV). Their results indicated a reflection varying between 48% at 2000°K and 36% at 1200°K. Consequently, according to Datz and Taylor, the fraction  $\beta$  for K on Pt,  $\beta_K$ , should be equal to about 0.60 at the temperatures used in our experiments (1400 - 1500°K).

By means of an ultra-high vacuum microbalance technique Schroen<sup>102</sup> obtained good agreement with the S. L. equation (5), without the insertion of a reflection coefficient ( $r_i = 0$  in eq. (6)), for K on Pt in the range 1200 - 1700°K. He also assumed that the reflection coefficients  $r_+$  and  $r_a$  did not depart from zero. Because of superior vacuum conditions we are inclined to prefer Schroen's results to those of Datz and Taylor (see also ref. 85) though some reserve is made with regard to the accuracy of the calculated work function of Pt:

4.94 ± 0.23 eV. This value seems rather low as compared with other data (see below). Therefore, and because of the high fraction  $\beta_K$  for K on Pt found by Schroen to vary from 0.99 (1200°K) to 0.96 ± 0.03 (1700°K) we may expect for our temperature region  $\beta_K$  to be equal to 0.99 ± 0.03.

For Na on Pt only results of Datz and Taylor are at our disposal\*. In the temperature range from 1600 to 2000°K they obtained values for the fraction  $\beta_{Na}$  between 0.83 and 0.79, respectively, as predicted by the S. L. equation (5) with the assumption of zero reflection coefficients (including  $r_i$ ) and implicating a work function of platinum equal to 5.50 eV ( $I_{Na} = 5.14$  eV). Since this value is in reasonable agreement with the value of 5.65 eV, as was found recently by Bouwman<sup>17</sup> in this laboratory for Pt films by means of photoelectric measurements, these data of Datz and Taylor for  $\beta_{Na}$  seem to be reliable. In the temperature range of interest here (1500 - 1600°K)  $\beta_{Na} \approx 0.83$ .

Throughout this work we used, therefore, the following data:

ionization efficiency of K on Pt:  $^{102} 100 \beta_K = 99 \pm 3$ ;

ionization efficiency of Na on Pt:  $^{31} 100 \beta_{Na} = 83 \pm 2$ .

We will now describe the device used (L, fig. III, 1) and the results obtained by means of it.

In the photoelectric cell a spec-pure platinum filament F (0.1 mm diameter, 12 mm total length) stretched between two tungsten rods T could be placed in front of that part of the cathode which was to be illuminated by monochromatic light in the photoelectric measurements (fig. IV, 4a and b). It was possible to shift the filament without losing the electrical contact needed for heating it to bright incandescence. For this purpose the tungsten rods T carrying the filament F formed sliding contacts with a pair of platinum wires P, placed inside the hollow glass supports S. The platinum wires were connected to tungsten rods in the cell wall by means of gold wires GW.

The glass shield S prevented the cathode from becoming covered with alkali metal during the period when S. L. measurements were carried out. Moreover, it proved to be useful for visual observation of the spatial orientation of the beams. The iron bar in a glass envelope  $M_3$  permitted F to be transported

\* NOTE ADDED IN PROOF.

After completion of the manuscript a recent article of Mayer and Rahn\*\* on the ionization coefficients of sodium atoms on platinum and tungsten has come to the author's attention. The ionization efficiency of Na on Pt ( $\phi_{Pt} = 5.4$  eV) is reported to be maximum at 1250°K ( $\beta = 0.86$ ) and equal to 0.83 at 1450°K. The latter value is consistent with the one used here.

\*\* Mayer, H. and A. Rahn, Z. Physik 212, 408 (1968).

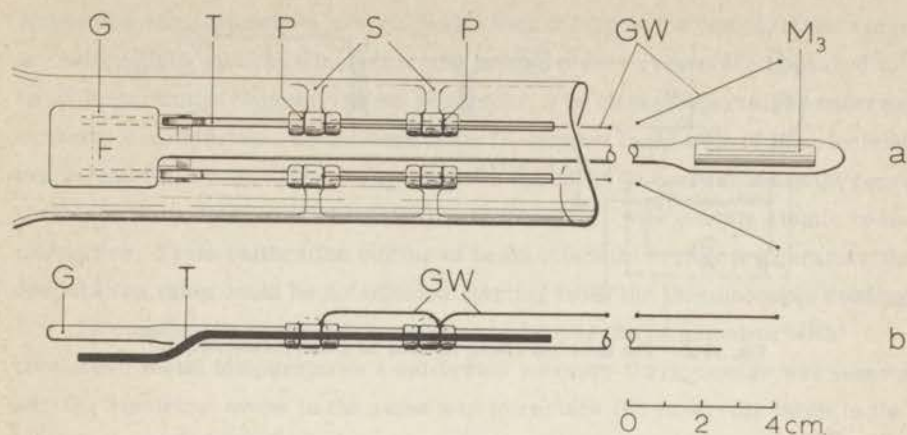


Fig. IV, 4. Assembly for Saha-Langmuir measurements inside the photocell.

by the operation of an electromagnet. In fig. IV, 4b the assembly is shown as seen from the side.

With this equipment atom beam intensities, layer thicknesses and alloy compositions could be determined on different places within the proper section of the beam. From the two ionizing surfaces, viz. Pt and W, employed usually in surface ionization experiments on alkali metals, we chose Pt for our study as it possesses the highest work function ( $5.65 \text{ eV}^{17}$ ). However, the melting point of Pt ( $1773^\circ\text{C}$ ) is much lower than that of W ( $3400^\circ\text{C}$ ); so the risk of burning through during outgassing forms a disadvantage.

The electrical circuit used for the S. L. measurements is shown in fig. IV, 5. The gold film inside the photocell served as a collector (C) for the ions and the ion current was passed through a high load resistor R ( $10^6\text{-}10^{12} \Omega$ ) which fed a lock-in amplifier E of the vibrating reed type (Vibron 33B, E. I. L.). Output voltage readings were monitored on a fast recorder (Philips) and the essentially instantaneous increase or decrease when opening or closing, respectively, the atomic beam ovens could be evaluated graphically.

The Pt filament was a. c. heated and biased positive by +100 V with respect to the ion collector C. (From 50 - 150 V the ion current was independent of the voltage in agreement with literature data:<sup>102</sup> above a voltage of about 25 V/cm the ion current remains independent of this voltage). As the platinum filament was spot-welded directly on the tungsten supports the effective ionization length of the hot filament was not equal to the total length, but was approximately 10 mm. Actually, in analyzing alloy compositions the exact length is of

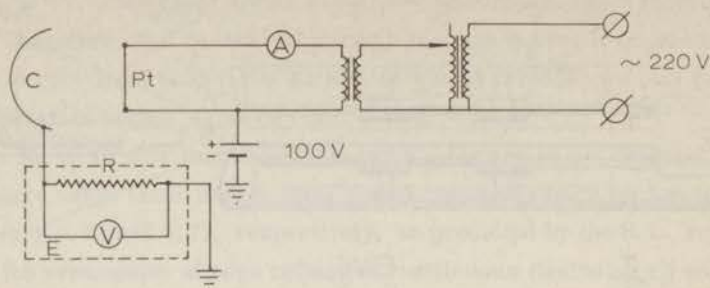


Fig. IV.5. The electrical circuit for Saha-Langmuir measurements.

no importance.

The temperature of the hot filament was measured with an optical pyrometer and varied between 1100 and 1300°C, but was equal to about 1220°C in most experiments. We did not observe a significant influence of the temperature on the ion current in this narrow range.

The measurements were carried out in a dark room so that only the light of the Pt filament could cause a - photoelectric - background current. If the temperature of the filament is high enough ( $> 900^{\circ}\text{C}$  for K) one observes an instantaneous increase of the ion current when opening an atomic beam oven; otherwise, the behaviour of the ion current is sluggish as not all alkali ions are repelled from the filament and thus lower its work function. At low intensities of the beam, we observed in our experiments a small rise following on the abrupt increase when opening an oven; this was presumably caused by surface diffusion of adsorbed alkali atoms from the cold ends to the hot part of the filament. At high beam intensities this effect practically disappeared.

Ion currents usually ranged from  $1 \times 10^{-7}$  to  $1.5 \times 10^{-6}$  A (K) and from  $1 \times 10^{-7}$  to  $2 \times 10^{-6}$  A (Na).

Sodium and potassium atomic beams could be analyzed separately or simultaneously. In an idealized working-schedule one should determine the rate of evaporation prior to each deposition. One should only have to make sure then that the filament is in its correct position, just in front of the spot formed by the incident light, and that the temperature of the atomic beam oven remains constant, also after removal of the filament during the actual deposition.

We found it, however, more practical to follow another procedure: beam

intensities were measured several times over a large oven temperature range for both metals with the filament on the proper place. (The place appeared to be an important parameter, as we shall see.) The oven temperatures referred to thermoelectric data, as obtained from the copper inner wall of the electrical ovens (see fig. IV, 3). These temperatures appeared to correspond quite reproducibly with certain ion currents and, consequently, with certain atomic beam intensities. From calibration curves of beam intensity versus temperature the evaporation rates could be determined starting from the thermocouple readings.

To connect the observed thermocouple temperatures somehow with true alkali metal temperatures a calibrated mercury thermometer was inserted into the electrical ovens in the same way to replace the reservoir tubes in the ovens, and both temperatures were compared. At a temperature of  $200^{\circ}\text{C}$  the thermocouple temperature was about  $6^{\circ}\text{C}$  higher than the thermometer reading, at  $300^{\circ}\text{C}$  the difference had increased to  $18^{\circ}\text{C} \pm 3^{\circ}\text{C}$ . These data are not important to establish the layer thickness as the S. L. method used by us is self-consistent and yields absolute values; but they are of interest when comparing them with, for example, vapour pressure data, or with equation (2).

We shall now discuss experimental surface ionization data obtained in the third photocell. The ion currents were evaluated graphically from the instantaneous change in the total ion current during a change of condition, viz. closing or opening the shutter of the beam oven.

All data are average values of several consecutive measurements at one oven temperature. They were taken after the temperature had reached its stationary value which corresponded with the dial setting of the oven Variac. In calculating beam intensities  $n$  (in atoms per  $\text{cm}^2$  per second) the following data were used:

- length of the platinum filament = 10 mm, diameter = 0.10 mm
- distance between molybdenum foil and lower diaphragm = 120 mm
- distance between filament and this diaphragm = 111 mm.

As the beam intensity diminishes with the square power of the distance, the "filament intensity" has to be multiplied by a factor of 0.85 to get the required "foil intensity".

In fig. IV, 6 results for ionizing potassium on platinum are presented. The number of potassium atoms per  $\text{cm}^2$  per second ( $n_K$ ) measured at the place of the filament by the S. L. method has been plotted against the oven temperature, given by the thermocouple reading. Different symbols refer to different series

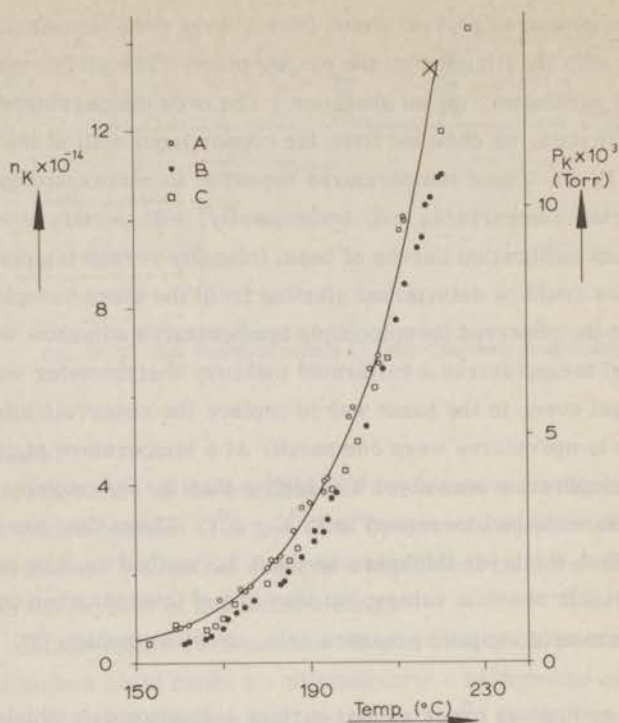


Fig. IV, 6. Number of potassium atoms incident on the hot platinum filament per  $\text{cm}^2$  and per second versus oven temperature. Different symbols refer to different positions of the filament. The solid curve represents the vapour pressure of liquid potassium.<sup>22</sup>

of measurements, during which the filament was in a certain constant position (A, B or C). The position of the filament was not the same for all series, but it appears that the points corresponding to each position fall on parallel curves (these are not drawn). Position C is evidently the same as position B. Position A represents the relevant position for evaluating low temperature alloy compositions.

As is also shown, the points e. g. of series A may well fit a (drawn) curve that gives the vapour pressure of potassium<sup>22</sup> in properly adapted units as a function of the true temperature corresponding with the thermocouple reading.

From fig. IV, 6 it follows that the atomic beam intensities varied rather strongly from one place to another within the area of deposition on the cathode. In the past, several authors made no allowance for variations in the spatial intensity distribution of molecular beams;<sup>102</sup> see, however, ref. 119.

Consequently, for the analysis of alloy compositions after deposition at

low temperature, a correct position of the filament is crucial. How far this analysis can also predict compositions of alloys after sintering seems questionable, however. If the alloys should acquire the same uniform composition over the whole cathode surface during annealing, flame photometric analysis would become a suitable method again for establishing the composition after sintering.

In fig. IV, 6 the point indicated separately by a cross relates to the result of a flame photometric analysis of a thick potassium film carried out directly after deposition. The result has been corrected for the reciprocal distance factor, mentioned above. Apparently, the intensity of the part of the beam ionized by the filament in position A happens to correspond quite well with the average intensity of the beam. We should emphasize, however, that this concurrence is accidental.

In fig. IV, 7 results of analogous experiments for the ionization of sodium on platinum are represented. The capitals A and B refer to the same positions as they did above. Only a few points could be obtained in position B.

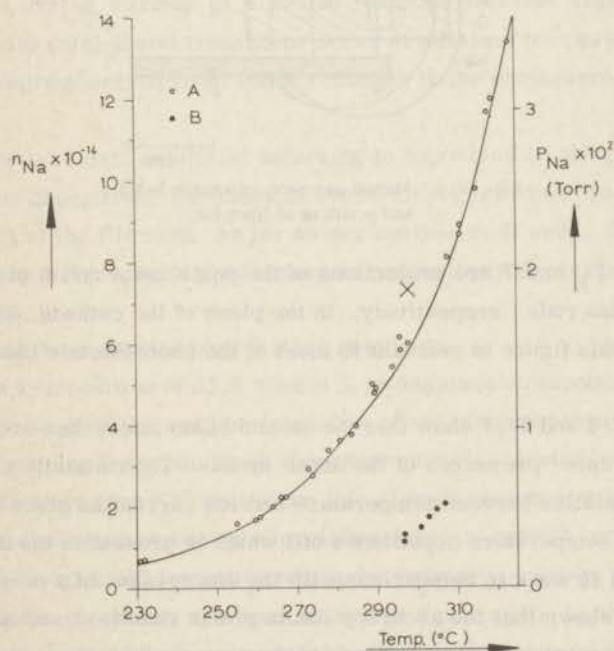


Fig. IV, 7. Number of sodium atoms incident on the hot platinum filament per  $\text{cm}^2$  and per second versus oven temperature. Different symbols refer to different positions of the filament. The solid curve represents the vapour pressure of liquid sodium.<sup>22</sup>

As in the case of potassium the drawn curve represents the vapour pressure of sodium<sup>22</sup> as a function of the true sodium temperature.

Obviously, the variation of beam intensity with position of the filament appears to be more pronounced than in the case of potassium. This fact is caused by a different orientation of the beams with regard to the position of the cathode, as could also be observed visually.

Flame photometric analysis of a thick sodium film (see the point indicated by a cross) reveals that other sites of higher layer thickness must occur on the surface.

This and other (visual) evidence enables the estimated spatial arrangement of the beams with respect to the cathode to be sketched (see fig. IV, 8). The circles denoted by K and Na represent the cross sections of the corresponding atomic beams in the plane of the cathode C. L gives the illuminated part of the

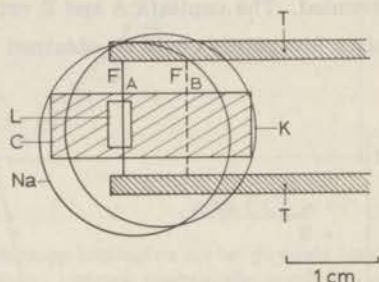


Fig. IV, 8. Mutual geometry of atomic beams and positions of filament.

cathode,  $F_A$ ,  $F_B$  and T are projections of the positions A and B of the filament and the tungsten rods, respectively, in the plane of the cathode. The situation envisaged in this figure is relevant to most of the photoelectric measurements on alloys.

Figs. IV, 6 and IV, 7 show that the atomic beam intensities are proportional to the vapour pressures of the alkali metals. Theoretically one should expect a correlation between temperature and ion current as given by equation (1). Since the temperature dependence of  $I$  which is present in the denominator of equation (1) is weak in comparison with the one present in  $p$  (see eq. (4)) it can be easily shown that the accuracy limits of our results do not allow unequivocal establishment of this dependence in the temperature range studied.

The principal cause of errors in all S. L. measurements is given by the error in the determination of the oven temperature by means of the thermocouple (we now consider the position of the filament as being constant). If we

assume an uncertainty of  $\pm 2^{\circ}\text{C}$  in the temperature reading, which is still rather low at  $300^{\circ}\text{C}$ , the uncertainty in the atomic beam intensity will amount to approximately  $\pm 10\%$  as a result of the exponential dependence of the vapour pressure on temperature. This low degree of accuracy will mask the  $T^{\frac{1}{2}}$ -dependence.

As stated above, S. L. measurements were mainly intended to obtain compositions of alloys after deposition at low temperature. For the most important group of alloys studied the calibration curves in figs. IV, 6 and IV, 7 (position A) were relevant.

It appeared that there were two methods of analysis which could provide a rough check of the S. L.-predicted compositions of alloys. Firstly, by means of flame photometric analysis after termination of the measurements. This was done in one case of a simultaneously evaporated alloy; we recall the fact that the analytical result then refers to a sintered alloy.

Secondly, by means of following the photoelectric yield as a function of temperature during warmup of a cooled film. In different regions of the phase diagram solid-liquid transitions occur at different temperatures, which could be readily observed from sudden changes in the photocurrent during annealing.

In table IV. 1 data are listed referring to a group of 13 alloys prepared by simultaneous deposition. The rates of evaporation correspond to those measured at position A of the filament. As far as our equipment allowed, the conditions for depositing and measuring photoelectric properties were invariably the same for all alloys.

Some of these results need further comment.

1. The composition of 33.3 atomic % potassium corresponds with the Laves phase  $\text{Na}_2\text{K}$  in the sodium-potassium phase diagram (see fig. VI, 1). An alloy containing less than 33 at. % potassium melts (partially) at  $6.9^{\circ}\text{C}$ , for an alloy with more than 33% potassium this already occurs at a temperature of  $-12.6^{\circ}\text{C}$ . In the latter region an alloy with potassium content between 33 and 42% K exhibits a second transition where the sodium-potassium compound reacts with the melt to form a larger amount of a new melt. As these solid-liquid transformations are accompanied by sharp small drops in the photocurrent they can be easily recognized and identified (see also chapter VI).

2. Alloy No. 12 was analyzed flame photometrically directly after deposition. Before analysis, the molybdenum foil was cut into two equal parts par-

Table IV.1

Determination of the composition from conditions of simultaneous deposition for a group of alloys studied in the third photocell.

Number	Time of deposition (min.)	Temp. Na-oven °C	Temp. K-oven °C	Rate of evaporation Na $\times 10^{-14}$	Rate of evaporation K $\times 10^{-14}$	Composition %K S.L.	Composition %K F.P.	Composition %K Ph. El.
1	40	320	166	12.0	1.08	8	-	< 33
2	30	326	179	14.7	2.04	12	-	< 33
3	40	322	184	12.8	2.59	17	-	< 33
4	35	316	180	10.4	2.14	17	-	< 33
5	40	296	177	5.53	1.84	25	-	< 33
6	47	289	186.5	4.57	2.92	39	-	> 33
7	40	281	186	3.57	2.84	44	-	> 33
8	32	286	205	4.17	6.70	62	-	> 33
9	41	278	199	3.22	5.24	62	-	> 33
10	40 $\frac{1}{2}$	266	203	2.13	6.17	74	-	> 33
11	45	261	212	1.75	9.45	84	-	> 33
12L	60	308	189	7.90	3.28	30	33	-
R	60	308	189	-	-	-	35	-

S.L. = according to Saha-Langmuir data

F.P. = " " flame photometric analysis

Ph. El. = " " photoelectric data

allel to the short edge. The left part L of the foil was of most interest with respect to photoelectric studies and S. L. measurements of these alloys (see fig. IV, 8). From Table IV.1 it appears that both parts of the molybdenum foil carried alloys of practically the same over-all composition, though the initial compositions before warming to room temperature must have been somewhat more different according to the S. L. data. Obviously, long range lateral diffusion and equilibration processes had taken place during annealing, in accordance with literature data.<sup>14</sup> This fact was substantiated during resintering of an alloy from its photoelectric behaviour. The transition observed during the first heating at 6.9°C had disappeared during the second one, which indicates a time dependent enrichment in potassium. Alloy No. 6 showed the reverse effect, however. A transition was observed there at -12.6°C during both sintering periods, but that near +6.9°C was only present during the second run, which points to a loss of potassium and a composition falling in the range of 33 - 42 at. % K.

Summarizing, the results obtained lead us to the following conclusions:

(i) Analysis *in situ* by the Saha-Langmuir method provides reliable determinations of alloy compositions after simultaneous deposition at low temperature. Additional information can be acquired in the case of sodium-

potassium alloys from photoelectric data during sintering processes. These data refer exactly to the correct part of the total film surface. They show that the S. L. results yield alloy compositions with a satisfactory degree of accuracy (outer limits of error:  $\pm 15\%$ ).

(ii) Flame photometric analysis gives over-all compositions of the deposited alloys. These are only of interest for sintered alloys. Discrepancies between the compositions obtained from S. L. data and flame photometric analyses have been shown to exist, but they appear to be restricted to about  $\pm 15\%$  under the experimental conditions for the study of the alloy series summarized in Table IV. 1.

(iii) As a consequence of the facts stated in (ii) a change in composition of the part of the alloy illuminated in photoelectric measurements will occur during a sintering period. This change, however, will not exceed 20%.

(iv) Results of S. L. measurements can also be used for determining layer thickness. An adequate method for checking data obtained in this way is not available and the correctness of the ionization fractions assumed cannot be verified. Therefore, an estimated error of about 20% still seems reasonable for this type of measurements, provided that the position of the filament corresponds with that of the image of the light source. The accuracy is mainly determined by the accuracy of temperature control, of the effective ionization length of the filament and of the adopted ionization efficiencies  $\beta$ .

## CHAPTER V

### PHOTOELECTRIC PROPERTIES OF POTASSIUM AND SODIUM

#### V. 1 INTRODUCTION

For a long time the photoelectric properties of alkali metals have been the subject of extensive investigation. Indeed, the history of observations in this area dates back to the very early experiments conducted by Elster and Geitel<sup>39</sup> about 1890. Evidently, the low work function and the high photoelectric sensitivity enabling studies by means of simple techniques considerably contributed to this early interest.

The photoelectric behaviour of alkali metals appeared to be complicated, and very sensitive to the composition and structure of the metal surface, to the angle of incidence of the light and to the state of polarization of the electric wave vector of the light ("vectorial selective photoeffect"<sup>58</sup>).

In 1931 Fowler's theory on photoemission was published (see chapter III). It was curious that most data on alkali metals did not fit this theory,<sup>19, 60, 73, 74</sup> although they approach better than any other metals the ideal case of a free-electron gas, on which the theory was based. Some authors<sup>74</sup> sought for an explanation in terms of contamination; others, accepting this deviation as a real property of alkali metals, tried to complete and extend the theory over a broader wave-length region.<sup>43, 84</sup>

When the conceptions of surface and volume photoeffect were discussed, as depicted in chapter I, interest was focused again to the alkali metals (see ref. 20, 76, 79, 89, 109, 115, 117, 120).

In 1954, Suhrmann<sup>109</sup> interpreted photoemission from potassium still as mainly a surface effect, besides having called attention to the optical proper-

ties of the bulk metal. In 1957, Mayer and co-workers<sup>76,115</sup> first presented evidence that photoemission from potassium films, deposited at low temperature under ultra-high vacuum, must be a volume effect in the whole spectral region. Especially the experiments of Thomas<sup>115</sup> concerning measurements of the photocurrent as a function of film thickness for different wave-lengths of the incident light seemed to offer an easy way to identify the type of the photoeffect (see chapter I).

Despite of the elaboration of experimental photoelectric data on sodium and potassium (for a survey, see ref. 47, 104), a clear picture of the photoelectric behaviour of films of these metals is still lacking. Yet such a knowledge is required for our study of alkali metal alloy films. Recent reports of Boutry et al.<sup>16</sup> (K), Lapp and Neumann<sup>67</sup> (K) and of Garron et al.<sup>45</sup> (Na) do not provide sufficient information for our purpose.

In the work described in the present thesis films were in general deposited at low temperature in order to obtain optimum control of alloy composition. Subsequent heating to higher temperatures (e. g. room temperature) was necessary to obtain the equilibrium state.

Hence, in the study of pure metal films attention was paid to the following topics:

- photoelectric yield as a function of layer thickness during deposition at 80°K.
- photoelectric spectral distribution curves (SDC's) at 80°K and at room temperature.
- reversible and irreversible changes in photoemission during heating and cooling.
- work function determination.

The experimental findings will be discussed separately for each of the metals and compared with previous work by other authors.

A more general discussion of those aspects which the metals have in common (e. g. nature of photoeffect) will be given in chapter VII, together with the discussion of the photoelectric properties of the alloys.

## V. 2 THE PHOTOELECTRIC PROPERTIES OF POTASSIUM FILMS

### V.2.1 Photoelectric yield as a function of layer thickness

Early work on this score was reported by Brady<sup>18,19</sup> and Mayer,<sup>75</sup> but

their experiments had mostly a tentative character and dealt with phenomena in thickness regions which are only of limited interest here.

More recently, Mayer and Thomas<sup>76, 115</sup> carried out a series of deposition experiments of potassium on quartz under scrupulously clean conditions at 77°K. They reported that the photoelectric yield became constant for all wave-lengths at a certain layer thickness; this thickness, depending strongly on the wave-length, varied regularly from about two atomic layers (at 300 nm) to 200 atomic layers (at 520 nm). The results were interpreted in terms of a volume effect, the layer thickness mentioned above corresponding to the escape depth of an excited electron at the wave-length studied.

We measured the photoelectric current during deposition of rather thick layers as a function of the layer thickness for three different wave-lengths of the incident radiation and for different evaporation rates. In practically all experiments the molybdenum substrate was cooled by liquid nitrogen to 80°K. Deposition times ranged from ten minutes up till an hour and deposition rates were relatively high (0.5 - 2.0 atomic layers per second).

In some experiments potassium was deposited on top of an alkali film which then functioned as a substrate; in that case an influence of the substrate on the development of the yield could, indeed, be observed (see section VI, 1), but the SDC obtained its final and normal form at about 100 monolayers.

In the photocell used for this work (No. 3, see chapter III) the photoelectric yield of freshly deposited alkali metal films did not remain constant after closing the atom source. The photocurrent of deposited pure potassium films invariably decreased during the first few minutes after evaporation and then slowly approached a constant value. The SDC, however, kept exactly the same form during this process, constituting an argument that these changes were not caused by contamination of the surface by residual gases. Also the amount of light reflected did not change after termination of deposition. Obviously, above phenomenon was due to a slow rearrangement of potassium atoms at the surface. The same effect has been observed by others for K on Pt<sup>75</sup> and for Cs on quartz.<sup>15</sup>

By heating the molybdenum foil to incandescence a previously investigated layer could be removed and a new experiment started under equal conditions. The intensity of the incident light remained constant during deposition.

In fig. V, 1a some examples of deposition experiments are given. The photocurrent was measured at 436 nm for film thicknesses up to 500 monolayers.

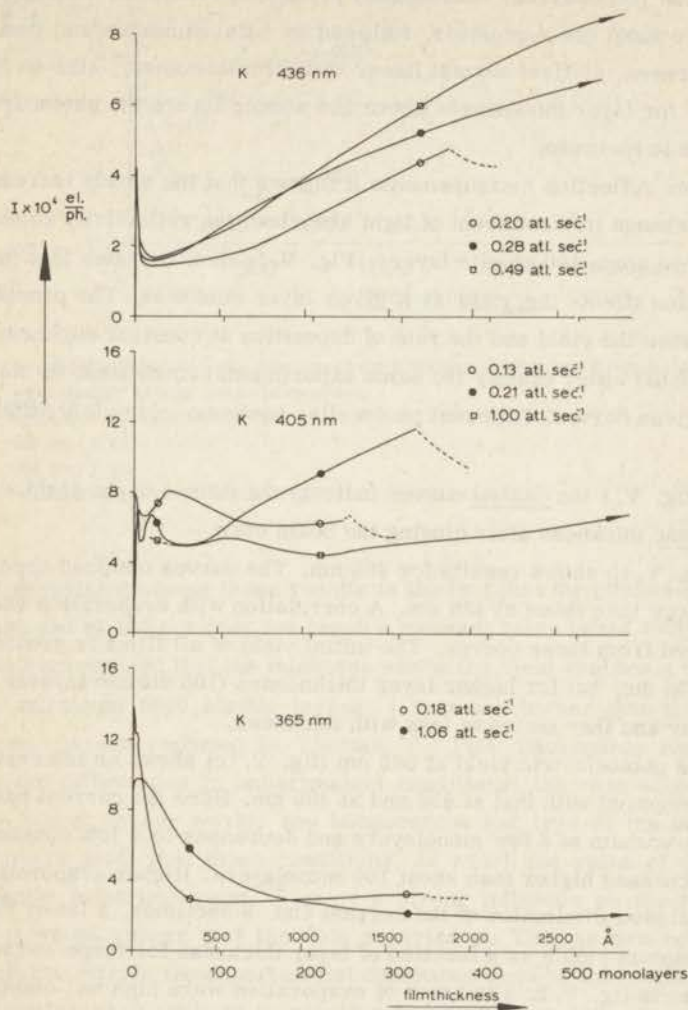


Fig. V.1. Photoelectric emission  $I$  (in electrons per incident photon) as a function of the thickness of potassium films, deposited at various rates on molybdenum at  $80^\circ\text{K}$ , excited by monochromatic radiation at 436 (a), 405 (b) and 365 nm (c) (atl. sec<sup>-1</sup> = atomic layers per second).

Arrows indicate that film preparation was continued.

Dashed curves represent the course of the yield with time during about 10 min. after closing the source, at constant film thickness.

The form of the curves is similar for all evaporation rates. For a sufficiently cleaned alkali-free substrate the yield is equal to zero at 436 nm. During evaporation the photocurrent immediately passes a pronounced maximum corresponding to about one monolayer, followed by a flat minimum and then a continuous increase, at first almost linear with film thickness, later on less steep. Note that for layer thicknesses above 500 atomic layers the photocurrent still continues to increase.

From reflection measurements it follows that the steady increase is not due to a change in the amount of light absorbed; the reflectivity remained constant above some 100 atomic layers. Fig. V, 1a demonstrates that the rate of evaporation affects the yield at a given layer thickness. The precise relation between the yield and the rate of deposition at constant thickness can only be elucidated under exactly the same experimental conditions, as was the case for the given curves. Different photocells, however, may yield different results.

In fig. V, 1 the dashed curves indicate the course of the yield with time at constant thickness after closing the beam oven.

Fig. V, 1b shows results for 405 nm. The curves obtained appear to diverge more than those at 436 nm. A correlation with evaporation rate cannot be derived from these curves. The initial yield of all films is greater than the one at 436 nm, but for higher layer thicknesses (100 atomic layers) the yields are lower and they increase less with thickness.

The photoelectric yield at 365 nm (fig. V, 1c) shows an interesting behaviour compared with that at 436 and at 405 nm. Here the current passes through a high maximum at a few monolayers and decreases to a low constant value for thicknesses higher than about 100 monolayers. Higher evaporation rates show a slower diminution of the current and, sometimes, a lower final value.

Quantum yields as a function of layer thickness for three wave-lengths are given in fig. V. 2. The rates of evaporation were high and comparable to those used in the experiments on alloys. The relative positions of these curves predict different forms of the SDC's for thin films ( $< 100$  atomic layers) and for thick films ( $> 300$  atomic layers). For thin films the spectral maximum is expected to be situated at about 365 nm (or less), for thick films it shifts towards higher wave-lengths (436 nm). This appears to be in agreement with experimental findings, as will be shown below. The dotted lines again indicate the progress of the photoelectric yield with time after closing the atomic beam oven.

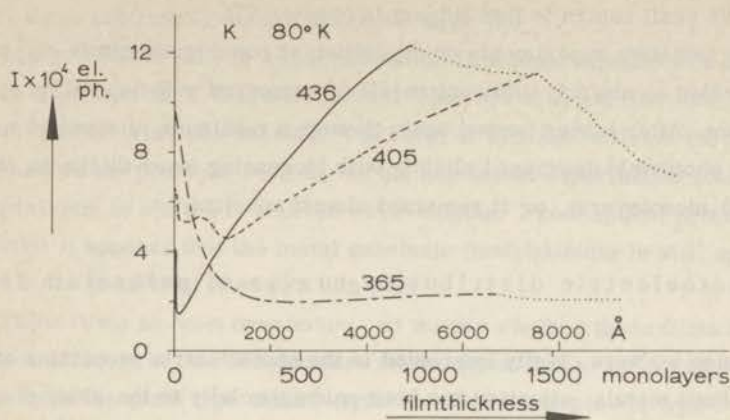


Fig. V. 2. Photoelectric emission as a function of the thickness of potassium films for different wave-lengths at high rates of deposition.  
 436 nm: 0.50 monolayers/sec.  
 405 nm: 1.00 " "  
 365 nm: 1.06 " "  
 For dotted curves: see caption fig. V, 1, "dashed curves".

Most surprising among these results is the fact that the photoelectric response at 436 and at 405 nm does not reach a constant value below 1500 monolayers. We even noticed that the thickness where the yield reaches a steady value may surmount 5000 atomic layers, i. e. much higher than the value of 100 atomic layers reported by Thomas.<sup>115</sup> This discrepancy may be caused by the differences in experimental conditions: the rate of evaporation (much higher in our work), the temperature and type of the substrate. From the mere fact, that these conditions, of which the rates of deposition are apparently most important,<sup>64</sup> exert a strong influence on the results obtained, it would appear that the data reported by Thomas are not of general validity outside the experimental conditions used by that author. The same restrictions then apply to conclusions based on these data, in particular the escape depths of excited photoelectrons.<sup>67, 76</sup>

As the results on deposition, reported here, are supported by evidence obtained in other photocells, there are now reasons to assume that besides escape depths more factors e.g. lattice defects, are involved in the realization of the behaviour of potassium films during "quenching condensation". We noticed, for example, that lowering of the rate of deposition while building up a layer, i. e. with increasing film thickness, produces a reduction of the photo-

current. We shall return to this subject in chapter VII.

A few tentative experiments on deposition at room temperature and at 436 nm yielded an entirely different result as compared with deposition at low temperature. After having passed again through a maximum at about 15 monolayers the photoyield decreased slightly with increasing layer thickness (up to about 1000 monolayers), or it remained almost constant.

### V.2.2 Photoelectric distribution curves of potassium films

Because we were chiefly interested in the photoelectric properties of compact alkali metals, attention has been paid especially to the study of thick potassium films. We measured SDC's after fresh deposition at  $80^{\circ}\text{K}$ , after subsequent sintering at  $293^{\circ}\text{K}$  and after cooling again to  $80^{\circ}\text{K}$  (designated with  $80^{\circ}\text{K}^*$ ). Also, a few films were deposited directly at room temperature.

In fig. V, 3 a selection of SDC's from 5 thick films after deposition at  $80^{\circ}\text{K}$  is presented. The data have been obtained in different photocells (1, 2 and 3). The photoelectric yield  $I$  in electrons per incident photon is plotted as a function of the wave-length  $\lambda$  (in nm). For the thick films the SDC's perfectly coincide if the heights of the maxima are normalized to unity. The given true values of these maxima are largely different from one film to another. Presumably, this spread is caused by differences in evaporation rate, layer thickness and geometry of the layer deposition. The form of the curves is always the same and is typical for a thick potassium film deposited at low temperature

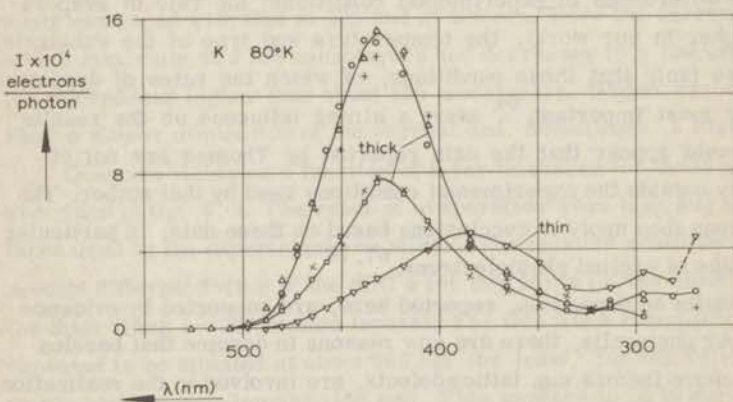


Fig. V, 3. Photoelectric spectral distribution curves of 5 thick (more than 500 monolayers) and 1 thin (about 60 monolayers) potassium films deposited at  $80^{\circ}\text{K}$  in different photocells.

(80°K) on an arbitrarily chosen substrate (type A).

In fig. V, 3 the SDC of a thin potassium film (approximately 60 atomic layers) deposited at 80°K is also shown. The rate of deposition was rather low ( $\sim 0.1$  atomic layer per second). The form of this SDC affirms the findings, mentioned in the previous section, on the deposition experiments (see fig. V, 2). The maximum is shifted to shorter wave-lengths. From optical properties (reflectivity) it appears that the metal substrate (molybdenum) is still apt to play a part in the behaviour of such a thin film.

Thick films at *room temperature*, no matter whether these films have been prepared directly at this temperature or via deposition at 80°K and sintering, always have the same type of SDC (type B). Some examples of type B curves are shown in fig. V, 4 (lower curves); for clarity, in fig. V, 5 a type B curve is represented on a larger scale. In fig. V, 4 the SDC of a thin potassium film (approximately 60 atomic layers or less, compare fig. V, 3) at room temperature is also shown. Remarkable are the occurrence of a very high spectral maximum and a shift of the threshold to longer wave-lengths.

On *cooling* thick films to 80°K the curve slightly changes ( $\rightarrow$  type C) (see fig. V, 5; 80°K\*). This change was found to be completely reversible.

The two types A and B of SDC's differ in some important respects:

1. The maxima are lying at different positions and are shifted from about 430 nm (A) to 400 nm (B). The photoelectric threshold is shifted over a short distance to longer wave-lengths (for type B:  $540 \pm 5$  nm, which yields a work function of  $2.29 \pm 0.02$  eV).
2. The dispersion of the heights of the maxima for type B is much smaller than that for type A.
3. The maximum yields of type A are about ten times larger than those of type B.

All these findings are in excellent agreement with those reported recently by Boutry et al.<sup>18, 64</sup> for thick potassium films, deposited at 77°K on polished glass. The angle of incidence was also equal to 45°. Therefore, we feel justified to add their result regarding the selective vectorial effect, which may be of indirect importance for this study: Curves of type A did not show this effect, whereas curves of type B exhibited a rather strong selective effect for the electric vector polarized parallel to the plane of incidence. This selective vectorial effect has recently been studied by Brauer.<sup>20</sup>

The SDC's of K at room temperature also agree otherwise well with those established in the literature<sup>20, 104</sup> (on both thick and thin films).

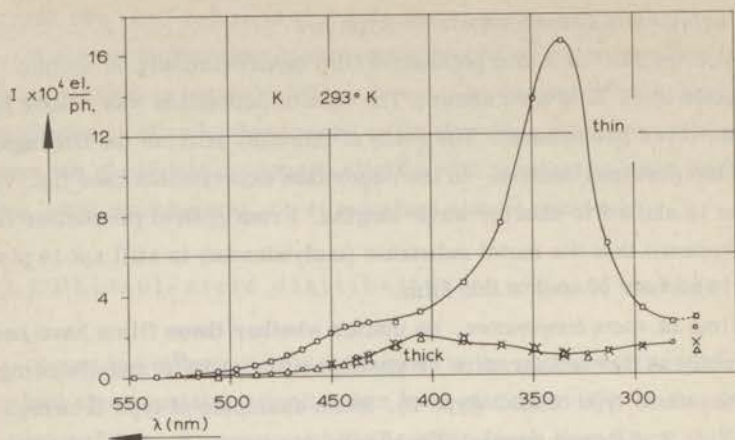


Fig. V. 4. Photoelectric SDC's of 3 thick and 1 thin potassium films obtained after sintering at room temperature in different photocells.

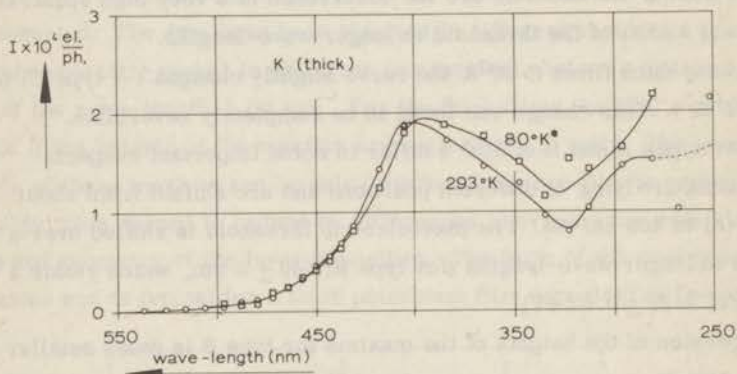


Fig. V. 5. Photoelectric SDC's of a thick potassium film after sintering at room temperature (○, 293°K) and cooling to 80°K (□, 80°K\*).

SDC's after re-cooling (type C) were not reported before.

### V.2.3 Sintering phenomena

To gain information about the origin of the drastic changes in the photoelectric SDC's during a variation in temperature, we measured the change in the photoelectric current at a selected wave-length while warming to room temperature a vapour quenched film.

Typical results at three wave-lengths are shown in fig. V, 6, where the

photoelectric yield per incident photon is plotted against time. They refer to *thick* films. It appears that:

- 1) The relative positions of the three sintering curves agree with the form of the SDC's before and after warming (cf. fig. V, 3 and fig. V, 5, resp.).
- 2) The emission current drops rather abruptly almost to its final value. This happens in a very small temperature range of the sintering process, some-

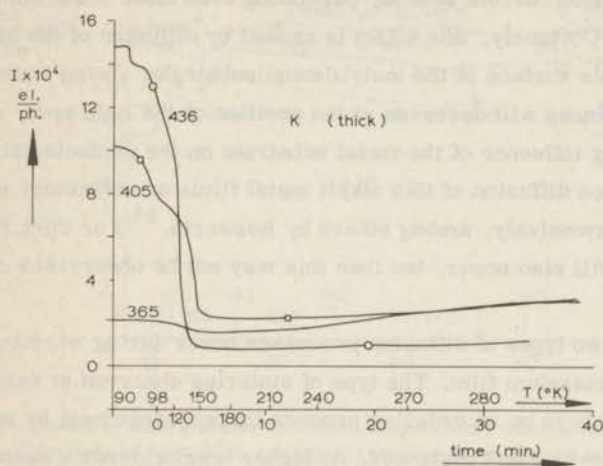


Fig. V. 6. Photoelectric emission of thick, vapour quenched K films as a function of temperature during warming for radiation of 365, 405 and 436 nm.

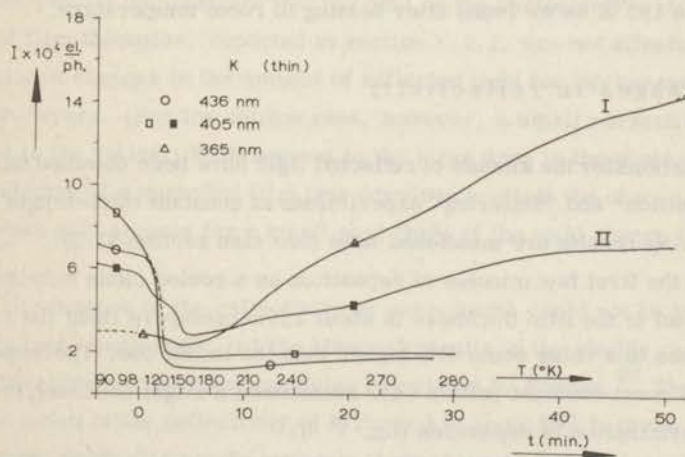


Fig. V. 7. Photoelectric emission of thin (I, II:  $\sim 300$  monolayers; other curves:  $\sim 500$  monolayers) vapour quenched K films as a function of temperature during warming for radiation of 365, 405 and 436 nm.

where between  $95^{\circ}\text{K}$  and  $130^{\circ}\text{K}$ . During the remaining period of warming, in general a small increment of the photocurrent is observed.

At variance with these results are sintering curves for *thin* films, presented in fig. V, 7, particularly those of the films I and II. These films show again a sharp drop shortly after removal of the liquid nitrogen, at temperatures below  $130^{\circ}\text{K}$ ; but at temperatures higher than about  $200^{\circ}\text{K}$  a monotonous increase of the emission current sets in, persisting even after room temperature has been reached. Obviously, this effect is caused by diffusion of the alkali metal over the whole surface of the molybdenum substrate. Owing to this transport the layer thickness will decrease at the position of the light spot, resulting in an increasing influence of the metal substrate on the photoelectric properties. The surface diffusion of thin alkali metal films on refractory metals has been studied extensively, among others by Bosworth.<sup>14</sup> For thick films a similar diffusion will also occur, but then this may not be observable in photoemission.

Apparently, two types of diffusion processes occur during warming of a vapour quenched potassium film. The type of sintering observed at very low temperature is likely to be an ordering process or rearrangement by means of diffusion of atoms over short distances. At higher temperatures a second type of ordering by means of long range diffusion takes place.

These results on sintering are supported by the findings of Dormont<sup>64</sup> who obtained essentially the same SDC's for vapour quenched potassium films after warming to  $195^{\circ}\text{K}$  as we found after heating to room temperature.

#### V.2.4 Changes in reflectivity

Indications for the amount of reflected light have been obtained during a few "deposition" and "sintering" experiments at constant wave-length (436 nm). The following results are mentioned here (see also section VI.3):

1. During the first few minutes of deposition on a cooled clean substrate (usually about 4; the film thickness is about 125 monolayers then) the reflection increases to a value some 40% higher than the initial one. Thereupon, it remains almost constant (within 5%). Sometimes a slight decrease is observed after termination of deposition (fig. V, 8).
2. Warming of such a pure alkali film causes a further stepwise increase of the reflectivity by about 30%, simultaneously with the sharp drop in the photocurrent (figs. V, 6 and V, 7). This is not shown in fig. V, 8.

- Cooling a film to  $80^{\circ}\text{K}$  causes a decrease of its reflectivity (fig. V, 8).
- Deposition of a film on top of a previously condensed film (at  $80^{\circ}\text{K}$ ) does not produce an appreciable change in reflectivity (not shown in fig. V, 8); if the underlying layer had been sintered, however, a slow reduction of reflecting power is observed (by about 20%, fig. V, 8).

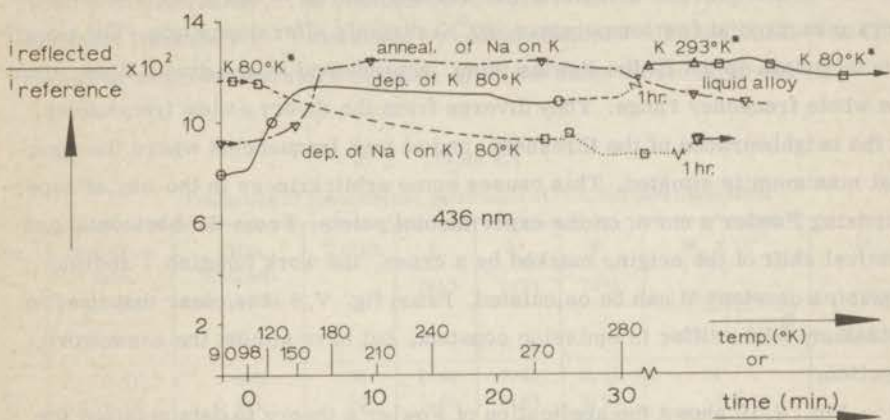


Fig. V, 8. Results of some qualitative reflection measurements, obtained during deposition of K on Mo (dep. of K) at  $80^{\circ}\text{K}$ , subsequent annealing and cooling ( $\text{K } 80^{\circ}\text{K}$ ), and during deposition of Na on top of presintered K at  $80^{\circ}\text{K}$  and subsequent annealing of this sandwich to give a liquid alloy film. Only continuously recorded changes in the reflectivity are reliable.

These results demonstrate that the data on the photoelectric yield as a function of film thickness, reported in section V. 2. 1, are not affected by the just mentioned changes in the amount of reflected light for thicknesses above  $\sim 125$  monolayers. (For low thicknesses, however, a small correction should be applied to the yields.) With respect to the large drop in the photocurrent during sintering of a quenched film (see previous section) the change in reflectance can only account for a small part (20%) of the total change in quantum yield.

The dependence of the reflectivity on wave-length could not be measured accurately (see chapter III), but the obtained results in the visible region were in rough agreement with literature data, calculated by Brauer.<sup>20</sup> These data show a variation in the reflectivity of K limited to about 20% between 300 and 500 nm; thus, the SDC's nearly maintain their shape in that region when the yields are expressed in absolute units (see also chapter III).

## V.2.5 Photoelectric parameters of potassium films

As was described in chapter III several methods are available for evaluating photoelectric work functions from SDC's.

Experimental data on thick potassium films plotted according to the classical Fowler method (ch. III, eq. (6)) are shown e.g. in fig. V, 9. The data were measured at low temperature ( $80^{\circ}\text{K}$ ) directly after deposition. The experimental points do not fit the Fowler plots, represented by the drawn lines, over the whole frequency range. They diverge from the theory at low frequencies, in the neighbourhood of the threshold, and at high frequencies where the spectral maximum is situated. This causes some arbitrariness in the way of superimposing Fowler's curve on the experimental points. From the horizontal and vertical shift of the origin, marked by a cross, the work function  $\phi$  and the emission constant  $M$  can be calculated. From fig. V, 9 it is clear that the two potassium films differ in emission constant, but have almost the same work function.

Fig. V, 10 shows the application of Fowler's theory to data obtained for a thick potassium film at room temperature ( $293^{\circ}\text{K}$ ). Again, the experimental points do not coincide with the theoretical curve and it is difficult to see which of the two drawn curves should be preferred. Parameters derived from both curves have, therefore, been included in Table V.I. In a purely formal sense one could also imagine that the experimental data are composed of two additional Fowler curves with two work functions  $\phi_1$  and  $\phi_2$  and with two emission constants  $M_1$  and  $M_2$ . Very similar deviations have been found by several authors,<sup>45, 67, 109</sup> also for other materials.<sup>4, 61</sup> The possibility of analysis by means of two different Fowler curves has been put forward several times<sup>4, 45, 61, 109</sup> as providing evidence for the existence of two types of emission centres with different work functions. We, like others,<sup>67</sup> do not support this view as many certainly non-homogeneous surfaces have yet shown a perfect fit to the Fowler plot. Furthermore, the strong selective vectorial effect, observed for sintered alkali metals and depending strongly on experimental conditions, can easily account for the observed divergence.

In figs. V, 11 and V, 12 linearized Fowler plots (see III, eq. (7)) are presented for the same respective data. As might be expected the fit of the data to a straight line is equally poor. Clearly, the linear form of the Fowler plot offers a more convenient way of evaluation.

The work function is given by the intercept on the abscissa; from the slope

the emission constant  $M$  may be calculated according to equation III (8):

$$M = (\text{slope})^2 \times 1.485 \times 10^{-8}.$$

In Table V. I results obtained from both forms of the Fowler theory are compared with each other. The photoelectric work function corresponding with the threshold frequency ( $\bar{\phi}_v$ ) and found by extrapolation is also included. The film studied at room temperature (number 3) is the same as the first one (1).

Table V. I  
Evaluation of photoelectric parameters of compact potassium films

Film No.	Deposition rate at, layers at, layers sec.	Film thickness at, layers	T (°K)	$\bar{\phi}_F$ (eV)	$\bar{\phi}_{LF}$ (eV)	$\bar{\phi}_v$ (eV)	$M_F \times 10^{11}$	$M_{LF} \times 10^{11}$
							electrons photon x deg. <sup>2</sup>	electrons photon x deg. <sup>2</sup>
1	0.46	680	80	2.45	2.45	2.41	21	18.9
2	< 0.46	< 600	80	2.45	2.45	2.43	8.3	7.43
3	-	high	293	2.25 or 2.44	2.25 or 2.45	2.31	1.55 6.4	1.60 7.07

Legend to Table V. I:

- $\bar{\phi}_F$  = photoelectric work function: Fowler theory (original)  
 $\bar{\phi}_{LF}$  = " " " " : " " (linear)  
 $\bar{\phi}_v$  = " " " " : Threshold frequency  
 $M_F$  = emission constant : Fowler theory (original)  
 $M_{LF}$  = " " : " " (linear)

The main differences between the sensitivity of potassium films deposited at low temperature (type A) and those sintered at room temperature (type B), expressed in the photoelectric parameters  $\bar{\phi}$  and  $M$ , are:

1. The work function is *decreased* on sintering, whatever method of evaluation is used.
2. The emission constant is lowered too, but, in a more pronounced way. Especially in those cases where one Fowler plot can cover most of the experimental points, thus yielding only one possible work function, this effect is very clear.
3. For films deposited at low temperature the emission constants show much more scattering than for films at room temperature.

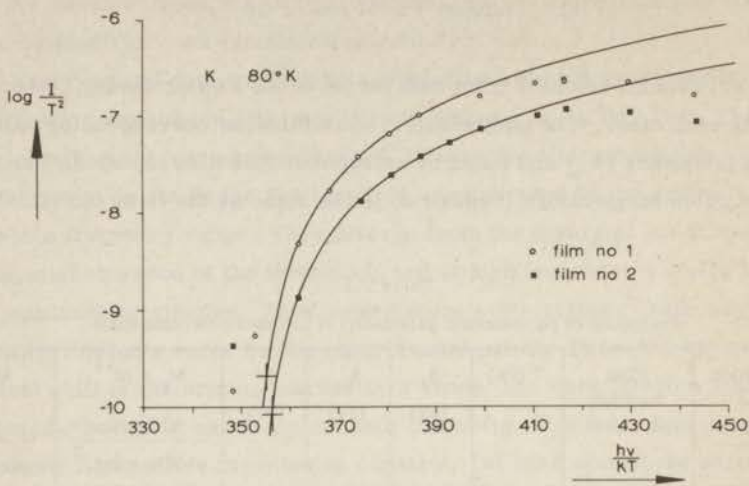


Fig. V, 9. Fowler plots from two thick, vapour quenched potassium films at 80°K. The crosses are the indices of the theoretical Fowler curves (see table V. I).

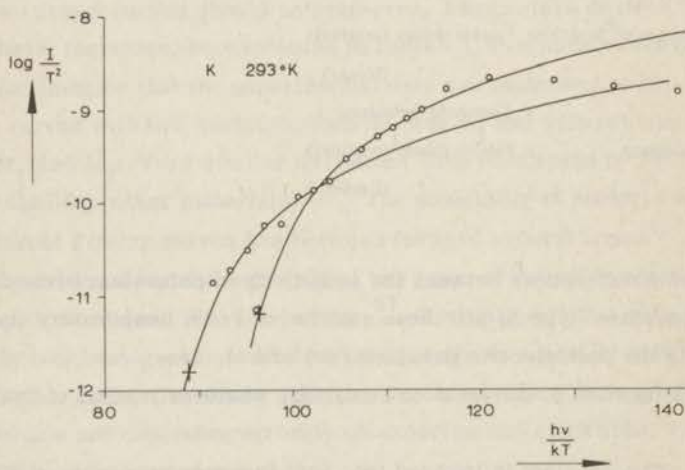


Fig. V, 10. Experimental photoelectric data for a thick potassium film at room temperature and two alternate ways of superimposing a theoretical Fowler plot with equally poor fit (see table V. I).

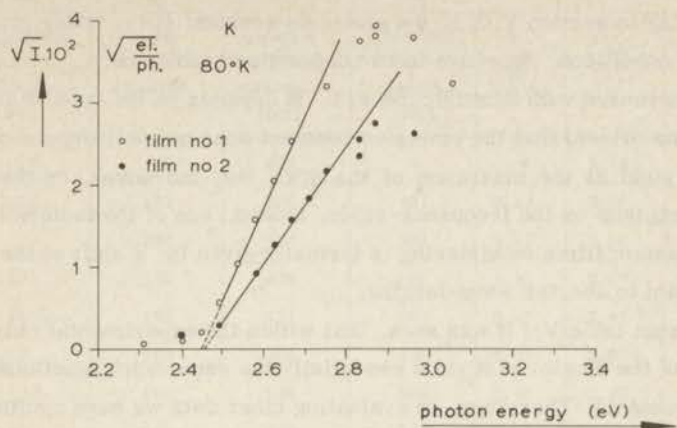


Fig. V.11. Linearized Fowler plots for two thick, vapour quenched potassium films at 80°K (cf. fig. V.9 and table V.I).

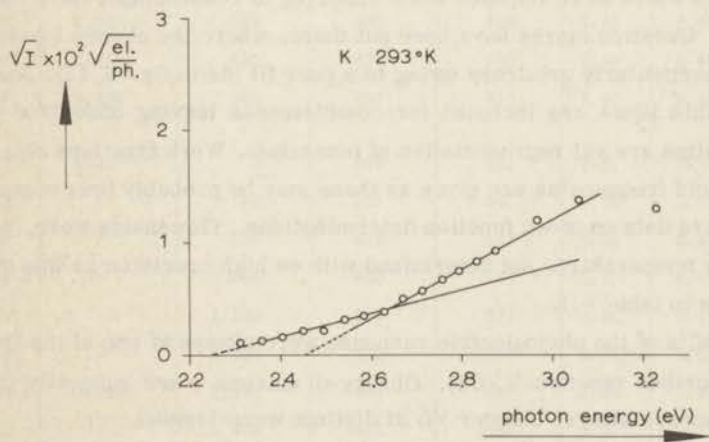


Fig. V.12. Linearized Fowler plot for a thick potassium film at room temperature; two modes of interpretation (cf. fig. V.10 and table V.I).

This spread in the values of the parameter  $M$  obviously reflects the spread in the heights of the maxima in the SDC's observed after deposition at  $80^{\circ}\text{K}$ . Referring to section V. 2. 2, the emission constant  $M$  is, under given experimental conditions, sensitive to two deposition conditions:

a.  $M$  increases with film thickness; b.  $M$  depends on the rate of deposition. It is also evident that the emission constant does not only depend on the *height* of the yield at the maximum of the SDC, but, moreover, on the *position* of this maximum on the frequency-scale. Indeed, one of the factors lowering  $M$  of potassium films on sintering is formally given by a shift of the spectral maximum to shorter wave-lengths.

From table V. I it was seen, that within the experimental error both forms of the Fowler plot yield essentially the same work functions and emission constants. Therefore, in evaluating other data we have confined ourselves to the linearized Fowler plot method.

In table V. II results on potassium films obtained in different photocells (indicated with 1, 2 and 3) are compiled. All details, necessary to describe the photoelectric behaviour, are given. Temperatures, provided with an asterisk, refer to temperatures different from the temperatures of deposition, or temperatures which were imposed after sintering at room temperature had taken place. Question marks have been put there, where the chosen Fowler plots were particularly arbitrary owing to a poor fit (as in fig. V, 12). Some results on thin films are included for completeness leaving undecided whether these films are yet representative of potassium. Work functions obtained from threshold frequencies are given as these may be probably best compared with literature data on work function determinations. Thresholds were, especially at low temperature, not determined with so high precision as was done for the films in table V. I.

The SDC's of the photoelectric response were always of one of the types already described (section V. 2. 3). Observed maxima were generally pronounced (compare alloys, chapter VI) at distinct wave-lengths.

The main results on the photoelectric parameters can be summarized as done in table V. III. As a matter of fact the results on thin films are subject to a much higher scatter (not indicated), but they are of no interest for the alloy work.

Table V. II  
Pure Potassium Films

Photo-cell	Temp. °K	Deposition rate at. layers/sec.	Layer thickness at. layers	Location of maximum (nm)	Threshold wavelength (nm)	$\Phi_V$ (eV)	$\Phi_{LF}$ (eV)	$M_{LF} \times 10^{11}$ electrons/ photon x deg. <sup>2</sup>
1	80	0.01?	12?	424	-	-	2.46	21.4
2	80	0.086	51	385	497	2.49	2.51	3.5
2	80	2	1,000	430	500	2.48	2.50	7.0
2	80	0.163	195	426	500	2.48	2.49	9.8
2	80	0.163 <sup>+</sup>	195	434	506	2.45	2.47	7.5
2	80	0.10	60	384	490	2.53	2.53	3.5
2	80	2	500	434	506	2.45	2.49	27.1
2	80*	-	500	395	526	2.36	2.41?	0.53
3	80	0.222	400	430	506	2.45	2.48	4.7
3	80	0.500	900	430	500	2.48	2.47?	7.2
3	80	0.296	750	425	506	2.45	2.42	5.8
3	80	0.356	850	423	506	2.45	2.46	17.3
3	80	0.356 <sup>++</sup>	850	430	560	2.21?	2.20?	1.2?
3	80	0.568	850	430	506	2.45	2.45	7.43
3	80	0.450	680	427	506	2.45	2.45	19.0
3	80	0.480 <sup>+</sup>	860	433	510	2.43	2.46	5.8
1	293	0.01	3	406	561	2.21	2.36	5.2
2	293*	-	50	335	548	2.26	2.32	1.6
2	293*	-	500	403	537	2.31	2.45	0.68
3	293*	-	400	402	537	2.31	2.41	0.74
3	293*	-	1,300	403	537	2.31	2.41	0.74
3	293*	-	2,000	402	537?	2.31?	2.19	0.39
3	293	0.595	1,070	408	537	2.31	2.30	1.4
3	293*	-	1,920	400	537?	2.31?	2.37?	0.50?
3	293*	- ++	2,700	360	640	1.94	2.03	0.45
3	293*	-	680	403	537	2.31	2.41	0.63

See legend to Table V. I.

+ on sodium

++ contaminated

\* after sintering

Table V. III  
Typical behaviour of potassium films

T°K	Conditions of deposition	Spectral max. nm	$\phi_V$ (eV)	$\phi_{LF}$ (eV)	$M_{LF} \times 10^{11}$ electrons photon x deg. <sup>2</sup>
80	low rate, thin film	385	2.50	2.52	3
80	high rate, thick film	430 $\pm$ 5	2.44	2.47 $\pm$ 0.03	4 - 20
293	thin film	335	2.25	2.3	1.6
293	thick film	404 $\pm$ 4	2.30	2.40 $\pm$ 0.05	0.60 - 1.50
80*	thick film	395	2.36	2.41 $\pm$ 0.02	0.5

See legend to table V. I.

\* after sintering

### V.2.6 Conclusion

In summary, for *thick* potassium films we found:

(i) After deposition at 80°K:

A photoelectric work function of 2.47  $\pm$  0.03 eV.

A spectral maximum in the photoelectric SDC at 430  $\pm$  5 nm, the height of which depends strongly on layer thickness and rate of deposition.

The emission constant is relatively high and varies parallel with the height of the spectral maximum.

(ii) At room temperature:

A photoelectric work function of 2.30  $\pm$  0.02 eV. This value is larger than those reported in the older literature, but agrees perfectly with very recent data.<sup>16, 67</sup>

A shift of the spectral maximum towards about 400 nm accompanied by a sharp diminution of the yield. Both effects lower the emission constant drastically on sintering. Furthermore, the mutual correspondence between different films has become much better then, as compared with vapour quenched films at 80°K.

(iii) Recoiled to 80°K after presintering.

The work function lies somewhere in between the values just mentioned. The SDC resembles that at room temperature (maximum now at 395 nm), as does the emission constant.

The behaviour is entirely different from the unique one of a film deposited freshly at 80°K.

For further discussion we refer to chapter VII.

### V.3 THE PHOTOELECTRIC PROPERTIES OF SODIUM FILMS

In discussing results on sodium films we will proceed approximately in the same way as we did for potassium films. Because sodium has a higher melting point and a lower vapour pressure than potassium it is more difficult in operation. To obtain sufficiently thick films in a reasonable time interval high oven temperatures (250 - 325°C) are required. Perhaps this is one of the reasons why sodium has been used somewhat less extensively in photoelectric investigations as compared with potassium.

Nevertheless, sodium was also studied many times by both experimentalists<sup>45, 73, 74, 89</sup> and theoreticians.<sup>7, 88</sup> Although sodium seems to approach the free-electron model better than any other metal deviations from Fowler's theory have been reported.<sup>45, 73</sup>

#### V.3.1 Photoelectric yield as a function of layer thickness

Only a few results on this topic are available in the literature.<sup>18, 19, 89</sup> Recent and reliable data on deposition experiments of sodium are due to Piepenbring.<sup>89</sup> Although these results were not presented in much detail they were strongly reminiscent of those found previously on potassium films (Thomas<sup>115</sup>). Thus, for distinct irradiation wave-lengths in the range from 290 to 400 nm the photoyield acquired a constant value for layer thicknesses in the range from 20 to 200 monolayers, respectively. These data were explained in terms of a volume effect; the layer thickness at which the yield became constant was interpreted as to correspond with the escape depth of the excited electrons.

It should be remarked that Piepenbring expressed the photoelectric current in arbitrary units and that data for wave-lengths above 400 nm were omitted. This seems to reduce their usefulness, because now no conclusion regarding the locality of a possible maximum in the SDC can be drawn, while, on the other hand, his results clearly suggest the presence of such a spectral maximum.

Some results on deposition experiments as found by us are presented in fig. V, 13 for three wave-lengths, viz. 436, 405 and 365 nm. The rate of de-

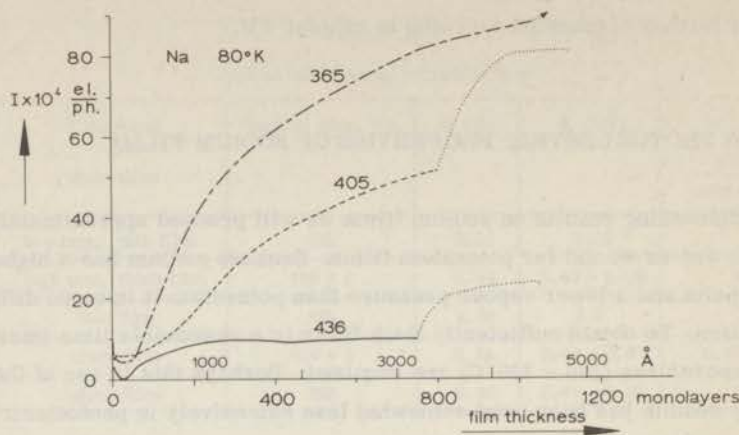


Fig. V.13. Photoelectric emission as a function of the thickness of sodium films for different wave-lengths at high rates of quenched deposition.

365 nm: 0.51 monolayers/second

405 nm: 0.44 "

436 nm: 0.42 "

For dotted curves: see caption fig. V.1, "dashed curves".

position (at 80°K) was rather high (about 0.4 monolayers per second).

At 436 nm the yield remains constant beyond about 200 monolayers. At 365 nm the yield increases rapidly to very large values and even at a thickness of 1000 monolayers no signs of levelling off are observed. The curve at 405 nm lies somewhere in between the two other ones and resembles the curve at 365 nm.

Especially during the first few minutes *after closing* the atomic beam oven spontaneous changes in the photocurrent do occur, as in the case of potassium. Interestingly, the emission current from sodium films is, in contrast to potassium, always raised in this process (see dotted lines in fig. V.13, covering about ten minutes).

Though the influence of deposition rate on the photoelectric yield at a given thickness was found to be less pronounced for sodium than for potassium, higher rates of evaporation tended to produce also higher yields.

From comparison with similar quenching deposition curves for potassium (fig. V.2) some remarkable differences can be noticed:

1. The mutual positions of the curves at the three wave-lengths are quite different.
2. For thin layers sodium possesses a lower sensitivity than potassium at all three wave-lengths.

3. For thick layers, of most interest here, sodium possesses a sensitivity at 365 and 405 nm which exceeds that of potassium several ( $\sim 5$ ) times.
4. The changes in the yield with time after closing the shutter are dissimilar.

Our results on sodium films were reproducible, but they are distinctly at variance with those reported by Piepenbring.<sup>89</sup> They are further supported by data on SDC's (see below). Without questioning the existence of a volume photo-effect we feel, moreover, that Piepenbring's determination of escape depths of photoelectrons is open to some serious objections, the same ones as given in section V. 2.1 for potassium. For further discussion of this point we refer to chapter VII.

### V.3.2 Photoelectric SDC's of sodium films

Photoelectric SDC's of sodium, even at room temperature, are less well established in the literature than those of potassium. For example, the existence of a spectral maximum at room temperature does not appear unambiguously from literature data. In Simon and Surhmann's book<sup>104</sup> a maximum is shown at 340 nm (see page 123); Mann and DuBridge<sup>73</sup> situated it at 370 nm, Maurer<sup>74</sup> at 355 nm; in the recent communication of Garron et al.<sup>45</sup> no maximum is reported in the spectral region between 250 and 520 nm.

Let us first consider *films vapour quenched at 80°K.*

Photoelectric data on six sodium films, obtained in two different photocells (2 and 3), are collected in fig. V, 14. They all refer to films with high layer thickness (300 - 2000 monolayers); the experimental conditions were exactly the same as during the study of the potassium films described in section V. 2.

It can be seen that all films show similar sensitivity curves. The shape of all curves is the same (type A) and is in concordance with our results on deposition experiments described above. It possesses the following characteristic features:

1. The photoelectric threshold, coinciding for all films studied, is situated at  $515 \pm 5$  nm (work function  $\phi_v = 2.41 \pm 0.02$  eV).
2. A very pronounced maximum is present at about 300 nm, surpassing the maximum of comparable potassium films at 340 nm by more than ten times. The presence of this maximum has never been reported before. Brady's measurements<sup>19</sup> did not extend far enough into the UV-region. Maurer<sup>74</sup> also observed a very high response, maximum at 345 nm, but he himself had no confidence in his results on vapour quenched and probably contami-

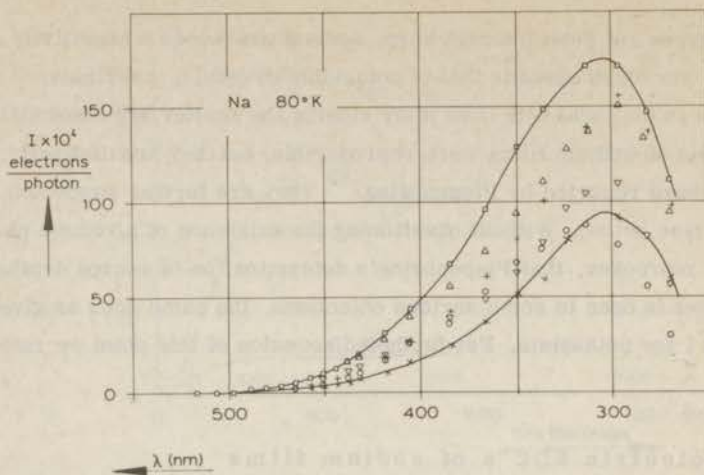


Fig. V, 14. Photoelectric SDC's of 6 thick (○: 300 monolayers; other symbols: 800 - 2000 monolayers) sodium films deposited at 80°K in different photocells. Only two curves have been drawn.

nated films. As stated above, Piepenbring made no assertion regarding the position of a maximum, but his results are misleading as far as they pretend a highest emission at 405 nm and not at 300 nm.

3. The *shape* of the SDC's is rather constant apart from small variations in the region of 300 - 400 nm. It is practically independent of film thickness (above some minimum value), rate of deposition and type of substrate\*.
4. The height of the maximal yield increases with increasing layer thickness and presumably also with higher deposition rate, though different photocells or different substrates may give departures from this rule.

The development of the SDC during built-up of a sodium film at low temperature appears from fig. V, 15. Results are shown for three film thicknesses: 8, 50 and 1500 monolayers. A film, approximately 10 atomic layers thick, does not yet display a spectral maximum, but the photoelectric threshold already equals the one of a thick sodium film.

Fig. V, 16 shows some examples of SDC's of sodium films measured at room temperature in three different photocells. The curve bending upwards at short wave-lengths represents results on two thin films, deposited at room temperature in the first cell. The lower curve, obtained after sintering thick vapour quenched films in cells 2 and 3, is typical for thick sodium films at

\* It should be remarked that in a few cases the SDC of a thick sodium film deposited on top of a fresh potassium film at 80°K differed slightly from the normal one (spectral maximum at 320 nm, instead of 300 nm).

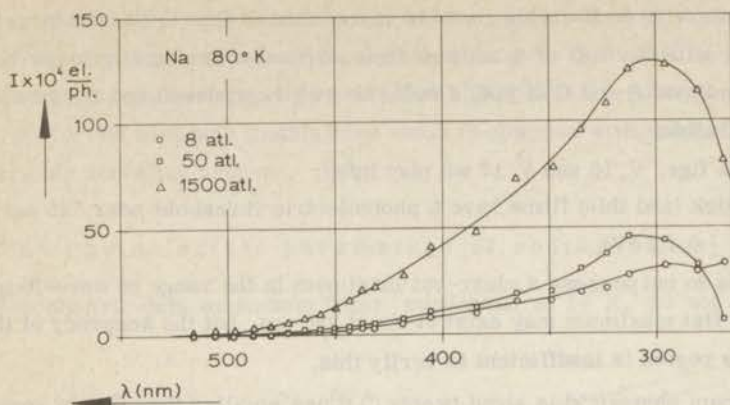


Fig. V. 15. Development of the yield during built-up of a sodium film on molybdenum at 80°K (atl. = atomic layers).

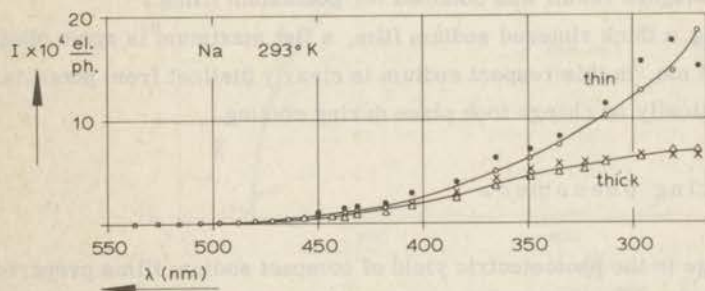


Fig. V. 16. Photoelectric SDC's of 2 thick (about 2000 monolayers) and 2 thin (less than 50 monolayers) sodium films at room temperature. Only two curves have been drawn.

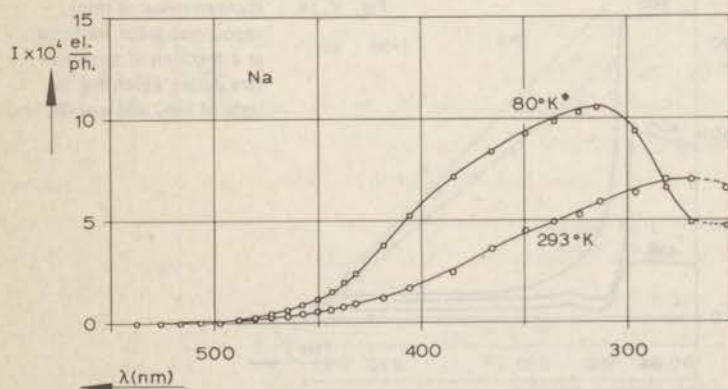


Fig. V. 17. Photoelectric SDC's of a thick sodium film after sintering at room temperature (○, 293°K; cf. fig. V. 16) and cooling to 80°K (○, 80°K\*).

room temperature (type B). This curve is reproduced in fig. V, 17 on a larger scale together with the SDC of a sodium film *after subsequent cooling to 80°K* (type C). Both types B and C of SDC's could be well reproduced and the transition was reversible.

From the figs. V, 16 and V, 17 we may infer:

1. Sintered thick (and thin) films have a photoelectric threshold near 525 nm ( $\phi_v = 2.36 \pm 0.02$  eV).
2. These films do not possess a clear-cut maximum in the range of wave-lengths studied. A flat maximum may exist at about 280 nm, but the accuracy of the data in this region is insufficient to verify this.
3. The maximum photoyield is about twenty (!) times smaller than that of vapour quenched films (cf. fig. V, 14).
4. Thin films show a higher yield than thick films in the neighbourhood of 300 nm. (An analogous result was obtained for potassium films.)
5. Upon cooling a thick sintered sodium film, a flat maximum is again observed at about 315 nm. In this respect sodium is clearly distinct from potassium where practically no change took place during cooling.

### V.3.3 Sintering phenomena

The change in the photoelectric yield of compact sodium films prepared by vapour quenching during warming is shown in fig. V, 18. The respective films correspond to those referred to in fig. V, 13.

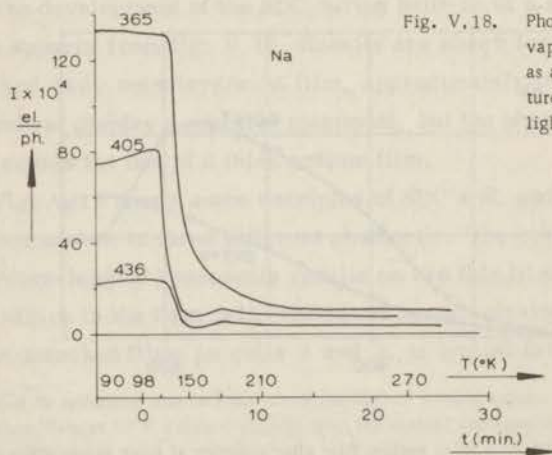


Fig. V, 18. Photoemission of thick, vapour quenched Na films as a function of temperature during annealing for light of 365, 405 and 436 nm.

At all three wave-lengths a very sharp, pronounced (up to a factor of 15) decrease occurs in a narrow temperature range at about  $130^{\circ}\text{K}$ . Note that the "transition temperature" lies somewhat higher than for potassium (cf. fig. V, 6); for the rest both metals have much in common with respect to this irreversible annealing process.

#### V.3.4 Photoelectric parameters of sodium films

Photoelectric data on sodium films, condensed at  $80^{\circ}\text{K}$ , do not give

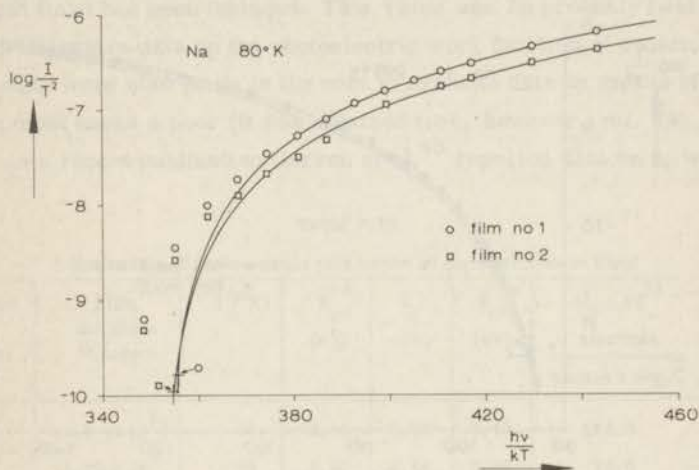


Fig. V, 19. Fowler plots for two thick, vapour quenched sodium films at  $80^{\circ}\text{K}$  (see table V. IV).

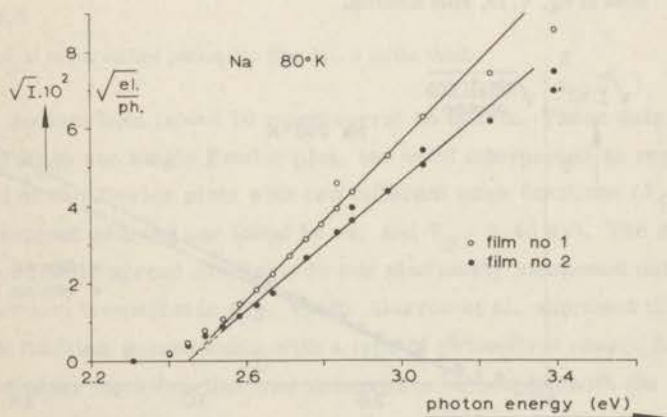


Fig. V, 20. Linearized Fowler plots for the films referred to in fig. V, 19.

a perfect fit to the Fowler curve. This is illustrated in fig. V, 19 for two different sodium films.

Since the maximum of the SDC is situated farther from the threshold frequency, the points could usually be fitted to the theoretical (solid) curve over a wider frequency range than was possible for data on potassium films (cf. fig. V, 9). The work functions are the same within experimental error; that is, the yield curves on the logarithmic scale can be superimposed by simple vertical translations (the zeroes of the Fowler curves are marked by a cross).

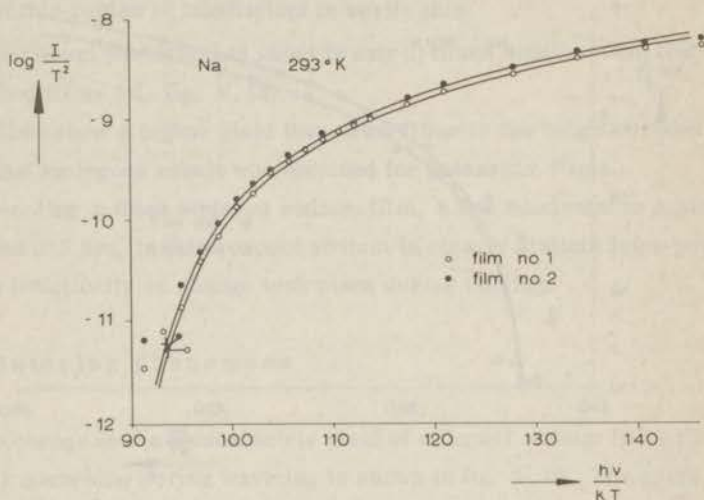


Fig. V, 21. Fowler plots for two thick sodium films at room temperature. The films correspond to those of fig. V, 19, after sintering.

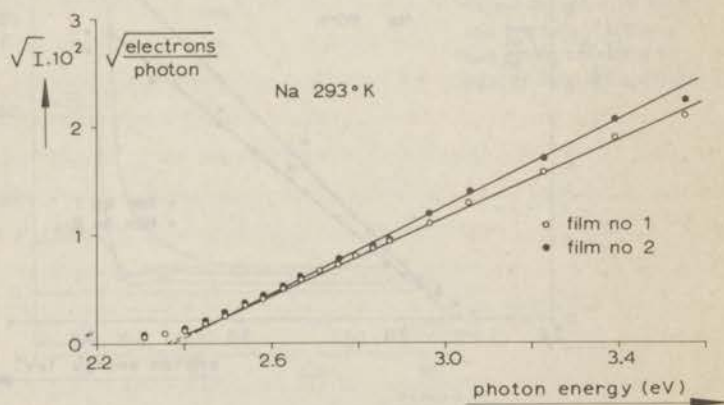


Fig. V, 22. Linearized Fowler plots for the data treated in fig. V, 21.

The corresponding linearized Fowler plots are shown in fig. V, 20.

From the fit of the data to the two types of curves, we may again infer that both methods are equivalent. Systematic deviations from theory appear in the neighbourhood of the threshold ("tail") and, only shown in fig. V, 20, near the maximum of the SDC. Both methods of evaluation have been further applied to data on the same films after annealing at room temperature. This is demonstrated in figs. V, 21 and V, 22. A remarkably good fit is obtained.

The values of the photoelectric parameters derived from the plots are enumerated in table V. IV. The work function corresponding with the long wave-length limit has been included. This value can be probably best compared with literature data on the photoelectric work function of sodium.

Attempts were also made in the past to evaluate data by means of Fowler's theory; in most cases a poor fit was obtained (see, however, ref. 74). For example, in a recent publication Garron et al.<sup>45</sup> reported data on a, what they

Table V. IV  
Evaluation of photoelectric parameters of compact sodium films

Film No.	Deposition rate at. layers sec.	Film thickness at. layers	T (°K)	$\phi_v$ (eV)	$\phi_F$ (eV)	$\phi_{LF}$ (eV)	$M_F \times 10^{11}$ electrons photon $\times$ deg. <sup>2</sup>	$M_{LF} \times 10^{11}$ electrons photon $\times$ deg. <sup>2</sup>
1	0.5 ?	$1.5 \times 10^3$ ?	80	2.40	2.45	2.45	16.5	16.2
2	0.91	$1.92 \times 10^3$	80	2.40	2.44	2.45	11.0	10.6
1			293	2.36	2.37	2.36	0.53	0.49
2			293	2.36	2.36	2.37	0.61	0.61

Legend: see table V. I

Film No. 1 was studied in the second photocell, film No. 2 in the third.

call, thick sodium film (about 70 monolayers) on quartz. These data did not give a good fit to one single Fowler plot, but were interpreted as representing the product of two Fowler plots with two different work functions ( $\phi_1 = 2.36$  eV, in full agreement with the one found by us, and  $\phi_2 = 3.45$  eV). The array of points was actually spread similarly to our previously mentioned data on potassium at room temperature (fig. V, 10). Garron et al. supposed that the lower work function corresponds with a type of photoeffect caused by surface states. The other work function was assumed to be coupled with the volume photoeffect. Their interpretation seems, however, open to objections. The discrepancy between their and our results can be explained in two ways:

Table V. V  
Pure Sodium Films

Photo-cell	Temp. °K	Deposition rate at. layers / sec.	Layer thickness at. layers	Location of maximum (nm)	Threshold wavelength (nm)	$\phi_V$ (eV)	$\phi_{LF}$ (eV)	$M_{LF} \times 10^{11}$ electrons / photon x deg. <sup>2</sup>
1	80	0.02	6	-	516	2.40	2.44	2.8
1	80	0.03	36	310	516	2.40	2.45	4.6
1	80	0.03	76	300	520	2.38	2.40	5.5
1	80	0.44	530	302	526	2.36	2.35	10.6
1	80	0.49	1,120	305	526	2.36	2.35	22.9
2	80	0.132	32	300	488	2.54	2.41	0.54
2	80	0.132	95	300	516	2.40	2.41	5.2
2	80	0.132	190	310	516	2.40	2.43	8.0
2	80	0.132	475	300	516	2.40	2.41	12.3
2	80	0.365 <sup>+</sup>	655	300	516	2.40	2.51?	9.3 ?
2	80	0.365	655	303	516	2.40	2.46	17.1
2	80	1.10	1,650	298	510	2.43	2.48?	11.3 ?
2	80*	-	1,650	320	506	2.45	2.47	2.10
2	80	0.940	845	295	510	2.43	2.49	6.8
2	80	0.365	220	298	506	2.45	2.49	8.5
2	80	0.421	1,520	298	516	2.40	2.46	16.2
2	80*	-	1,520	315	497	2.49	2.48	2.32
2	80*	-	1,520	296	506	2.45	2.44	1.28
3	80	0.432	1,300	310-340	516	2.40	2.43	36.7
3	80	0.432	260	313	516	2.40	2.47?	9.7 ?
3	80	0.432	260	315	516	2.40	2.45	12.0
3	80	0.91	1,910	301	516	2.40	2.45	10.6
3	80	0.99 <sup>+</sup>	1,480	319	516	2.40	2.44	24.8
1	293*	-	76	-	605	2.05	2.06	0.26
1	293*	-	325?	-	590	2.10	2.41	0.39
1	293	1	500	312	506	2.45	2.53	3.28
1	293	0.027	8	258?	526	2.36	2.33	0.49
1	293	0.027	16	-	526	2.36	2.34	0.60
1	293	0.027	32	285?	526	2.36	2.36?	0.65?
1	293	0.027	55	280?	526	2.36	2.36	0.84
2	293*	-	190	-	526	2.36	2.38	0.57
2	293*	-	1,650	-	516	2.40	2.36	0.51
2	293*	-	1,520	275	526	2.36	2.36	0.49
2	293*	-	1,520	-	516	2.40	2.38	0.47
2	293*	-	1,520	-	537	2.31	2.44	0.29
3	293*	-	1,910	-	526	2.36	2.38	0.61

See legend to table V. I.

<sup>+</sup> deposited on potassium

\* after sintering

1. The steep increase of the photoelectric yield for photon energies surpassing 3.45 eV ( $\lambda < 360$  nm) was observed by us only for thin films (cf. fig. V, 16). Perhaps the film thickness was too low in Garron's experiments.
2. Sodium films exhibit a strong vectorial selective effect at room temperature. Under different experimental conditions, e.g. angle of incidence of the light, different SDC's and different Fowler plots can be obtained, whereas the threshold remains the same.

As for potassium, results on sodium films measured in different photo-cells are listed in table V.V. All relevant details are included; the SDC's always had one of the characteristic shapes described in section V.3.2. Data with a low degree of accuracy, due to a poor fit to Fowler plots are indicated with question marks. For other comments we refer to the text of table V. II.

The results on sodium films can be recapitulated as done in table V. VI.

Table V. VI  
Typical behaviour of sodium films

$T^{\circ}\text{K}$	Conditions of deposition	Spectral max. nm	$\phi_{\text{V}}$ (eV)	$\phi_{\text{LF}}$ (eV)	$M_{\text{LF}} \times 10^{11}$ electrons photon $\times$ deg. <sup>2</sup>
80	low rate, thin film	300	2.40	$2.42 \pm 0.05$	1 - 5
80	high rate, thick film	300	2.40	$2.45 \pm 0.03$	5 - 40
293	thick film	-	2.36	$2.36 \pm 0.01$	0.3 - 0.9
80*	thick film	$315 \pm 5$	2.45	$2.45 \pm 0.03$	1 - 3

Legend: see Table V. I.

\* after sintering

### V.3.5 Conclusion

Summarizing the main photoelectric properties of sodium we arrive at the following statements:

(i) After deposition at  $80^{\circ}\text{K}$ :

A photoelectric work function of  $2.45 \pm 0.03$  eV, or, if determined from the threshold frequency,  $2.40 \pm 0.03$  eV. These values almost coincide with those of pure potassium films.

An unusually high maximum occurs in the SDC at 300 nm.

The emission constant exceeds that of comparable potassium films and varies strongly from one film to another.

(ii) At room temperature:

For unpolarized radiation at an angle of incidence of  $45^{\circ}$  sodium films do not exhibit a distinct spectral maximum in the wave-length region above 280 nm.

The photoelectric yields are markedly lower than for vapour quenched films. The work function, which can be determined with high precision, equals  $2.36 \pm 0.02$  eV.

The emission constant is much less liable to variations than it is for vapour quenched films and is lowered drastically.

(iii) After presintering cooled again to  $80^{\circ}\text{K}$ :

The work function is raised to  $2.45 \pm 0.03$  eV.

A spectral maximum reappears at about 315 nm.

The emission constant increases.

The properties are clearly different from the properties of either group just mentioned.

Some of the present results will be further discussed in chapter VII.

## CHAPTER VI

### PHOTOELECTRIC PROPERTIES OF SODIUM-POTASSIUM ALLOYS

In 1894 Elster and Geitel<sup>39</sup> discovered that the photoelectric emission from the liquid equimolecular alloy of sodium and potassium showed a pronounced vectorial selective effect, i. e. it was greatly altered in amount when the plane of polarization of the incident light was varied. Later work<sup>58</sup> proved that molten pure sodium and potassium do not exhibit (at least in the visible spectrum) the same high ratio of the *selective* to the *normal* effect, as found in the equimolecular alloy. Subsequently, Ives and Stilwell<sup>59</sup> studied the entire series of alloys with respect to the vectorial photoeffect of white light.

As far as we know, an investigation of the alkali metal alloys with monochromatic light has never been undertaken up to date.

Photoelectric studies of other alloys with monochromatic light have occasionally been performed in the past.

Work on liquid amalgams was primarily intended to establish a correlation between work function and surface tension.<sup>32</sup> With amalgams of alkali metals it appeared that upon addition of comparatively small amounts of the alkali metal (cesium, potassium or sodium) to mercury the photoelectric work function decreased drastically.<sup>68</sup> This was interpreted to be caused by an enrichment of the alkali metal component (with lower surface tension) in the surface of the amalgam, as can be rationalized on the basis of simple thermodynamic relations. For less dilute Hg-Cs alloys (> 5 at. % alkali metal) the work function exhibited a minimum situated below the values of the pure constituting metals.<sup>69</sup> No interpretation of this peculiarity was published.

With various experimental techniques minima of the work function were also found for other alloys (for example, in the photoelectric study of Cu-Ni

alloys;<sup>100</sup> see chapter D).

Recently, photoelectron energy distribution measurements were applied to some alloys in order to gain information concerning their band structure.<sup>21, 103</sup> It was found that the rigid band model is satisfactory for Ni-Al alloys<sup>21</sup> (92% Ni), but not for Cu-Ni alloys,<sup>103</sup> which are better described in terms of the virtual-bound-state model assuming the formation of new, virtual bound levels from the nickel d-states (see also ref. 118).

Photoelectric data on vapour quenched alloy films are available only for one system, viz. a Sn-10 at. % Cu alloy film,<sup>9</sup> deposited at 8°K by means of flash evaporation of an alloy wire. The photoelectric sensitivity was found only half that of a comparable pure Sn film, though the work function of the alloy film was somewhat lower.

In this chapter experimental results will be presented for the photoelectric properties of the sodium-potassium system. The phase diagram is shown in fig. VI, 1.

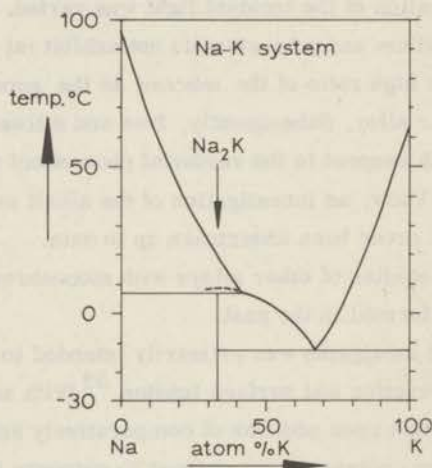


Fig. VI, 1. Solid-liquid equilibrium diagram for the system sodium-potassium.<sup>63</sup>  
Eutectic point : -12.6°C  
Peritectic point: + 6.9°C

All alloys were prepared by simultaneous deposition at about 80°K, during which the photoemission at one wave-length (436 nm) was monitored. From SDC's of these films the photoelectric parameters were evaluated. Subsequently, the films were warmed to room temperature and again investigated in the same way. The sintering process was followed at one wave-length, as before. Then

the annealed films were cooled again and their SDC's measured.

Most of the alloys were studied in photocell No. 3 described in section III. 2. The compositions of the alloys were derived from Saha-Langmuir data (see Table IV.1). As will be shown, yield measurements during annealing provided for an additional check of the predicted composition. Earlier results on 6 simultaneously deposited alloys studied in photocell No. 2 appeared to agree with the findings on the other alloy series studied in photocell No. 3. As the exact composition of these alloys could not be established *in situ*, they were *a posteriori* derived from their photoelectric properties.

In this chapter we shall confine ourselves chiefly to the presentation of experimental results; only occasionally we will touch on certain implications, whereas the results will be discussed in a more elaborate way in chapter VII.

## VI.1 PHOTOELECTRIC YIELD DURING DEPOSITION OF ALLOY FILMS

### VI.1.1 Successive deposition

In the initial stage of this study attempts were made to prepare alloys by means of successive deposition at  $80^{\circ}\text{K}$ . As stated in chapter V this procedure does not lead to the formation of an alloy at  $80^{\circ}\text{K}$ , but the film will exhibit the photoelectric characteristics of the metal deposited last. Only after sintering of such sandwich film both components will be mixed and then form a real alloy film.

In fig. VI, 2 the development of the photoelectric yield at 436 nm is shown during two successive deposition experiments in photocell No. 2.

In the first experiment sodium was deposited on top of a previously prepared potassium film (on the molybdenum substrate) maintained at  $80^{\circ}\text{K}$ . In the second one this sequence was reversed. The times and rates of deposition for each of the metals were the same in both experiments, but sodium was deposited at a much higher rate (about 0.5 monolayers per second) than potassium (about 0.1 monolayer per second). Fig. VI, 2 shows that initially the photoelectric yield of either alkali metal during its deposition on molybdenum is in exact agreement with the results reported in chapter V. Deposition of the second alkali metal, however, gives rise to a peculiar sequence of changes in the yield. For Na deposited on K a pronounced minimum of the yield was always observed, followed by a continuous increase. The usual emission peak after opening the oven

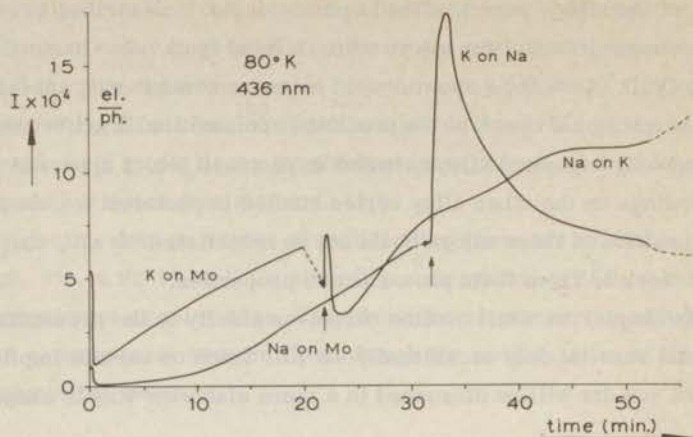


Fig. VI, 2. Development of the yield per incident photon during successive deposition. In both experiments the times and rates of deposition are the same (Na: 30 min. at 290°C; K: 20 min. at 170°C); only the sequence is reversed. Vertical arrows indicate the start of deposition of the second alkali metal.

was small. For K on top of Na the yield curve passes through a steep maximum, after which the yield decreases continuously over the entire range investigated. For the layer thicknesses studied here the final yield still depends on the type of substrate under otherwise unchanged conditions. The ultimate yield of the system Na-on-K-on-Mo differs from that of Na-on-Mo. The form of the SDC is the same for all sodium films.

Perhaps the most interesting phenomenon observed in these experiments is the occurrence of the maxima during deposition of one alkali metal on top of the other, strikingly analogous to what is well known to occur when an alkali metal is condensed on top of a refractory metal. When an alkali metal is deposited on top of the other, it is evident that the maximum cannot be caused by an ionization or strong polarization of the alkali metal atoms, as is usually assumed when alkali metal atoms are adsorbed on a refractory metal. Consequently, the steep maximum of the emission in the case of two alkali metals cannot be ascribed to a lowering of the work function. It is probably not caused by a change in optical properties either, as follows from our reflectivity measurements. The question, how this intriguing phenomenon might be understood will be discussed in chapter VII.

## VI.1.2 Simultaneous deposition

During simultaneous deposition, it is of high importance to maintain the rates for both metals constant, as the composition of the outer region of the film will determine its photoelectric behaviour.

Curves of yield versus deposition time, measured in photocell 3, are given in fig. VI, 3 for light of 436 nm and a substrate temperature of 80°K. The total rate of deposition exceeded 4 Å/sec. for all films. The observed behaviour during simultaneous deposition of alloys can be best summarized by dividing the total composition range into three parts with  $\gamma_K$  = atomic fraction of potassium:

- 1)  $0 < \gamma_K \leq 0.20$  (diluted potassium alloys)
- 2)  $0.20 < \gamma_K \leq 0.85$  (concentrated alloys)
- 3)  $0.85 < \gamma_K < 1.00$  (diluted sodium alloys).

As far as deposition is concerned, the behaviour of diluted potassium alloys resembles that of pure sodium films, except that for very low potassium content the increase of the photocurrent at 436 nm is much steeper than for pure sodium (alloy with 8% K). For alloys with  $\gamma_K \approx 0.10$  yields are lower

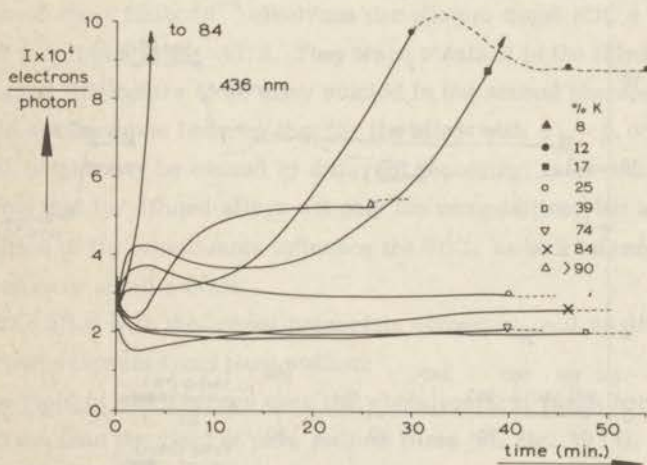


Fig. VI, 3. Yield per incident photon during simultaneous deposition at 80°K. For details of deposition, see Table IV.1. The alloy containing more than 90% K was prepared in photocell No. 2. Only one calculated point has been indicated for each curve.

Dashed curves: yield after closing the beam ovens.

Final yields: 8% K (No. 1 in table IV.1) -  $84 \times 10^{-4}$  electrons/photon (:)

17% K (No. 3 " " " ) -  $11 \times 10^{-4}$  " "

than for pure sodium but higher than for pure potassium films. The rather steep increase of the photoyield as a function of layer thickness commences only after about 10 minutes (layer thickness of about  $2500 \text{ \AA}$ ) (Compare chapter V, fig. V, 2 and fig. V, 13).

Only part of the curves for 8 and 17% K is shown in the figure; the further course of the current consisted in a regular increase.

The "concentrated alloys" show a behaviour strikingly different from that of the pure metal constituents. The photoelectric yield reaches very quickly its final value. This value is situated below that for the other alloys or pure components. A slight decrease of the emission current observed during the first four minutes is approximately accounted for by the increase of reflectivity. This is shown in fig. VI, 4, where the relative amount of light reflected is plotted as a function of the time of deposition.

In fig. VI, 3 only results on three concentrated alloys are shown, but the same behaviour was observed for other concentrated alloys in both photocells 2 and 3. No observable change occurs after closing the atomic beam ovens. From deposition experiments followed at another wave-length (365 nm) a similar course of the photocurrent was obtained, although the initial yield was higher (cf. fig. V, 2) and the subsequent decrease somewhat slower.

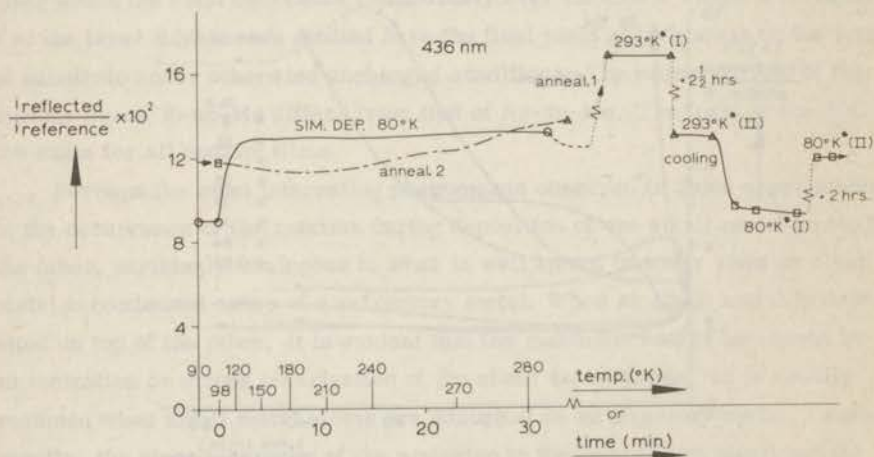


Fig. VI, 4. Results of some qualitative reflection measurements, obtained during simultaneous deposition (sim. dep.) and subsequent annealing-cooling cycles of a concentrated alloy. Only continuously recorded changes in the reflectivity are reliable.

The diluted sodium alloys show some resemblance with pure potassium films, but the yield is lower during the whole deposition process and its increase is slower.

Note the difference between diluted sodium and diluted potassium alloys. A small proportion of potassium causes a uniquely high quantum yield, while a small addition of sodium to potassium has a much less spectacular effect. This difference might be caused by geometrical factors. Sodium atoms having only half the size of potassium atoms can be more easily incorporated without disturbing the potassium structure than in the reverse case.

In contrast to the pure metals, for most of the alloys the photoelectric current did not show spontaneous changes after the shutters were simultaneously closed. The alloy indicated with a black dot showed, however, a more complicated sequence of changes (see dashed curve in fig. VI, 3).

## VI. 2 PHOTOELECTRIC DISTRIBUTION CURVES OF VAPOUR QUENCHED ALLOY FILMS

The photoelectric SDC's reflect the widely divergent emission properties of vapour quenched sodium-potassium alloy films as a function of composition during deposition. Most of the alloys exhibited maxima with a height of about  $5 \times 10^{-4}$  electrons per photon, but in the sodium-rich region extrema reached a value of about  $200 \times 10^{-4}$  electrons per photon. Some SDC's of alloys in this region are shown in fig. VI, 5. They were obtained in the third photocell, only the dashed line refers to an alloy studied in the second photocell. This curve has almost the same form as that for the alloy with  $\gamma_K = 0.08$ ; the difference in peak height may be caused by different deposition rates and geometry. Thus, it seems that for diluted alloys not only the composition, but also the rates of deposition of its constituents influence the SDC, as was inferred from our results on pure alkali metals.

The alloy with the lowest potassium content  $\gamma_K = 0.08$  differs in three important respects from pure sodium:

1. The yield is much larger over the whole spectral range between 300 and 500 nm than the yield of pure sodium films (cf. fig. V, 14).
2. The SDC exhibits a very broad maximum.
3. The threshold wave-length is shifted to a higher value (lower work function:  $\lambda_0 = 530$  nm;  $\phi_v = 2.34$  eV).

Other alloys containing up to about 25% K have SDC's of a regular form, comparable to those obtained for pure alkali metals. The spectral maxima decrease regularly in height with increasing potassium content (they all lie below the values

for corresponding pure sodium films) and are shifted from 300 to about 330 nm.

For films containing more than 25% K the shape of the SDC's undergoes a drastic change (see in fig. VI, 5 the 39% K alloy-SDC, redrawn on a larger scale in fig. VI, 6). The SDC's have lost their smooth character. The yields are lowered again (underscored by the different ordinate scale in fig. VI, 6), the maxima are rounded off and are situated in the vicinity of  $360 \pm 30$  nm. All al-

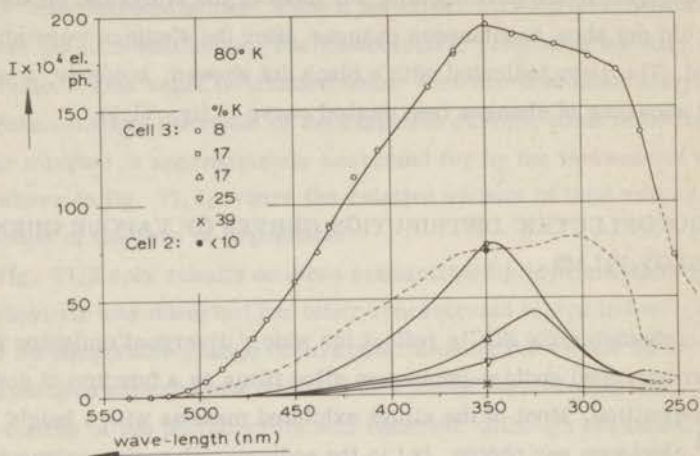


Fig. VI, 5. Photoelectric SDC's of vapour quenched sodium-potassium alloys in the range  $0 < \gamma_K \leq 0.39$ . For details of preparation, see table IV.1. (The alloy ( $\gamma_K = 0.17$ ) indicated with an open square corresponds with No. 3). Only for one curve all experimental points have been given.

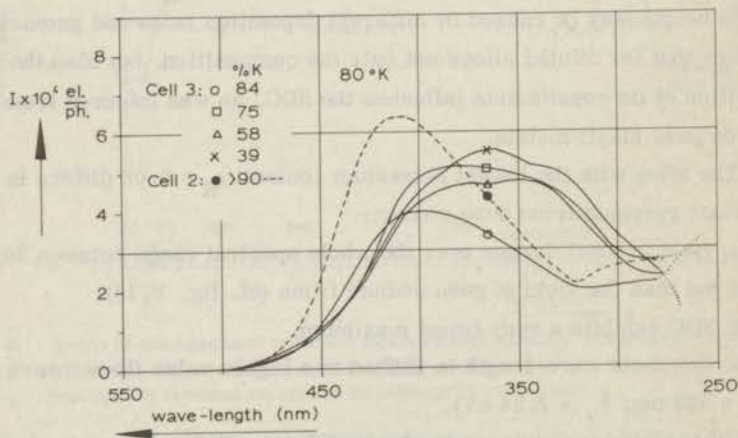


Fig. VI, 6. Photoelectric SDC's of vapour quenched sodium-potassium alloys in the range  $0.39 \leq \gamma_K < 1.00$ . For details of preparation, see table IV.1.

loys with compositions between 25 and about 85 at. % K show these features and the yield curves almost coincide with each other.

Potassium-rich alloys ( $\gamma_K > 0.85$ ) resemble typical pure potassium films (cf. fig. V, 3). The dashed curve refers to a film studied in the second photo-cell, which must have been very rich in potassium (about 95% K) according to the applied evaporation temperatures of the alkali metals. In contrast to the diluted potassium alloys no outstanding yield-maximum surpassing the yield of pure potassium is observed.

The photoelectric parameters of the alloys will be evaluated in section VI, 5, together with those of sintered alloys. For a discussion of the experimental findings we refer to chapter VII.

### VI.3 SINTERING PHENOMENA OF SODIUM-POTASSIUM ALLOY FILMS

The photoelectric yield measured at a constant wave-length was followed during the annealing of alloys between 80°K and room temperature in order to investigate the effect of sintering. A distinction must be made between two types of processes:

- 1) irreversible annealing effects, always observed during the first heating of a film deposited at liquid nitrogen temperature;
- 2) reversible temperature effects, observed e. g. when a presintered film is heated from 80°K to room temperature.

As can be inferred from the phase diagram (fig. VI, 1) several phase transitions occur in the sodium-potassium system. As we found that the phase separations at -12.6°C and at +6.9°C affect the photoelectric current, the temperature of the observed transition(s) provides a sensitive check of the composition of the alloy being studied.

It further follows from the phase diagram that at room temperature only one liquid alloy phase must be expected in the composition range between about 30 and 85 at. % K. The dilute alloys with  $\gamma_K < 0.30$  and  $\gamma_K > 0.85$  consist of two phases at room temperature, viz. a melt and one pure solid metal.

As before, it appears that the alloys may be divided into groups of concentrated and dilute alloys, each of which exhibits characteristic sintering phenomena.

In fig. VI, 7 three sintering curves are shown at 436 nm for diluted potassium alloys and one for a concentrated alloy, all studied in the third photo-

cell. The sintering of the alloy containing 8% K is not entirely shown because its initial yield ( $90 \times 10^{-4}$  electrons per photon) is beyond the adopted yield scale. The curve representing the decrease during the first eight minutes is very steep and continuous. The other sintering curves, also resulting in a decrease of the photoyield, exhibit maxima and minima. This "structure" first appears about 2-5 minutes after all liquid nitrogen has disappeared ( $t = 0$ ,

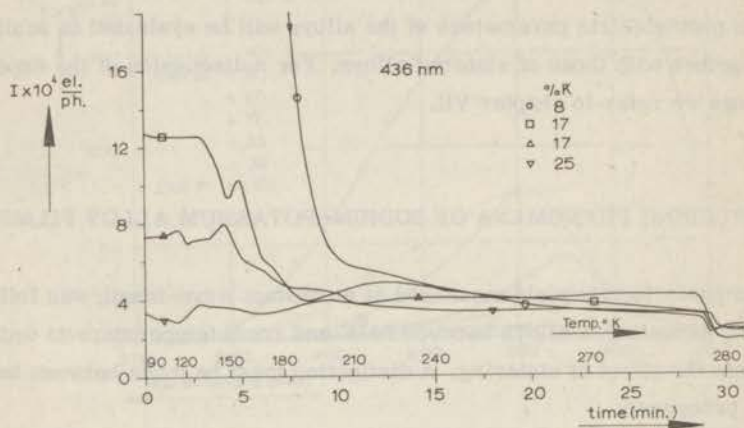


Fig. VI. 7. Photoelectric annealing curves of three dilute Na-K alloys, and a concentrated alloy, observed during initial heating from the temperature of deposition ( $80^\circ\text{K}$ ). Only a few points have been indicated.

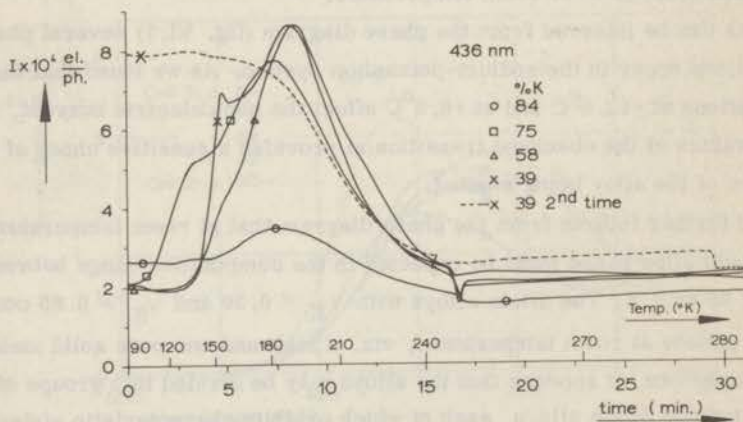


Fig. VI. 8. Photoelectric annealing curves of four concentrated Na-K alloys, observed during initial heating from the temperature of deposition ( $80^\circ\text{K}$ ). The dashed curve is obtained on re-sintering after rapid cooling from the highest temperature.

$T \approx 90^\circ\text{K}$ ). The sintering curve of the concentrated alloy ( $\gamma_{\text{K}} = 0.25$ ) displays no more the sharp drop in the photocurrent, which was previously observed to be common as well for pure alkali films at this wave-length.

As pure sodium and potassium films never show such a curve "structure" these maxima might reflect the occurrence of certain ordering processes in alloys, either in the bulk, or at the surface, or both.

All alloys in fig. VI, 7 exhibit a sharp jump in the photoelectric yield at a temperature above  $273^\circ\text{K}$ . Obviously, this is caused by the eutectic melting at  $6.9^\circ\text{C}$  (see phase diagram fig. VI, 1).

Fig. VI, 8 shows typical curves for the annealing of the photoelectric yield of concentrated alloys recorded while the samples were brought to room temperature. Although the ultimate yields at 436 nm have almost coinciding values for all compositions, the initial yields and the annealing behaviour of the pure metals, the dilute alloys and the concentrated alloys are strikingly different. The occurrence of very pronounced *maxima* for concentrated alloys is the most surprising phenomenon observed during sintering. Such a maximum is absent during annealing of a presintered film in this composition range\* (see dashed curve for a 39% K alloy), whereas the discontinuities after about 16 and 30 minutes are reproduced. We will return to these details below. It can be noticed that the peak in the yield curve shows some "structure", namely, a "shoulder" is present in the ascending part.

The phenomena evidently indicate that the annealing of these alloys is a multiple-step process. At a temperature (about  $180^\circ\text{K}$ ) where annealing is essentially completed for the pure components and sodium-rich alloys and where their behaviour is reversible, the emission from the concentrated alloys reaches a maximum and a second process sets in upon further heating (up to about  $220^\circ\text{K}$ ). From the dashed curve it appears that this step follows approximately the pattern which is obtained if a presintered liquid alloy is first rapidly cooled to liquid nitrogen temperature and then heated again. In this descending region we may expect the alloy splitting up into two solid phases ( $\text{Na}_2\text{K}$  and one pure alkali component), but we cannot claim to have observed that phase separation by virtue of the change in photocurrent.

There is evidence that rapid cooling of a liquid alloy ("splat cooling") is a much less effective way of quenching than vapour quenching and, indeed, quenching of a liquid alloy is known to produce always a metastable solid solution

\* One sodium-rich alloy showed a weak maximum only during resintering (see Table VI, I, No. 3). This was much lower than the yield at  $80^\circ\text{K}$ .

in the crystalline state, whereas vapour quenching may produce a random mixture in the amorphous state (cf. e.g. concentrated Cu-Ag alloys<sup>36, 70</sup>). Thus, a metastable crystalline alloy might be expected also here after rapid cooling.

We should add that on cooling an alloy film the yield did not always reach a magnitude approximately equal to the maximum value observed during the initial annealing. This can be seen in more detail in Table VI. I, where quantum yields at distinct stages of an annealing cycle are listed for the alloy series of photocell No. 3. The data obtained during annealing (fourth column, table VI. I) resemble more the data gained at 80°K\* than the respective data at 80°K (third column) or at 293°K (fifth and seventh column, respectively). This holds particularly for the alloys No. 5, 6 and 7. The alloys No. 8, 9, 10 and 11 displayed spontaneous changes when they were maintained at room temperature. For this group the yields at 293°K (column 5 and 7) diverge also more than for the other alloys.

Table VI. I

Development of photoelectric yield I (in electrons/incident photon) at different stages of an annealing cycle at 436 nm (see Table IV. I).

Number	Composition at% K	$I \times 10^4$		Maximum during annealing	$I \times 10^4$	$I \times 10^4$	$I \times 10^4$
		After deposition, Before SDC	80°K After SDC		293°K*	80°K*	293°K**
1	8	80.5	→ 90.0	-	2.47	4.07	2.62
2	12	9.30	→ 8.40	-	2.52 <sup>+</sup>	3.87	2.41
3	17	10.8		-	2.36	2.26	2.74 <sup>++</sup>
5	25	3.03		3.78	2.20	4.52	2.26
6	39	2.02		8.71	2.14	7.55	2.17
7	44	2.12		5.22	2.21	3.10	2.67
8	62	1.37	→ 1.69	6.57	2.25 <sup>x</sup>	2.43	3.08
9	62	1.89		8.51	2.19 <sup>x</sup>	4.11	2.46
10	74	2.08		7.67	2.20 <sup>x</sup>	2.88	3.03
11	84	2.62		3.46	1.73 <sup>x</sup>	2.37	2.66
	0	3.08	→ 8.4	-	0.80	2.09	-
	100	13.7	→ 13.5	-	0.97	0.50	-

<sup>+</sup> after adding ice-water mixture:  $I = 2.60 \times 10^{-4}$

after removing ice-water mixture:  $I = 2.37 \times 10^{-4}$

<sup>++</sup> reached via maximum at  $I = 4.83 \times 10^{-4}$

<sup>x</sup> changes observed as a function of time

Table VI.1 shows that the photoelectric yield of the vapour quenched state is almost independent of composition for concentrated alloys (see also section VI. 2), and passes a maximum during the first heating. From similar measurements we have evidence that also at other wave-lengths (e. g. 365 nm) maxima occur for concentrated alloys upon heating.

It is especially interesting to compare the annealing curves of concentrated and K-rich alloys (fig. VI, 8) at higher temperatures with those of diluted potassium alloys (fig. VI, 7). All former alloys display an annealing step at about  $250^{\circ}\text{K}$ , which obviously corresponds to the segregation into a two-phase equilibrium state at the eutectic melting temperature. Note that the observed eutectic temperature lies a few degrees ( $\pm 8^{\circ}\text{K}$ ) below the literature value for compact alkali metal alloys. Furthermore, none of the drawn annealing curves show a clear transition at higher temperatures, as is observed for all sodium-rich alloys (fig. VI, 7) and which corresponds to the incongruent melting at  $7^{\circ}\text{C}$ .

However, the alloy with  $\gamma_{\text{K}} = 0.39$  exhibits two successive phase changes during the second (reversible) heating (dashed curve in fig. VI, 8). This indicates that in this case the particular alloy must have a composition between 33 and 42 at. % K, as only in that interval two abrupt changes can be expected because of two melting events. As the second drop in the photocurrent, corresponding with the reaction of  $\text{Na}_2\text{K}$  with the melt to give Na and another melt, was absent during the first annealing, the composition predicted by the Saha-Langmuir data does not seem to be quite consistent with the photoelectric behaviour. However, if we assume that:

- a) the original composition after deposition was a few percent (at least 3) richer in potassium than that predicted by the S. L. data, and
- b) long range diffusion at room temperature gives rise to a local sodium enrichment (due to a higher sodium concentration elsewhere on the foil), or potassium depletion, of the alloy to a degree of a few (say 5) percent (see section IV. 2),

a simple explanation for the observed phenomena is possible. Alloy No. 5 showed a similar inconsistency with regard to its composition (see section IV.2).

With regard to the *changes in reflectivity* during annealing of a film, only a few results were obtained, but they illustrate an important point.

1. Simultaneously with the irreversible annealing stage of all vapour quenched alloy films the reflectivity increases by about 30% (not shown in fig. VI, 4).

2. In the temperature region where the eutectic melting is expected the reflectivity decreases ( $\pm 15\%$ ) (not shown in fig. VI, 4 but in fig. V, 8).
3. Upon cooling a presintered alloy the amount of reflected light further decreases by about 30% (see fig. VI, 4).
4. After repeated annealing the reflectivity remains almost constant below the eutectic temperature; above that temperature it slowly rises to a value corresponding with the final value of the first heating (see fig. VI, 4).

These results prove that the usually drastic changes of the photoelectric response at 436 nm during warmup of vapour quenched alloy films cannot be rationalized in terms of changes of the optical properties only, but they support the view that during an annealing cycle the physical properties of the bulk are changed. Stepwise changes in the reflectivity coincide with stepwise, and usually more pronounced, changes in the photoelectric properties.

## VI. 4 PHOTOELECTRIC DISTRIBUTION CURVES OF PRESINTERED Na-K ALLOY FILMS

### VI. 4.1 At room temperature

Photoelectric SDC's of sodium-potassium alloys were obtained at room temperature after annealing of vapour quenched alloy films. The alloys with  $0.30 < \gamma_K < 0.85$  are liquid at this temperature, the remainder consisting of a liquid and a solid phase.

We have explored a series of alloys in two different photocells (No. 2 and 3). A number of representative examples are shown in fig. VI, 9 covering the whole composition range.

The current measurements at room temperature could be carried out rather accurately (with error limits of  $\pm 5\%$ ), causing a low degree of uncertainty in the form of the SDC's. On the other hand, some arbitrariness might occur with respect to the composition of the annealed alloys, since at room temperature diffusion rates of alkali atoms are high,<sup>8</sup> thus enabling lateral displacements over large distances, whereas the area of the light spot is only a small part of the total alloy surface.

From fig. VI, 9 it appears that:

- 1) A broad spectral maximum at about  $340 \pm 15$  nm is present for alloys of all compositions.

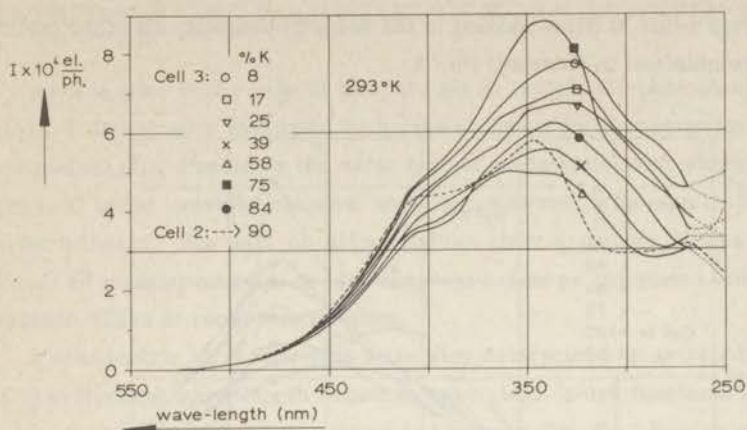


Fig. VI, 9. Photoelectric SDC's of sodium-potassium alloys at room temperature (after deposition at 80°K and warmup).

- 2) The SDC's are not smooth, but show a "shoulder" at about 400 nm which becomes more pronounced with increasing potassium content. This feature is especially conspicuous in the dashed curve, which refers to a very potassium-rich alloy ( $\pm 95\%$  K) measured in photocell No. 2.
- 3) All alloys exhibit roughly the same photoelectric response, particularly in the long wave-length region (above 450 nm). We may, therefore, expect equal work functions and approximately equal emission constants.
- 4) The spread of the maximal yields is rather small, compared to that for the quenched films (at 80°K). No simple relation between the shape of the SDC and composition seems to emerge from the obtained data.

The results cannot be interpreted by a simple additivity of the sensitivities of sodium and potassium films at room temperature. For further discussion we refer to chapter VII.

#### VI.4.2 After cooling to 80°K

Since practically no migration of atoms is possible upon solidification of a liquid binary alloy, the solid bulk and surface of the alloy are expected to have approximately the same, but now crystalline, arrangement as the liquid alloy has.

In fig. VI, 10 photoelectric SDC's are shown for a number of sodium-potassium alloy films, presintered and cooled to 80°K (designated: 80°K\*). The

dashed curves refer to films studied in the second photocell, all other (solid) curves were obtained in photocell No. 3.

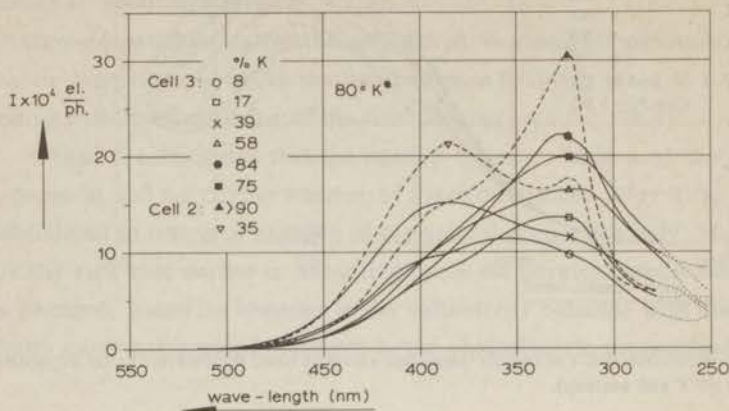


Fig. VI, 10. Photoelectric SDC's of sodium-potassium alloys at  $80^\circ\text{K}$  after presintering at room temperature.

Diluted potassium alloys resemble over most part of the spectral region fairly well pure sodium films after the same treatment (spectral maximum at 330–360 nm). The alloy containing 39 at. % K shows a singular SDC with a spectral maximum at 390 nm, and a "shoulder" at about 330 nm. A more or less similar SDC was also obtained for an alloy film prepared in photocell No. 2, the composition of which was not well known. Though the work function of these films is equal to all other ones, the yield rises much more steeply than for the other alloys. This unique behaviour might be connected with the presence of the intermetallic compound  $\text{Na}_2\text{K}$  containing 33.3% K. The difference between compositions of 33 and 39%, especially after sintering, does not exceed the limits of error of composition determination (see ch. IV).

For higher concentrations of potassium a pronounced maximum develops at about 325 ( $\pm 10$  nm). The height of this maximum increases regularly with increasing potassium content to high values. Comparison with the curve for a pure potassium film at  $80^\circ\text{K}^*$  indicates that a small admixture of sodium to pure potassium changes quite drastically the photoelectric properties of potassium films at  $80^\circ\text{K}^*$ .

## VI.5 PHOTOELECTRIC PARAMETERS OF SODIUM-POTASSIUM ALLOYS

As was done in the case of the pure alkali metals the photoelectric parameters  $\phi$  and  $M$  were evaluated by means of linear Fowler plots (see chapter III, equation (7)). Precisely the same type of deviations, with which we were concerned in the previous chapter, were encountered in the application of Fowler's theory. The data on alloys did not show a poorer fit than those on pure alkali metals; usually, the fit was even better as compared to the data on potassium films at room temperature.

Photoelectric work functions were also determined by extrapolating the SDC's in the long wave-length region to zero yield. Work functions thus obtained, designated with " $\phi_v$ ", proved to be lower than the "Fowler work functions" in almost all cases. However, this method of analysis obviously does not yield any parameter corresponding to the emission constant.

### VI.5.1 Films prepared by means of vapour quenching at 80°K

The variation of the photoelectric parameters  $\phi$  and  $M$  with composition is shown in fig. VI, 11 for vapour quenched sodium-potassium alloys prepared in the photocells 2 and 3.

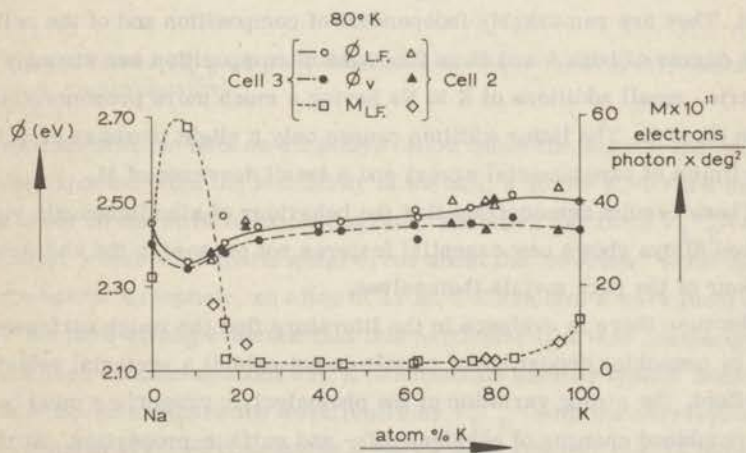


Fig. VI, 11. Work function ( $\phi_v$ ,  $\phi_{L.F.}$ ) and emission constant ( $M_{L.F.}$ ) of sodium-potassium alloys after simultaneous deposition at 80°K.

The rate of deposition and the thickness of the layers was substantially lower for the alloys studied in photocell No. 2. The evaporation rates of sodium in this cell were always lower than approximately 0.3 monolayers per second; those of potassium were lower than about 0.5 monolayers per second. The rates of deposition do not influence the work function, but they are relevant as regards the emission constant. These facts can explain, for example, the rather low emission constant obtained for a sodium-rich film in photocell 2 (containing about 14 at. % K), the SDC of which resembles a sodium-rich alloy film studied in photocell 3 (8 at. % K) possessing a much higher emission constant.

Fig. VI, 11 comprises the following evidence:

1. A minimum occurs in the work function versus composition diagram for diluted potassium alloys. The existence of this minimum is verified by the extrapolated work functions. It has a position about 0.1 eV below the value of pure sodium films.
2. The minimum in the work function diagram is accompanied by a very pronounced maximum of the emission constant.
3. Alloy films containing more than about 20 at. % K and less than about 85% K (concentrated alloys) exhibit a constant work function within the experimental error ( $\pm 0.02$  eV).
4. The emission constants  $M$  for alloys in this region are substantially lower than those of the pure components under equivalent conditions of preparation. They are remarkably independent of composition and of the cell used.
5. The curves of both  $\phi$  and  $M$  as functions of composition are strongly asymmetric, small additions of K to Na having a much more pronounced effect than Na to K. The latter addition causes only a slight increase of  $\phi$  (within the limits of experimental error) and a small decrease of  $M$ .

These results demonstrate that the behaviour of simultaneously vapour quenched alloys shows new essential features not present in the characteristic behaviour of the pure metals themselves.

Because there is evidence in the literature that the rough surfaces produced by quenching deposition of metals do not exhibit a vectorial selective photoeffect, the strong variation of the photoelectric properties must be related to the combined changes of physical bulk- and surface-properties. Work functions may be considered of special interest regarding surface-properties, whereas emission constants are also related more or less to bulk-properties, viz. the structure of the emitter.

## VI.5.2 Films sintered at room temperature (293°K)

The photoelectric properties of vapour quenched alkali metal alloy films are drastically changed upon warming to room temperature, during which irreversible changes are taking place (see section VI. 4).

Fig. VI, 12 shows data for work functions and emission constants of sodium-potassium alloys at 293°K. Note that the emission constants are plotted in a different scale compared to fig. VI, 11.

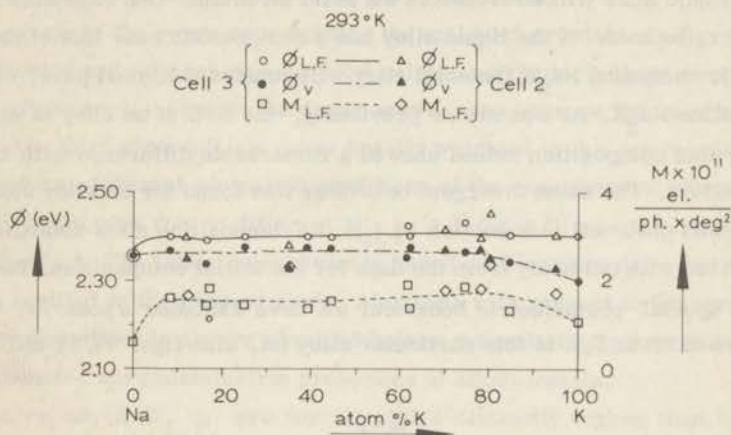


Fig. VI, 12. Work function ( $\phi_{L.F.}$ ,  $\phi_v$ ) and emission constant ( $M_{L.F.}$ ) of Na-K alloys after sintering at room temperature.

It appears that the data on all alloys follow much the same trend as could already be expected from the similarity of the SDC's at 293°K. Notice that no extrema occur in the work function diagram. The work functions  $\phi_{L.F.}$  of the alloys scatter within the experimental error about the "average" value of 2.40 eV. There is one exception: an alloy of 17 at. % K exhibits a work function of 2.21 eV. We have strong evidence that this particular film was contaminated.

The alloys containing about 62% K demonstrate another typical feature of this work when we compare the work functions  $\phi_{L.F.}$  with the corresponding emission constants. Films possessing a higher work function tend to have also a higher emission constant. This is, however, not a significant result. For alkali metals there exists some arbitrariness with regard to the position of the straight line in the linearized Fowler plot. Within the limits given by the experimental points one can draw the straight line either steeper and with larger

intercept or flatter and with lower intercept on the abscissa.

### VI.5.3 Films cooled to 80°K after presintering (80°K<sup>\*</sup>)

The SDC's of these films showed that the photoelectric properties varied more than in case of films at room temperature. The values of the photoelectric parameters shown in fig. VI, 13 confirm this impression. During solidification and subsequent rapid cooling no changes are to be expected regarding the structure and the surface composition of the alloys. The disorder present in the liquid state will be frozen in the solid structure. One exception must, however, be made: if the liquid alloy has a composition near that of the intermetallic compound Na<sub>2</sub>K the solid alloy will consist of almost pure, ordered, crystalline Na<sub>2</sub>K. As was shown previously, the SDC of an alloy of approximately this composition indeed showed a remarkable difference with that of other alloys. The same divergent behaviour was found for an alloy studied in the second photocell (see section VI.4.2). Its composition after annealing cannot be derived with certainty from the data for the initial composition. But in view of its special photoelectric behaviour we have assigned *a posteriori* a composition of 35 at. % K to this particular alloy (cf. also figs. VI, 11 and VI, 12).

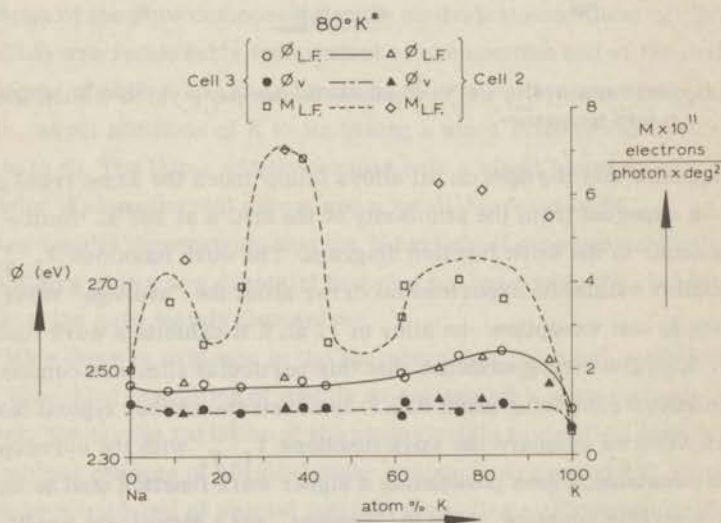


Fig. VI, 13. Work function ( $\phi_{LF}$ ,  $\phi_v$ ) and emission constant ( $M_{LF}$ ) of Na-K alloys cooled rapidly to 80°K after sintering at 293°K.

Fig. VI, 13 shows that for all compositions the photoelectric work functions derived from threshold frequencies are lower than those obtained from linear Fowler plots. In our opinion, the maximum of the  $\bar{\phi}_{L.F.}$ 's that seems to occur for potassium-rich alloys is rather a consequence of the shortcomings of the applied method of evaluation than a consequence of photoelectric properties themselves. This maximum which is accompanied by a maximum of the emission constant is absent in the  $\bar{\phi}_v$ -pattern (except for one point at about 95% K). Therefore, we conclude that the work functions of presintered sodium-potassium alloys, brought back to 80°K, are all equal to  $2.41 \pm 0.03$  eV, this value being intermediate between those of the pure components.

The form of the curve representing the emission constants in fig. VI, 13 is complicated and several experimental points, particularly those obtained in the second photocell do not fit the drawn curve, also because the results obtained in the third photocell are more heavily weighted in that curve. As was argued before, different geometric conditions of the experimental set-up in photocell 2 may give rise to different  $M_{L.F.}$ 's if these films exhibit a vectorial photoeffect. The latter supposition is based on literature data, but has not been verified in the present study. Alertness with respect to the vectorial selective photoeffect is always required before generalizing interpretations can be given for the photoelectric properties of alkali metals.

The values of  $M_{L.F.}$  are for all alloys distinctly higher than for the pure components. The maximum present at about 35% K is attributed to the crystalline phase  $Na_2K$ . The results will be further discussed in a broader context in chapter VII.

#### VI.5.4 Position of the spectral maximum at various stages of an annealing cycle

For the photoelectric SDC's of sodium-potassium alloys the occurrence of a spectral maximum is characteristic. In general, the spectral maxima of alloys are less clear-cut and less nicely shaped than the maxima found for the pure metals.

Data on the position of the maxima observed are collected in fig. VI, 14. None of the respective sets of experimental data at a certain temperature fit one smooth curve. Because the maxima were flat the uncertainty of the points amounts to 20 till 40 nm. Therefore, the drawn curves give only trends of the location of spectral maxima for alloy films. The curve for the presintered films measured at 80°K is still questionable.

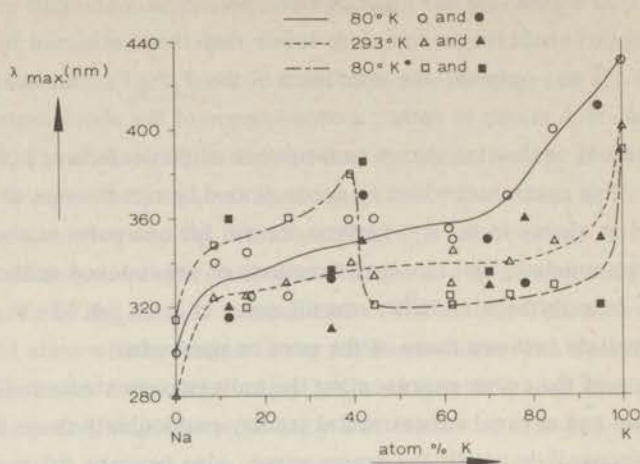


Fig. VI.14. Position of spectral maxima in the photoelectric SDC's of sodium-potassium alloys. Black symbols refer to films studied in cell No.2, "open" symbols to films in cell No. 3.  
 ○, ● : films after quenched deposition at 80°K  
 △, ▲ : films sintered at 293°K  
 □, ■ : presintered films cooled to 80°K.

Our vapour quenched alloy films (80°K) always have SDC's with a spectral maximum lying between 320 and 360 nm. The position of the maxima favour a moderate increase of the emission constant with increasing K-content, particularly in the region of K-rich alloys. (The emission constant should, of course, increase with increasing wave-length of the maximum, at constant integrated yield.) Therefore, the remarkable pattern of emission constants of alloys at 80°K (fig. VI,11) is clearly not related to positions of spectral maxima, but to emission capacities.

The same holds for the alloys studied at room temperature, after sintering. The (almost constant) position of the maxima cannot give rise to the distinctly higher emission constants as compared with the pure metals.

When alloy films are cooled, the positions of the maxima scatter over a wider range than at room temperature. At about 39 at. % K the position of the maximum is at highwave-lengths, which may be connected with the presence of the  $\text{Na}_2\text{K}$  compound. The large value of the emission constant at this composition is evidently associated with the favourable position of the maximum in the SDC, whereas the high emission constants in the potassium-rich region are the result of high emission yields. Closer inspection of the sodium-rich region in fig. VI, 13 reveals that the individual emission constants are also markedly

connected with the position of the corresponding spectral maxima (fig. VI, 14).

Summarizing we may state that in some cases the emission constants and the positions of the spectral maxima vary with composition in a related manner. In most cases, however, the behaviour of the emission constants cannot be understood in a simple way and is due to intrinsic emission properties. Though the above considerations emphasize that a straightforward interpretation of emission constants is embarrassed by the interplay of several distinguishable effects - intrinsic emission capacities and qualities of photoelectric SDC's are interwoven in the derived emission constants and vectorial selective effects may also complicate the scheme under certain conditions - these considerations also indicate that a number of major variations in the emission constants can serve as a starting point for further discussion. This will be given in the following chapter.

## CHAPTER VII

### GENERAL DISCUSSION - WORK FUNCTION AND PHOTOELECTRIC EFFECT

In this chapter the experimental results described in chapters V and VI are discussed in more detail. Firstly, attention is devoted to the work function data.

As the magnitude of the work function may depend on the method of determination, a basic thermodynamical definition of the work function is given. The photoelectric work functions of sodium-potassium alloys obtained at different temperatures are compared with those of the pure metals, particular interest being paid to the occurrence of minima in diagrams of work function versus composition.

Further, we consider the photoelectric SDC's. Although the photoelectric emission process is not well understood at the moment, we feel that the present work on alkali metal and alloy films has revealed some important features of the nature of this process.

#### VII.1 WORK FUNCTIONS

##### VII.1.1 Thermodynamic definition of the work function

The work function can be defined in a thermodynamical sense independently of special models, as follows.

Let us consider a system of electrons in two phases: metal plus vacuum. We define for this system Gibbs free enthalpy  $G$ :

$$G = U - TS + pV,$$

and its differential is:

$$dG = dU - TdS - SdT + pdV + Vdp, \quad (1)$$

where  $T$ ,  $S$ ,  $p$  and  $V$  have obvious meaning.

For systems where a charge  $q$  ( $-e$  for an electron) is transferred across the potential difference  $\varphi_{\text{total}}$ , we have for energy differential  $dU$  (First Law of Thermodynamics):

$$dU = TdS - pdV + \mu dn + q\varphi_{\text{total}} dn, \quad (2)$$

where  $\mu$  is the chemical potential and  $n$  is the number of electrons.

For convenience, we divide the potential  $\varphi_{\text{total}}$  into two parts: the so-called *double layer potential*  $\chi$ , and the *electrostatic potential* imposed upon the metal  $\psi$ , and we set the zero for both in vacuum, far from the metal.

Then, inserting (2) into (1)

$$dG = -SdT + Vdp + \mu dn - e\chi dn - e\psi dn$$

or 
$$dG = -SdT + Vdp + \eta dn \quad (3)$$

where  $\eta = \left(\frac{\partial G}{\partial n}\right)_{p, T}$  = *electrochemical potential*, and  $\mu = \left(\frac{\partial G}{\partial n}\right)_{p, T, \varphi_{\text{total}}} = 0$ .

It is immediately evident that for two phases I and II in equilibrium the condition for equilibrium reads:

$$dG = dG_I + dG_{II} = 0$$

and, because  $dn_I = -dn_{II}$  for closed systems, it follows:

$$\eta_I = \eta_{II}$$

It can be shown that in the case of a free-electron gas this  $\eta$  is identical

\* To avoid confusion we shall reserve the term "surface potential", often found in the literature for this potential, for another quantity that we will meet in chapter VIII.

with the energy parameter of the Fermi-Dirac distribution function:

Probability that a state at energy  $\epsilon$  will be occupied =

$$f(\epsilon) = \frac{1}{\exp(\epsilon - \eta)/kT + 1}$$

provided that the energy  $\epsilon$  is again measured from a zero representing an electron at rest at infinity.

For a charge (potential) free metal the *true work function*  $\bar{\phi}$  is given by

$$\bar{\phi} = -\eta \quad (4)$$

The inner potential  $\varphi_{\text{inner}}$  sometimes met in the thermodynamic definitions of  $\bar{\phi}$ <sup>37, 54</sup> vanishes if the above definitions are used.

In general, we need to define the work function  $\bar{\phi}$  in such a way that it is a constant parameter for the metal, not depending on the potential put on the metal. This is met with the *definition*

$$\bar{\phi} = -\mu + e\chi = -(\eta + e\psi) \quad (5)$$

Further we need that  $\bar{\phi}$  reflects the changes in the potential laying across the (uniform) surface, i. e. of the surface double layer.

Therefore,  $\bar{\phi}$  is defined as the work necessary to bring an electron from the Fermi level to the charge free vacuum, up to a certain distance from the metal (usually put equal to  $10^{-4}$  cm), where the electron still "sees" the double layer as an infinite one and where it is subject to the outer potential, but where the potential of image forces is already zero.

Since  $\chi$  (electrostatic potential of the double layer) will be *different* for different faces of a single crystal, the work function  $\bar{\phi}$  will also vary from face to face.

When two electronic conductors 1 and 2 are kept at the same temperature and are connected electrically, electrons will flow from one to the other until an equilibrium state is reached. In this equilibrium state the electrochemical potentials  $\eta_1$  and  $\eta_2$  of the electrons in both conductors must be equal. This implies that there must be a difference in electrostatic potential between a point just outside conductor 1 and a point just outside conductor 2, given by the difference in work function:

$$-e(\psi_1 - \psi_2) = \phi_1 - \phi_2 \quad (6)$$

This is the so-called "contact potential difference" between 1 and 2.

It is especially important to note that the contact potential difference will in general also be different from zero when 1 and 2 refer merely to different crystal faces of the same conductor or to different grains of the surface of a polycrystalline conductor. The relationships between the various thermodynamic quantities, as defined above, are illustrated for one particular case in fig. VII, 1. The energy diagram represents schematically the situation for a crystal the surface of which is composed of two different crystallographic planes 1, 2. Note that  $\eta$  and  $\mu$  are the same for two crystal planes of the same metal.

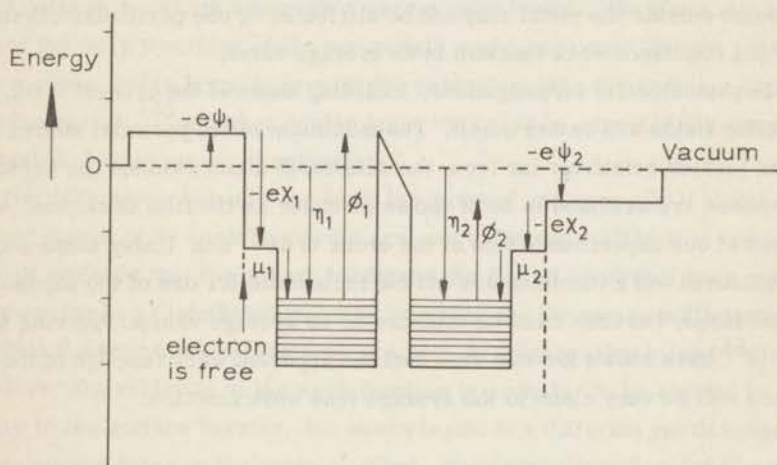


Fig. VII, 1. Schematic representation of the energy diagram of a crystal, the surface of which is composed of two different crystallographic planes with different true work functions  $\phi_1$  and  $\phi_2$ . The figure shows that  $\phi_1 - \phi_2 = -e(\psi_1 - \psi_2)$ , where  $-e$  is the charge of an electron.

As appears from fig. VII, 1 the differences in the work functions of distinct surface planes of the same crystal are equal to the differences in the potentials of the corresponding double layers (these are usually of the order of 0.5-1.0 Volt). Smoluchowski<sup>105</sup> has shown how these differences are possibly generated.

What we measure in actual practice, however, is not the true work function, as defined above, because most measuring techniques impose a different reference level outside the metal. Usually, a collector is employed, its electrostatic potential being positive, lowering the potential barrier near the metal surface.

For surfaces on which various crystal faces are exposed the experimental values of the work function (apparent work functions) are weighted averages of the contributions of these faces. The way in which a particular plane contributes to the average value depends on the manner of averaging, inherent to the method of measurement. If the imposed reference level is located very near the crystal and if the emitting crystal planes are large, each crystal plane will have its own potential energy maximum where the double layer of that particular plane is felt. These conditions are realized for the combination of large crystals and high collecting fields. Where these conditions prevail, different apparent work functions will be found for different crystal faces. If the opposite conditions prevail, i. e. small crystals and low collecting fields, the potential energy maximum outside the metal may not be attributed to one particular crystal face; the measured work function is an average value.

In photoelectric investigations, including those of the present work, the collecting fields are rather small. The maximum of the potential energy curve is then located relatively far from the outermost metal atoms. The crystal dimensions are assumed to be of the same order as the film thickness, which in most of our experiments was of the order of  $10^{-5}$  cm. Under these conditions the measured work functions are not characteristic for one of the exposed crystal faces, but they must be interpreted as average values. Herring and Nichols<sup>54</sup> have shown for this case that the apparent work function of the entire surface will be very close to the average true work function.

### VII.1.2 Discussion of the work function data

#### a. Pure metals

A theoretical calculation of the work function is very difficult and has been only performed by Bardeen<sup>7</sup> in the case of sodium. In order to determine the potential of the surface double layer which contributes considerably to the work function (the "binding" energy, entering  $\mu$ , is the other part) it is necessary to make an explicit calculation of the electronic charge density at the surface of the metal. Bardeen<sup>7</sup> concluded that the surface barrier is primarily due to exchange and polarization forces, and that ordinary electrostatic forces play a minor rôle. Approximate agreement was obtained between the work function of the free-electron model and the experimental values of the work function of sodium. When the correlation forces were omitted in the calculation

the work function was 2.0 eV and the double layer 1.0 eV; when these forces were included the results were 2.35 eV and 0.4 eV, respectively. The latter work function is in good agreement with our value for sodium at room temperature ( $\bar{\phi} = 2.36$  eV).

It is remarkable that the work function of potassium films as obtained from the threshold frequency (2.30 eV, see chapter V) approximates closely the corresponding one of sodium. Potassium films quenched at 80°K even tend to have distinctly higher work functions than comparable sodium films, whereas on the other hand presintered potassium films have a lower work function at 80°K.

If we assume that the "binding" energy of electrons in sodium is greater than in potassium, which assumption seems quite logical, the close similarity between the work functions of the two metals would implicate that the potential of the surface double layer is greater for potassium than for sodium. According to Smoluchowski,<sup>105</sup> a higher double layer may also be expected for more polarizable, bigger atoms of potassium.

The differences between the work functions of one pure alkali metal at different stages of an annealing cycle are, nevertheless, difficult to understand. There is evidence that the energy bands and the Fermi level still have not lost their meaning in a disordered material provided the atoms are sufficiently close that the atomic wave functions of atoms on neighbouring sites overlap. Therefore, the variation of the work function is probably to be related to changes in the surface barrier, for example due to a different participation of various crystal faces in the surface. Thus, after annealing of metal films often an increase of the work function has been reported. This increase was usually attributed to the appearance of more stable crystal faces at the surface which possess a higher work function.<sup>41</sup> But, in a number of cases such a change in work function was absent.<sup>9</sup>

For potassium and sodium we found a clear *decrease* of the photoelectric work function on annealing. Boutry et al.<sup>16</sup> also obtained for potassium after vapour quenching at 77°K a work function of 2.39 eV, which decreased to 2.30 eV at room temperature.

In a very recent report Lapp and Neumann<sup>67</sup> made a distinction between polycrystalline (during deposition), liquid and monocrystalline (solidified from the melt) potassium films at and above room temperature. The work functions were equal to, respectively:  $2.39 \pm 0.01$  eV (due to the preponderance of (110)-

planes at the surface under the conditions of deposition used\*),  $2.30 \pm 0.02$  eV and  $2.30 \pm 0.02$  eV (due to a more smoothly shaped surface also comprising planes with other indices, e. g. (211), (100)). Their value of 2.30 eV is in good agreement with our result for a sintered K film ( $293^{\circ}\text{K}$ ) but we obtained a value of 2.39 eV only for films quenched at  $80^{\circ}\text{K}$ . The discrepancy may be caused by their unusual way of measuring yields *during* deposition.

Our results obtained after rapid recooling of the films to  $80^{\circ}\text{K}$  cast some doubts on Lapp and Neumann's interpretation. In the case of potassium the work function after recooling lay in between those of the vapour quenched film at  $80^{\circ}\text{K}$  and the sintered film at  $293^{\circ}\text{K}$ ; for sodium the work function after recooling was even higher than the one before sintering. As it is very unlikely that the distribution of crystallographic planes at the surface changes during recooling, it seems not unreasonable to assume that the change in the photoelectric work function reflects a change in the photoemission process of alkali metals.

#### b. Alloys

Our results on sodium-potassium alloys show that, with one exception, all data on photoelectric work functions are situated between the values of the pure components, or, are approximately equal to the value of one component. The exception: diluted potassium alloys after deposition by vapour quenching exhibiting a slightly lower work function (about 0.1 eV below the value of pure sodium). How can these results be explained?

The work function of any material depends essentially on two quantities. First, the energy with which the electrons are bound to the metal ions and the other electrons. Second, the energy of the surface double layer separating the interior from the exterior is decisive. These two quantities correspond with  $\mu$  and  $\chi$ , respectively, defined in section VII. 1. 1.

With respect to the first parameter it is hard to make any detailed statement. If all energy band parameters remain the same upon alloying, which implies that the two metals must have the same band scheme, one should expect that the work function would vary linearly with composition between the values of the pure constituents provided that the position of the bottom of the energy bands remains also the same. Christman<sup>26</sup> calculated the position

\* The assumption that the surface was *exclusively* composed of (110)-planes, made by Lapp and Neumann, is possibly in conflict with the basic principle proved by Stranski, that metals in equilibrium always expose at least two crystal faces.

of the Fermi level in sodium-potassium alloys. He found a deviation of the position of the Fermi level from the "ideal mixing" position in the direction of the larger atom (K), but all Fermi energies were lying in between the values for the two pure metals. These Fermi energies were calculated, however, for a reference level different from that of work functions.

With respect to the second factor it is also very difficult to make any quantitative prediction. It is without doubts, however, that the condition of the surface, determining the potential barrier at the surface, is of extreme importance for the work function. Variations in the constitution of the surface of alloys must be expected to produce easily the variations in the work functions usually observed.

Several ways can be distinguished in which variations in the surface of alloys may arise. Firstly, the composition of the surface may depart from the composition of the bulk if the surface energies of the two components are different and mobility is sufficient. This can also be expected in the case of Na-K alloys which are liquid at room temperature and in which K has a much lower surface tension (at 100°C: 111 dyne/cm) than Na has (at 100°C: 191 dyne/cm).<sup>46</sup> Apparently, this type of rearrangement did not lead to anomalies in the work function pattern of our sintered alloys: at 293°K and after recooling no minima were observed (see chapter VI). With respect to the surface composition it is difficult to reach a more detailed conclusion from the work functions of sintered alloys owing to the following facts. As we showed in chapter V, in the case of potassium a discrepancy occurs between the photoelectric work functions obtained in different ways ( $\frac{1}{2} \nu$  and  $\frac{1}{2} L.F.$ ), whereas in the case of sodium such a difference is absent due to an excellent fit of the data to the Fowler plot. In addition, the difference between the work functions of the two metals turned out to be small and its sign even depended on the method of evaluating data on potassium. In case any tendency towards an enrichment of the surface in potassium is present, as suggested by the photoelectric SDC's (see section VI.4 and VII.2), this is neither unambiguously borne out nor definitely denied by our work function data. The results, however, point indeed to a rather uniform composition of the surface, irrespective of the bulk composition of alloys. For the same reasons work function data of Na-K alloys do not provide unequivocal information about the type of phase(s) present at the surface of the alloys. (Cf.: Lapp and Neumann<sup>67</sup> found no change in the work function of liquid potassium when it was solidified).

Furthermore, changes in the surface potential may be brought about by

changes in the type of crystal planes present at the surface of the alloy. Interestingly, in their early report Ives and Stilwell<sup>59</sup> also related the variation of the vectorial selective photoeffect of Na-K alloys as a function of composition to certain orientations of the surface atoms or molecules. This kind of interpretation was supported by the fact that the ratio of emissions was greatly reduced in value when the alloy was heated. Certain semi-molten alloys actually showed crystalline planes at their surfaces, as was observed visually. These alloys always possessed higher selective-normal ratios than when they were completely molten. The authors were not able, however, to suggest a more refined model (concerning the precise orientation of the atoms at the surface) for explanation of their remarkable results. Like for pure alkali metals a relationship of work function to surface planes does not emerge unambiguously from our data on alloys.

For the occurrence of the unique minimum in the work function of vapour quenched sodium-rich alloy films an explanation might be found in a favourable configuration of atoms at the surface. For example, one could imagine that even small amounts of potassium are able to disturb the sodium lattice considerably, as potassium atoms have twice the size of sodium atoms. If the difference in size is presumed to invoke that relatively more potassium atoms are separated out into upmost surface layers, whereas the underlying layers contain a relatively smaller number of potassium atoms, a slight excess polarization or charging of the potassium atoms in the surface layer is to be expected. According to Christman<sup>26</sup> a charge of the order of several hundredths of an electron is transferred in alkali metal alloys, always from the larger to the smaller atom.

For potassium-rich alloys an analogous effect is not expected, although in those alloys potassium should also build up primarily the surface.

As for the pure alkali metals, the differences between the photoelectric work functions of the alloys at different temperatures or at different annealing stages (especially the difference between films after sintering and recooling) are difficult to interpret. Probably these differences are connected with the mechanism of the photoelectric effect itself. Note that all alloys behaved in this respect in the same way as the pure alkali metals.

### VII.1.3 Conclusion

Recapitulating the main results of the analysis of work function data we

may state:

- (i) The theoretical basis of the work function as a function of surface and volume properties is insufficient to justify detailed conclusions from work function data.
- (ii) The work functions of the metals sodium and potassium are situated more closely together than has been recognized to date. It seems that a predictable difference in  $\mu$  is compensated by a corresponding difference in  $\chi$  of the opposite sign.
- (iii) The changes in the work function during sintering of disordered alkali metals and alloys cannot be ascribed to the disappearance of unstable crystal faces since it is found that the work function decreases during sintering.
- (iv) The changes of the photoelectric work function on alloying sodium with potassium are inconspicuous. Under equilibrium conditions the alloys do not display a minimum in the work function. Under non-equilibrium conditions, after vapour quenched deposition, such a minimum does occur and has been tentatively explained.

## VII.2 PHOTOELECTRIC SENSITIVITIES AND SPECTRAL DISTRIBUTION CURVES

### VII.2.1 Factors governing the photoemission process.

Photoelectric emission from solids is a rather intricate phenomenon. It involves a combination of several interactions, each of which being of considerable complexity and not well understood at present. In this section an attempt is made to review the most important aspects of the generation of a photocurrent.

When we start from the assumption that photoemission from solids is essentially a volume effect (see chapter I), though admitting that the energy barrier is extremely dependent on the constitution of the surface, it can be described as a multiple-step process. Electrons are first optically excited into states of higher energy; then some of them travel to the surface of the solid, and escape into vacuum. Factors determining whether an electron reaches the surface involve interactions such as electron-phonon and electron-electron scattering. Light is predominantly absorbed within a few tens of nm in the solid, exciting

electrons into unfilled states above the Fermi level. Electrons with energies higher than the vacuum level, i. e. the Fermi level plus the work function, are then able to escape from the emitter if they arrive at the surface within a certain escape cone.

#### a. Photoexcitation

In the first step of the photoemission process the light penetrates into the emitter. Electrons with energy below the Fermi level are excited to unoccupied states of higher energy. These transitions are often described as direct, indirect, or nondirect.

When the electrons of the solid are described by Bloch-functions a transition to a higher unoccupied state caused by the interaction with a photon is *direct* if crystal momentum  $\hbar\vec{k}$  is conserved. A transition from state  $k$  to  $l$  will contribute to the absorption of a quantum  $h\nu$  or to the photoelectric current provided that  $\nu = \nu_{kl}$ ,  $h\nu_{kl}$  being the energy difference of the electron between the excited and the ground state. The second selection rule for the optical transitions in solids is the conservation of momentum  $\vec{k} = \vec{l}$ . In *indirect*, or phonon-assisted, transitions the conservation law for momentum is modified - part of the electron momentum may be transferred to phonon momentum. In addition to these two types of transitions, optical transitions may occur in which the conservation of  $\vec{k}$  is not an important selection rule. These are called *nondirect* transitions. Many metals and semiconductors have mostly exhibited nondirect transitions though evidence for some direct transitions has been also seen.

In the literature there is no agreement as to the type of optical absorption process which is dominant in alkali metals. According to Meessen<sup>79</sup> vertical (or direct) transitions are not allowed for alkali metals and the absorption is due to indirect transitions. On the other hand, Brauer<sup>20</sup> has pointed out that the photoelectric properties of potassium, including the vectorial effect, can be derived quantitatively when assuming that the optical transitions are direct. Mayer and El Naby<sup>77</sup> also obtained evidence for direct transitions. Recent work on alkali metals, however, has emphasized the importance of nondirect optical transitions in these "simple" metals.<sup>2, 87, 88</sup>

If photoexcitation is accomplished by nondirect transitions, the probability of exciting an electron is proportional to the product of the initial and final density of states:<sup>10, 21</sup>

$$P(E) = C N_C(E) N_V(E-h\nu) \quad (7)$$

where  $P(E)$  is the probability per unit energy interval of exciting an electron from an initial state at energy  $E-h\nu$  to a final state at energy  $E$ ;  $C$  is a coefficient (assumed to be constant) which includes the square of matrix elements connecting the initial and final states;  $N_C(E)$  is the density of unoccupied states above the Fermi level at energy  $E$ ; and  $N_V(E-h\nu)$  is the density of occupied states below the Fermi level at energy  $E-h\nu$ . The assumption of constant matrix elements is crude, but enables photoemission data to be readily interpreted in a self consistent manner.

#### b. Scattering processes

Once the electrons are excited to higher energy states they may be subject to scattering processes prior to their escape. The three main interactions, the electrons may undergo in the assumed energy range (2-5 eV), are: electron-phonon, individual electron-electron and collective electron-electron (plasmon) scattering events.

The interactions of photoelectrons with phonons are nearly elastic. They do not change the energy of electrons to an extent observable in photoemission.<sup>10</sup> They do, however, affect the escape probability. Electrons near the surface have more chance to escape if they undergo many electron-phonon collisions, because an electron that reaches the surface and does not escape, but is reflected back into the material, can be redirected towards the surface by additional scattering and may have several more chances to escape. On the other hand, electrons which stay within a small region of the sample for a longer time because of electron-phonon collisions are subject to an increasing probability of undergoing inelastic scattering processes, e. g. electron-electron collisions, and they may never reach the surface. Which effect dominates depends upon the ratio of the mean free paths for electron-electron and for electron-phonon scattering.<sup>108</sup>

Scattering by lattice defects does not considerably disturb the energy distribution of the quantum yield. On the other hand, lattice defects may exert an influence on the excitation probability as far as they provide an additional mechanism to conserve momentum of the  $k$  vector.

Electron-electron interactions take place between photoexcited electrons and electrons in the ground state. An energy equal to the difference between

the state of the photoelectron before and after scattering is exchanged. Since both the photoelectron and the ground state electron must go into unoccupied states after collision, events are most probable in which much of the excitation energy above the Fermi level is lost by the photoelectron. The energy with which an electron escapes from the metal and even the probability of escape are greatly affected by the extent of electron-electron collisions.

Another important process of de-excitation of an excited photoelectron is a collective interaction with electrons (plasmon creation). Plasmon scattering can only occur if the energy of the excited electron exceeds a certain threshold  $h\nu_p$ , where  $\nu_p$  is the characteristic frequency of the plasmon. Since the electron cannot transfer an energy, higher than the energy  $h\nu$  it received from the photon, the creation of a plasma oscillation is only possible if  $h\nu > h\nu_p$ . Plasmon creation is sometimes a strong scattering mechanism: in potassium ( $h\nu_p = 3.72 \text{ eV}$ <sup>112</sup>) it is argued to be important,<sup>76</sup> in silver the plasma resonance at  $h\nu_p = 3.85 \text{ eV}$  was found to cause practically no scattering.<sup>10</sup>

Scattering by Auger processes can cause an additional contribution to the quantum yield. The Auger process was found to be of appreciable importance in the case of silver.<sup>10</sup> For sodium the bottom of the band is 3 eV below the Fermi level. It can be shown that in the range of photon energies up to 3 eV above the threshold frequency Auger processes do not play a rôle in the photoemission process. Therefore, they are of no further interest here.

Experimental data on electron energy distribution curves were reported by Dickey for Na and K.<sup>33</sup> The results on sodium indicated that the optical transitions were *nondirect* and an important contribution of low energy electrons arose from once scattered electrons.

### c. Escape

Escape is governed primarily by two factors:

- (1) one which limits the escaping electrons to an escape cone whose size depends on the photoelectron's vector momentum (otherwise reflection will occur);
- (2) one which accounts for elastic scattering. The two factors taken together make up an "escape function". When this escape function is multiplied by the probability of excitation, given in equation (7), the result is the energy distribution of the emitted electrons (neglecting for the moment the effect of electron scattering processes):

$$N(E) = C S(E) N_C(E) N_V(E-h\nu) \quad (8)$$

where  $N(E)$  is the energy distribution of emitted photoelectrons, and  $S(E)$  is the escape function. If the escape function is assumed to be constant (as is often done for high photon energies) the energy distribution is almost equal to the product of the initial and final density of filled and empty states, respectively.

The yield  $I$  is given by:

$$I(\nu) = \int_{E_W}^{\infty} N(E) dE \quad (9a)$$

where  $E_W$  = the energy at the vacuum level. In general the quantum yield per incident photon is measured. When the reflectivity is equal to  $r(\nu)$  we obtain:

$$I(\nu) = I'(\nu) / \{1 - r(\nu)\} \quad (9b)$$

If scattering processes are negligible and if the escape function is constant with  $E$ , photoelectron energy distribution measurements can be used to determine directly the density of states (eq. (8)). Comparison of the thus calculated yield to the observed yield can further be used to determine indirectly the density of states between the Fermi level and the vacuum level, which range is not accessible in energy distribution measurements alone.<sup>10</sup>

When electron-electron scattering becomes important an analytical approximation<sup>108</sup> may be used to estimate the contribution of inelastic scattering to the external energy distribution. Another procedure is to include explicitly both electron-electron and electron-phonon scattering in a Monte Carlo analysis.<sup>108</sup>

There are several nice examples in the recent literature concerning the application of photoelectric energy distribution curves to the determination of electron band structures. Though this method has been used with considerable success, a few questions can be signalized in this field as well.

The scheme of the energy bands in Cu and Ag as derived from experiments showed good agreement with theoretical calculations.<sup>10</sup> For Ni, however, there was no agreement between theory and experiment.<sup>11</sup>

In the mentioned paper on Cu and Ag, the escape function  $S(E)$  was assumed to have a simple form. The presence of a monolayer of cesium on the surface was found only to suppress the work function, but for relatively high photon

energies the yield and the electron distribution curves were unaffected by the cesium. Wooten and Huen,<sup>120</sup> however, found drastic changes in the form of the energy distribution curves of aluminium after adsorption of a monolayer of cesium, even in the range of high photon energies (about 10 eV). This fact illustrates once more that photoemission is very sensitive to the constitution of the surface layer. Even a partial coverage of the surface of the emitter may cause profound changes in the escape function. Furthermore, it cannot be excluded that such a layer brings about an additional scattering mechanism.

These examples show that there are various difficulties which hamper an easy interpretation of photoelectric data (energy distribution curves and, to a higher degree, yield distribution curves).

The approach to the interpretation of photoelectric data outlined above appears to have, on the one hand, a rather sophisticated character leaving room for many vague speculations; on the other hand, it may still comprise unwarranted simplifications. For example, alkali metals are known to have a very simple band structure, but the photoelectric behaviour, including photoelectron energy distribution curves, is complicated. Even the optical properties are poorly understood. A full discussion of photoelectric properties of pure alkali metals is hampered by a lack of knowledge of the important optical and geometrical properties of the surface layers. The same holds *a fortiori* for alkali metal alloys.

In the past, little attention was paid to the influence of structural properties of the emitter on its photoelectric response. It was assumed that for disordered materials the concepts of band structure, which are only well defined for ordered ones, could still be used. In consequence, if the photoelectric effect could be described primarily in terms of band structure, the degree of ordering would only have a minor influence on the photoelectric properties.

However, on the basis of the results reported in this thesis we conclude that in the case of alkali metals and alloys the structural properties, as dependent on the conditions of preparation, and sintering, are of crucial importance to the photoelectric properties. For these materials it is, therefore, not justified to compare experimental data obtained by different authors, if the experiments were carried out under different conditions. Apart from this general conclusion we shall now consider some more specific questions.

## VII.2.2 "Volume" versus "surface" photoeffect

We return to the question of the controversy between the concepts of the volume and the surface photoeffect (see chapter I). Surveying all results on pure metals and on alloys obtained after deposition by means of vapour quenching, we are struck by their strong divergence, e. g. with respect to the position of the maxima in the SDC's. For alloys the heights of the spectral maxima may vary, indeed, by more than an order of magnitude with composition. In the case of pure metal films the irreversible annealing step is attended with drastic changes (for certain wave-lengths also one order of magnitude) in the photoelectric yield, without proportionately equal changes in the optical properties. It is difficult to see how such widely varying yields for one and the same material can be caused merely by changes in the constitution of the surface monolayers. Furthermore, the remarkable results obtained during quenching deposition of metals and alloys are hard to reconcile with the concept of the surface photoeffect.

Several pieces of evidence point to the prominence of the volume photoeffect in alkali films. First, the irreversible drop in the photocurrent occurs at temperatures where also irreversible ordering processes take place and where we found a sharp increase of the amount of light reflected. Light absorption and reflection are known to be bulk properties. The measured reflectivity is certainly not a property of the surface alone, as was demonstrated by our successive deposition experiments of, for example, Na on top of fresh K films (the reflectivity did not change at all during deposition of the first monolayers, see chapter VI).

Secondly, we mentioned before (see chapter I) that the structure of the bulk of alloys prepared by simultaneous vapour quenching can differ widely from one composition to another. This produces strongly divergent physical properties. In similar experiments on other metals Baumann<sup>9</sup> observed that the drop in the photocurrent was accompanied by large changes in the resistivity, which, again, is primarily a bulk property.

For these reasons we are inclined to believe that in alkali metals and alloys the volume photoeffect prevails.

From the successive deposition experiments, alluded to above, it follows, however, that the photoelectric effect is also very sensitive to the constitution of the surface. The small peak of the yield occurring immediately after starting deposition can yet be understood in terms of a volume effect if we assume that

only the escape function is momentarily different, but that the photoelectrons still originate from deeper lying layers. Also, a specific photoemission process of different mechanism may be temporarily involved.<sup>80</sup>

It will be shown below in more detail how the experimental results on metals and alloys, e. g. during deposition and sintering, can be rationalized in terms of the volume effect.

While we thus agree with Mayer *c. s.* on the predominance of the volume photoeffect in alkali metals, we wish to point out that much of our experience is at variance with their results and their interpretation.<sup>89, 115</sup>

### VII. 2. 3 "Escape depths"

As was described in chapter V, from the development of the photoelectric yield as a function of layer thickness at 77°K and at different wave-lengths of the incident radiation, an important conclusion was drawn by Mayer, Thomas and Piepenbring<sup>76, 89, 115</sup> with respect to the magnitude of the escape depths of photoelectrons emitted by alkali films. The escape depths appeared to depend strongly on the alkali metal and on the wave-length of the incident light. The wide variations of the escape depths were entirely attributed to the influence of electron-electron scattering (sodium<sup>89</sup>) and to scattering by plasmons (potassium and cesium<sup>89, 115</sup>). Mayer and Thomas<sup>76</sup> (and later also Lapp and Neumann<sup>67</sup>) applied their results to data on films at room temperature, without making a clear distinction between the properties of vapour quenched films and those of annealed compact material.

One of the most striking results of the present work, however, is the very pronounced difference between the photoelectric properties of vapour quenched and annealed films (see chapters V and VI). The existence of this difference is further demonstrated by the presence of the irreversible annealing behaviour. (Cf. also: tentative deposition experiments at 293°K, section V. 2. 1).

Our results on potassium films differ from those of Thomas mainly within the layer thickness from which on the yield remains further constant. If escape depths are determined from our results according to their receipt, we arrive at values, which are unrealistically high. They are much higher than the penetration depth of the incident light (see e. g. Brauer<sup>20</sup>). As this is, of course, impossible the explanation by Thomas and Mayer cannot be used here. The magnitude of the penetration depth of the light is estimated about two times the layer thickness at which reflectivity becomes constant (which is about 100 mono-

layers at 436 nm). Besides, we observed an additional dependence of the "escape depth" on the rate of deposition.

Mayer presented data which seem to show that the escape depth of photoelectrons depends on the frequency of the incident light. The shape of the SDC's, consequently, should vary with the film thickness unless the thickness exceeds the maximum escape depth. In our experiments, however (see e. g. results on sodium), the SDC's reached their final *shape* already at rather low layer thicknesses, long before the absolute yields at the maxima of the SDC's revealed "saturated" values with increasing layer thickness. Besides, the form of the SDC at room temperature was distinctly different from the unique one of vapour quenched films.

Our results on pure sodium films are in even more striking contrast to the results of Piepenbring.<sup>89</sup> In particular, the relative positions of our yield curves as a function of layer thickness totally differ from his results. The resemblance between sodium and potassium is much smaller than his results did suggest. These differences cannot be ascribed to the differences in rates of deposition only, as follows from our experiments carried out at low rates of deposition.

In view of these facts we conclude that deposition experiments at low temperature, as carried out by Mayer and co-workers should not be used to determine the escape depths of photoelectrons. Escape depths obtained in this way should, certainly, not be used in the analysis of data measured at room temperature as was done by Lapp and Neumann.<sup>67</sup>

On the other hand, the particular variation of the escape depths as proposed by Mayer seems not quite unlogical and finds support in later theoretical calculations of scattering processes.<sup>96</sup> Also, the importance of plasmon creation as a scattering mechanism in potassium is not excluded.

#### VII.2.4 Influence of the film structure

On several occasions we already alluded to the rôle of the structure of films in their photoelectric properties. In recent years much has become known about the physical properties of metal and alloy films prepared by means of vapour quenching (see chapter I and ref. 9, 23, 36, 44, 70, 71). These films sometimes display strikingly different physical properties as compared with well crystallized bulk material at the same temperature. The structural properties were studied by means of X-ray diffraction and electron microscopy, and the annealing behaviour was investigated by measuring resistivities. One

of the general results was that pure metals always crystallize in their normal lattice at deposition temperatures of  $20^{\circ}\text{K}$  whereas simultaneously deposited alloys may then build up a "liquid-like" amorphous structure, if the two components are incompatible in size and in alloying ability. In transition regions of composition both structures may be formed, for example crystalline areas in an amorphous matrix. It appears that the sodium-potassium system meets the two criteria, which were proposed by Mader<sup>71</sup> for the formation of amorphous structures at  $80^{\circ}\text{K}$ , namely, a) limited terminal solubility of the two components, and b) a size difference greater than 10% between the component atoms.

From the analogy to the mentioned literature data, let us assume as a working-hypothesis that the pure metals and the very dilute alloys crystallize during deposition by means of vapour quenching, at least partially, in their normal (or a modified) lattice, whereas the concentrated alloys ( $0.20 < \gamma_{\text{K}} < 0.85$ ) build up a predominantly amorphous "structure". Dilute alloys may form crystalline domains surrounded by "relaxed" material of low density (an amorphous matrix). Unfortunately, the equipment did not allow to do X-ray measurements, which obviously could easily verify our hypothesis.

During deposition of pure alkali metal films at a highly supersaturated vapour pressure they will condense in a crystalline structure. This term must, however, be properly understood: The condensed phase will contain many lattice defects and even the formation of amorphous regions in the metal films cannot be excluded. The state of the atomic aggregate in the films may depend strongly on the rate of deposition and on the layer thickness according to the theory of nucleation and growth. In view of the prolonged strong increase of the photocurrent with layer thickness the assumption that alkali metals condense at  $80^{\circ}\text{K}$  in a state containing at least crystalline areas seems reasonable. During deposition of additional layers a continuous growth of metastable crystalline conglomerates takes place, which change continuously in number and volume (dendritic growth). On the basis of this model an increase in photoelectric emission at thicknesses even above 1000 monolayers can be understood, whereas this would not be possible when assuming that an amorphous structure without any crystalline domains is formed\*.

\* The first suggestion of Suhrmann (see his book,<sup>104</sup> footnote p. 88) that the increase of the photocurrent for potassium films as observed by Thomas was probably due to the structure of the film-surface, which would consist of an increasing number of atoms with a higher specific surface energy and a lower work function, as a function of layer thickness, seems not correct. The work function reaches already a constant value below 100 monolayers. Our interpretation is more in agreement with his other suggestion that the excitation probability is dependent on the layer thickness.

In our model we postulate that the crystalline conglomerates, possessing many lattice imperfections, are very active in photoemission although their work functions are not lower. One might further expect that they are abruptly transformed to a stable crystalline structure at a sharply defined temperature, as indeed appeared to be the case in our sintering experiments. In this coalescence phenomenon the photoelectric yield is drastically lowered for most part of the wave-length region studied.

The following argument based on the theory of the volume effect now seems attractive. The three main steps in the photoemission process are excitation, scattering and escape. The escape probability though, indeed, dependent on the surface structure is not expected to change as continuously with increasing layer thickness as was observed. Electron-electron scattering is strongly dependent on the energy of the incident photons\*. Therefore, this scattering exerts a high influence on the form of the SDC's. Scattering of electrons by phonons and lattice imperfections is elastic and therefore not important.

Hence it seems plausible that the continuous increase of the photocurrent with increasing layer thickness is chiefly due to an increase of the excitation probability. This can be understood if we assume that the perturbations of the periodic potential brought about by lattice imperfections form an important mechanism in the conservation of momentum. It is feasible that with increasing layer thickness the number of lattice imperfections situated within the volume as defined by the surface and the escape depth of the emitter increases for a prolonged period due to the whimsical way of crystal growth\*\*.

As stated above, the form of the SDC's is probably mainly determined by the scattering processes, or, what is equivalent, by the escape depths of photoelectrons. Because the *shape* of the SDC's was independent of layer thickness, this would mean that the scattering processes are not much changed with increasing layer thickness and number of defects. This is consistent with the current concepts of scattering mechanisms.

The present model can also account for the sharp drop in the emission

\* We assume that electron-electron scattering depends, furthermore, on the degree of ordering (see below), but this cannot explain the results of deposition.

\*\* It should be remarked that for potassium and sodium the continuous increase of the photocurrent during quenching deposition is most pronounced at the maxima of the SDC's (430 and 300 nm, resp.). Possibly, the excitation probability at these wave-lengths is most sensitive to the concentration of lattice defects. This could also explain the dependence of the position of the spectral maximum on the structural properties before and after sintering. It can also not be excluded that at the frequency of the maximum the escape depth is the largest (less electron-electron scattering).

during annealing of a metal film. This would be caused by the disappearance of lattice defects. On the other hand, the abrupt character of the drop strongly suggests that also a structure-transformation takes place. The process should then be accelerated by the liberation of heat during the transformation.

The spontaneous changes immediately after finishing deposition of a metal film are presumably caused by minor changes of the same type, induced by the arrival of the last hot atoms at the surface (until the moment of closing the source), and by changes in the surface layer which modify the escape probability. Interestingly, Ives and Stilwell<sup>59</sup> found at room temperature an increase of the ratio selective-normal effect for smooth, solid sodium as the cell stood, suggesting an increasing crystalline character of the surface, whereas specular solid potassium did not show this type of behaviour.

A small addition of K to Na giving a diluted potassium alloy presumably causes a large increase of the excitation probability, whereas the scattering efficiency is proportionally less increased. Moreover, from work function data there is evidence that in this case the escape function may also be changed.

The addition of small amounts of Na to K does not produce a similar effect. The distinction can probably be caused by the difference in size of the component atoms.

Concentrated alloys do not behave like pure metals and dilute alloys but attain their ultimate yields at relatively low film thicknesses (about 200 "monolayers",  $10^3 \text{ \AA}$ ). This value corresponds approximately to the layer thickness from where on the reflectivity does not change any more (also not in the case of pure alkali metals). Because it seems unlikely that the "constant yield effect" is a result of two opposing tendencies cancelling each other for such a broad range of compositions, we may assume that none of the factors governing the photoemission process are changed during the further development of the films. From comparison with the pure alkali metal films we may infer that the condensed phase is not crystalline, but reaches quickly a structure which is not further changed. We propose that an *amorphous* random "structure" is formed. Presumably, however, the difference between the amorphous state thus obtained and the disordered crystalline structure of the alkali metals is smaller than the respective designations do suggest: both types of condensed phases are highly disorganized; but, for the concentrated alloys, the arrival of comparable amounts of two kinds of atoms, differing strongly in size, avoids at all the formation of any periodicity. Thus, concentrated alloy films reach their final

yield very quickly during deposition by vapour quenching. These yields are much lower than the final yields of pure alkali metals and dilute alloys, and they are almost independent of composition. The low yield is probably caused by the presence of strong scattering in the random structure (e. g. electron-electron scattering) causing a low value of the escape depth. Changes in excitation and escape probabilities are expected to be of minor importance.

In the present model the sintering behaviour observed for alloys can also be qualitatively understood. Dilute alloys behave in a way comparable to pure metals, with minor differences. Concentrated alloys, however, anneal all in a similar way, strikingly different from that of pure metals. For ordering of these alloys several steps are necessary. At approximately the same temperature interval where the atoms of the alkali metal films jump into their proper lattice positions, thus building up an ordered structure, the component atoms present in the bimetal condensed phase also rearrange to form a metastable crystalline structure. The latter can be compared with a solidified melt. During further annealing the alloy film decomposes into the appropriate co-existing phases. Sintering thus has become a more stage process, as observed in photoemission (see chapter VI). This interpretation of the data is supported by the results on presintered alloy films after rapid cooling (see ch. VI). Several alloys, for which no changes were observed at room temperature, then again exhibited approximately the same yield as the "metastable" alloy phases.

The strong increase of the photocurrent occurring during the first stage of the sintering process can be explained in terms of a strong decrease of scattering (or, as an increase of the escape depth) whereas the excitation probability is still higher than in pure metals because of the presence of impurities in the lattice. On further sintering the excitation probability would decrease again. However, the escape function, depending among others on the electron-phonon scattering characteristics, may also alter during this process.

Furthermore, recent work on alkali metals<sup>16, 64</sup> lends support to the idea that during the first step of sintering the photoelectric effect becomes vectorial selective indicating a fundamental difference in photoelectric behaviour between vapour quenched and annealed films. We did not investigate polarization selectivity of the photoeffect.

## VII.2.5 Spectral maxima

The occurrence of a spectral maximum at room temperature in the SDC of potassium (400 nm) and probably at higher frequencies in that of sodium can be caused by the creation of plasma oscillations or by the effect of electron-electron scattering, as was suggested by Mayer. The other explanation featuring the strong decrease of the absorption of light in the UV-region, while assuming constant escape depth, thus leading to a lower yield in that region (Surhmann<sup>109</sup>) deserves also consideration.

Several objections can be raised against the view that plasmons are the only cause of the occurrence of spectral maxima. First, at room temperature the position of the maxima is not in concordance with the plasma frequency: For K:  $h\nu_p = 3.72$  eV, max. at 3.10 eV; for Na:  $h\nu_p = 5.71$  eV, max. at 4.8 eV (?). Secondly, at low temperature before as well as after sintering, the spectral maxima are situated at higher wave-lengths. (K: 430 nm, Na: 300 nm). Such a temperature-dependence is not expected from the theory of plasmons.

Plasmons play, however, also an important rôle in the optical properties of alkali metals and by virtue of the optical properties they may be of relevance to the photoelectric properties of these metals. Unfortunately, we were unable to measure reflectivity in the UV-region in our photocell. Hence, our photoelectric data in the UV-region are not proportional to absolute photoelectric yields.

We may therefore infer that the origin of the occurrence of spectral maxima in the SDC's of pure alkali metals is still not completely resolved. On the other hand it is clear that structural *bulk* properties of the metals are of importance for their position. The temperature of the measurement has an influence, especially for sodium. Probably plasmon scattering as well as electron-electron scattering and electron-phonon scattering mechanisms are involved. It is moreover conceivable that many-body effects (collective pairing of the kind used to explain superconductivity) which are supposed to cause some peculiarities in the optical properties of alkali metals<sup>88</sup> are also of interest as regards the photoelectric properties. At the present moment no rigorous theory of the collective resonances, including e.g. electron-hole pairs (excitons), electron-electron s-wave pairs, surface plasmons, is available.

The position of the maximum of vapour quenched *alloy* films varies profoundly with composition. For concentrated alloys the position of the very flat maximum remains the same over a broad range of compositions (20-85 at. % K).

This flat maximum can be a consequence of a less selective, but efficient scattering mechanism in these alloys (e. g. electron-electron scattering).

Alloys at room temperature are all very similar as regards their SDC's. Again, the maximum is usually rather flat which points to a less specific scattering mechanism as compared with pure alkali metals at this temperature. The yields at various frequencies are higher while the work functions are not clearly changed. A higher excitation probability is, therefore, expected for ordered alloys as compared with the pure components. This is consistent with results on other alloys. The "saddle point" at 400 nm coinciding with the maximum for K points either to a special rôle of potassium in the bulk or to an influence of potassium on the surface properties. Since we may expect that potassium will be preferentially adsorbed on the surface the latter interpretation seems most likely. It may involve changes in the escape function, but also scattering phenomena at the surface.

The temperature-dependence of the SDC's for sintered alloy films seems difficult to understand. Is the increase of the yield after recooling a consequence of the action of phonons? Phonon scattering is only considered to change the escape function in the direction of increasing escape probability with increasing temperature. On the other hand, electron-electron scattering may also become more important then (see section VII. 2. 1).

Probably these changes, which are well reproducible, might also be connected with other processes involved in photoemission, such as those responsible for the vectorial selective effect.

## VII. 2. 6 Conclusion

From the foregoing discussion it is evident that many of the experimental data reported in the preceding chapters cannot be explained satisfactorily in a quantitative and sometimes even not in a qualitative way making use of the theory of the photoelectric effect in its present state. On the other hand, it is felt that this study can contribute to further progress in the field. It has been demonstrated that structural properties are of higher importance for the photoemission process than has been recognized to date.

In order to gain a more detailed interpretation of all data, extension of the experimental results presented in this thesis might be profitable. First, a thorough investigation of the optical properties of Na-K alloys will allow to calculate yields in absolute units (per photon absorbed). This quantity is far more

instructive. Secondly, the measurement of the energy distribution of photoelectrons emitted by Na-K alloys will contribute importantly to a better insight, because this type of measurement supplies a resolution of data on quantum yields. Thirdly, a study of the physical, in particular the structural, properties of vapour quenched Na-K metal and alloy films will provide more detailed information regarding the validity and the qualities of the structural models proposed in this thesis on the basis of photoelectric data.

## CHAPTER VIII

### PHYSICAL ADSORPTION OF XENON ON POTASSIUM

#### VIII.1 INTRODUCTION

Measurements of work function changes upon adsorption of gases on metal surfaces are of interest in studying both chemisorption and physical adsorption.<sup>30, 37</sup> By means of contact potential measurements Mignolet<sup>81</sup> found a considerable decrease in work function due to the physical adsorption of xenon and other gases on a number of metals. His results were confirmed by diode-thermionic,<sup>82</sup> photoelectric<sup>53, 110</sup> and field emission<sup>38, 98</sup> measurements.

The change in work function  $\Delta\phi$  caused by xenon adsorption varies for different metals, but the surface potential\*

$$\text{S. P.} = -\Delta\phi/e = (\phi_0 - \phi)/e \quad (1)$$

is always positive or zero.

The same is true for the adsorption of benzene, for which Surhmann<sup>111</sup> observed that the surface potential increases with the work function of the adsorbing metal. Such a simple correlation between S. P. and  $\phi_0$  cannot be established, however, for xenon adsorption. There is only a qualitative trend that metals of high work function such as Ni and W give rise to high surface potentials (0.85 V and 1.1 V, respectively), while, on the other hand, a value of zero is reported by Mignolet for the surface potential of xenon on potassium.<sup>81, 83</sup> This author puts, however, his result into brackets as he was not able to decide whether xenon had indeed been adsorbed by potassium. This doubt is further increased by later results of Pierotti and Halsey,<sup>90</sup> who found *no* adsorp-

\* This meaning of the "surface potential" should not be mistaken for the other definition it may have in the literature and which corresponds with that of the "double layer potential", as used in chapter VII.

tion of krypton on sodium at  $75^{\circ}\text{K}$ , within the experimental error of their volumetric investigation. At relative pressures above 0.9 only condensation was observed.

Mignolet's data illustrate a general problem of high importance. If the surface potential of xenon on alkali metals should, indeed, be nearly zero, this would imply that the metal-xenon bond is much less polarized than in the case of xenon adsorption by transition metals. According to current theories on physical adsorption<sup>48, 99</sup> such a low polarization would be indicative for a low heat of adsorption, justifying Mignolet's doubts whether adsorption takes place at all at pressures  $p < p_s$ ,  $p_s$  being the equilibrium pressure of solid xenon.

For our general understanding of the bond character in physical adsorption it is therefore of great importance to determine the surface potential and to estimate the heat of adsorption of xenon on alkali metals. This is the aim of the work described in this chapter. It is hoped that the experimental data on the two parameters mentioned will permit to clarify the quantum mechanical nature of the physical adsorption bond.

A method is required which detects adsorption even when no change in work function occurs. In this respect the photoelectric emission method appears superior to the contact potential technique used by Mignolet. As described in chapter III, photoelectric emission yields information on two parameters: the work function  $\phi$  and the emission constant  $M$ . The occurrence of adsorption can be recognized from its change in the parameter  $M$ , even if  $\phi$  remains unchanged. As was shown in chapters V and VI, the evaluation of photoelectric data on alkali metals is complicated by the appearance of a selective maximum in the spectral distribution curve. This deviation from Fowler's theory as well as the presence of a "tail" in the threshold region will not reduce, however, the applicability of the photoelectric method for deciding whether or not physical adsorption does take place.

## VIII. 2 EXPERIMENTAL

The photoelectric cell described in chapter III was used in a number of tentative experiments of xenon adsorption on the pure alkali metals and on the alkali metal alloys. The techniques and the devices used are described in chapters II and III.

We found that under *normal* working conditions and at xenon pressures of

the order of  $10^{-4}$  Torr the photocurrent slowly increased with increasing xenon pressure. The effect appeared due to collision ionization as it was absent if the anode voltage was lower than about 10 V. (The ionization potential of xenon is equal to 12 V).

In the same photocell, but under proper conditions of the measurements, higher xenon pressures up to the saturation vapour pressure of solid xenon at  $77^{\circ}\text{K}$  did not lead to an observable change in photoemission for any of the alkali films studied. This indicated that the heat of adsorption of xenon on alkali metals may be much smaller than on most other types of substrates.

On the other hand, these experiments are inconclusive as to the absence of adsorption because of the fact that there will necessarily be a difference between the temperature of the Dewar part of the cell and the temperature of the cathode, which difference will become larger when xenon is admitted to the high relative pressures needed to achieve adsorption (see chapter III).

Therefore, a different type of photocell is required, in which thermal contact between the cathode and the part of the cell filled with liquid nitrogen is better. The photoelectric cell shown schematically in fig. VIII,1 fulfilled this condition\*.

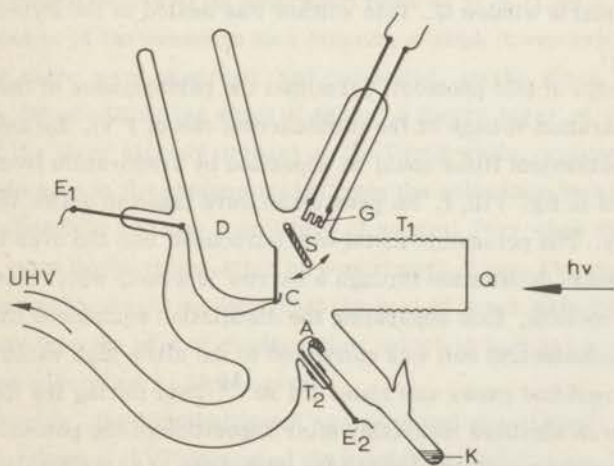


Fig. VIII,1. The photocell used in the study of xenon adsorption (see text).

\* The author wishes to thank Drs. R. Bouwman of this laboratory for the loan of this photocell and for the permission to adapt it to the requirements of this work.

The body of the cell was made of Pyrex glass. The cathode C consisted of a plan-parallel glass support which could be coated with a potassium film. The cathode-plate was molten to the Dewar part of the photocell D which could be filled with liquid nitrogen. The photocurrent was collected by a platinum wire protruding from the lower edge of the cathode-plate and contacting the deposited potassium layer. The current was fed through the glass housing of the photocell via a tungsten rod  $E_1$ .

The anode consisted of a heavy gold film, evaporated onto the inner walls of the cell from the tungsten helical filament G after previous vacuum melting of the gold beads. Resistance heating of this filament was accomplished by means of the two tungsten supports drawn, which emerged outside the photocell.

The shield S consisted of a magnetically movable door protecting the cathode from the gold source. The arrows indicate the direction of motion of the shield. The platinum anode lead A provided the electrical connection between the gold film and the anode voltage supply. The lead A was embedded in the glass wall of the cell and connected to a tungsten support  $E_2$  fused in a quartz made part of the side-tube. The quartz seal avoided the occurrence of leak currents, but necessitated the presence of the graded Pyrex-quartz seal  $T_2$ . The incident light fell perpendicularly onto the lower part of the cathode through the quartz window Q. This window was sealed to the Pyrex cell via a transition  $T_1$ .

The design of this photocell permitted the performance of the cell at a very low saturation voltage of the photocurrent (about 1 V). By using an electrical oven potassium films could be deposited by evaporation from the reservoir indicated in fig. VIII, 1. No provisions were taken to define the molecular beam sharply. The potassium metal was introduced into the oven tubing by means of vacuum distillation through a narrow junction, which was subsequently closed by melting, thus separating the distillation equipment from the phototube. The photoelectric cell was connected to the ultra-high vacuum line. The pressure of residual gases was about  $4 \times 10^{-10}$  Torr during the measurements.

Xenon was admitted invariably after deposition of the potassium film at liquid nitrogen temperature. During the deposition of potassium and the admission of xenon the photocurrent was monitored at a constant wave-length of the incident light (436 nm).

### VIII.3 RESULTS

Three experiments on potassium were carried out in this photocell. Though the angle of incidence of the light was always  $90^\circ$  (perpendicular) the development of the photocurrent, as measured at 436 nm, and the form of the spectral distribution curve after deposition were very similar to those obtained in the "alloy" photocells, where the angle of incidence was  $45^\circ$ . The quantum yields were about twice those obtained in the previously used photocells. This is probably due to differences in geometry, mentioned above, and to the very high rates of deposition in the present experiments (10 at. layers/sec?).

As before, the photocurrents increased during the whole period of building up a layer (20 minutes), except in the first experiment in which the photocurrent reached a constant value at an early stage of deposition. In that case the current also remained perfectly constant after removal of the oven. In the other two cases a small decrease was observed when the electrical oven was taken away. This decrease was much smaller than in the previous cells (see chapter V).

The experiments, in which xenon was admitted, confirmed the findings of the other photocell that no change in photocurrent takes place when the xenon pressure is raised nearly to its saturation value at  $77^\circ\text{K}$  ( $1.84 \times 10^{-3}$  Torr). From the course of the pressure as a function of time it was evident that large quantities of xenon were adsorbed, and condensed, on the glass walls of the Dewar part. By admitting big slugs of xenon, a heavy layer of it was built up on top of the layer already present on the Pyrex walls, without causing detectable changes in the photoemission from the potassium layer. The slugs were large enough to produce a pressure of several Torr when the whole photocell was at room temperature after an experiment. From the absence of any change in the photocurrent we infer that the heat of xenon adsorption on potassium is lower than the heat of condensation, which in turn is lower than the heat of xenon adsorption on Pyrex glass.

Subsequently, the liquid nitrogen was removed successively by quick evaporation of portions of it. This caused the condensed xenon to accumulate at the lower part of the Dewar to which the light spot was also directed, but no changes in photoelectric emission were observed.

When the level of the liquid nitrogen reached approximately the top edge of the light spot on the potassium film, however, a lowering of the photocurrent was observed. The magnitude of the decrease differed from experiment to ex-

periment and could also be influenced, for example, by admitting or pumping off xenon. One example of these experiments under xenon at saturation vapour pressure is shown in fig. VIII, 2, where the photoelectric yield  $I$  (in electrons

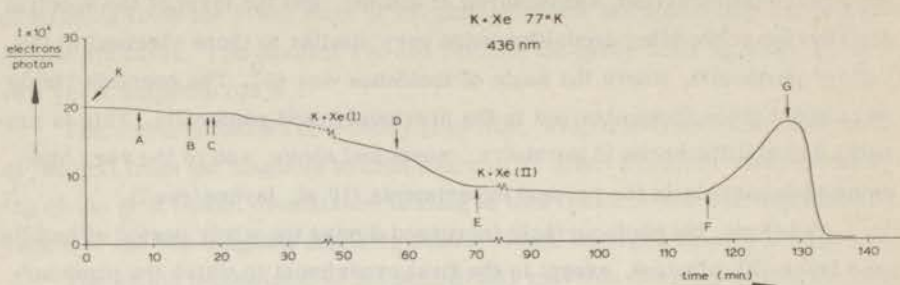


Fig. VIII, 2. Photoelectric emission from a freshly deposited K film for light of 436 nm as a function of time during slow removal of liquid nitrogen from the Dewar in the presence of xenon at saturation pressure.

per incident photon) is plotted as a function of time, while corresponding changes in the spectral distribution curve are shown in fig. VIII, 3.

Before xenon was admitted a spectral distribution curve was evaluated, designated with "K" in fig. VIII, 3. This curve agrees well with the typical curve for vapour quenched potassium films (see chapter V).

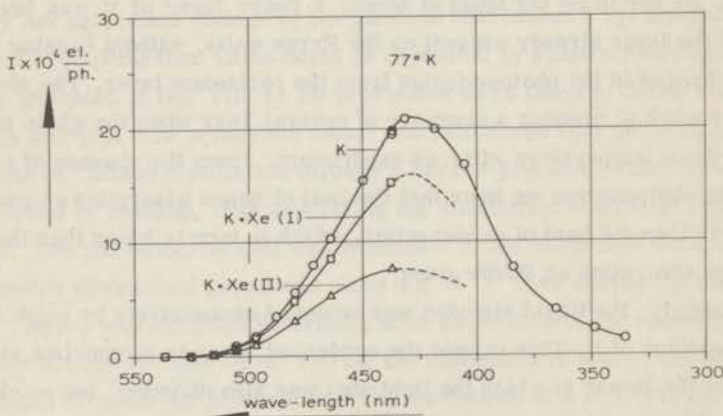


Fig. VIII, 3. Part of the spectral distribution curve of a vapour quenched potassium film at various stages of an adsorption experiment (cf. fig. VIII, 2).

At A in fig. VIII, 2 the xenon pressure was equal to about  $3.7 \times 10^{-4}$  Torr (corrected value). At B the xenon pressure had become immeasurable ( $> 1.7 \times 10^{-3}$  Torr) and at C the cell was saturated with xenon. The minor changes observed thus far in the yield are just the spontaneous changes always occurring after deposition of a potassium film.

When the level of the liquid nitrogen is only a few mm above the top-edge of the light spot a gradual decrease of the photoyield is observed. At the break in the time-axis, designated with "K + Xe (I)", the monitoring of the photocurrent was interrupted for measuring part of the spectral distribution curve. The latter is also represented in fig. VIII, 3. The whole spectral distribution curve appears to be transformed, but the long wave limit has kept its position. After termination of this measurement the meniscus of the liquid nitrogen was still above the light spot. A small amount of cooling agent was added at E.

At the second break in the time-axis, at "K + Xe (II)", an additional spectral distribution curve was measured, shown in fig. VIII, 3. At all wave-lengths the yields were again lowered substantially, but the position of the threshold (520 nm) remained unaffected.

During the further lapse of time the photoelectric yield remained remarkably constant, though the level of the liquid nitrogen was sinking steadily. At F the meniscus passed the lower edge of the light spot; promptly, a steep increase of the yield was observed. At G the original quantum yield was restored. After removal of all liquid nitrogen the photocurrent dropped rapidly toward a very low value owing to sintering. The liberated amount of xenon gas ( $\pm 30$  Torr) was found to suppress the photocurrent after sintering: upon pumping off this xenon the photocurrent was considerably enhanced (a factor of about two).

In another experiment all results, mentioned above, were reproduced.

For the record, linearized Fowler plots of the data are shown in fig. VIII, 4 from which photoelectric work functions and emission constants are derived. Note that the data at the left side of the maximum well fit a straight line (cf. chapter V). In table VIII. I the characteristic quantities have been summarized.

From these data we may formally infer that the changes in the photoelectric yield observed in the experiments with xenon at the recorded wave-length were not caused by a change in work function, but exclusively by a change in emission constant.

The work functions  $\phi_{L.F.}$  are significantly lower than those obtained in photocell No. 3, whereas the positions of the threshold are equal within the error limits.

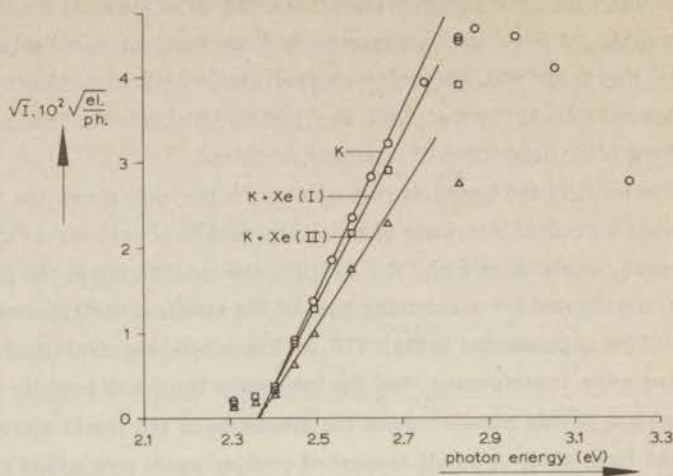


Fig. VIII.4. Linearized Fowler plots for a potassium film, vapour quenched at 77°K, at various stages of an adsorption experiment.

Table VIII. I

Photoelectric parameters before and after admission of xenon to a vapour quenched potassium film at 77°K.

	$\phi_v$ (eV)	$\phi_{L.F.}$ (eV)	$M_{L.F.} \times 10^{11}$ electrons / photon x deg. <sup>2</sup>
K	2.40	2.37	17.0
K + Xe(I)	2.39	2.37	14.1
K + Xe(II)	2.39	2.365	9.2

Legend:  $\phi_v$  = photoelectric work function as determined from threshold  
 $\phi_{L.F.}$  = ditto, as determined from linearized Fowler plot  
 $M_{L.F.}$  = emission constant as determined from linearized Fowler plot.

#### VIII.4 DISCUSSION

No detectable changes in the photocurrent have been found when potassium has been brought into contact with saturated xenon pressure at the given temperature of adsorption. Xenon always preferred to condense on other places of the apparatus (e.g. glass walls) cooled to the temperature of adsorption. This witnesses the very low condensation coefficient of xenon at alkali metal (and alloy) surfaces.

If a potassium surface represents the only part of the apparatus cooled to the temperature of adsorption (or if at least this is the biggest part of the cooled surface), a decrease of the emission constant is observed showing the built-up of a xenon layer on the potassium surface under these conditions. The method does not allow us to decide, whether the layer is multimolecular (in the beginning of emission lowering), or that we see only the final effect, i. e. condensation of xenon on potassium at its saturation pressure. The presence of a xenon layer on potassium may, indeed, give rise to the observed lowering of the emission constant, because the expectation is that the layer lowers the escape probability (see chapter VII). From the fact that the work function of potassium does not change we conclude that the xenon layer has no dipole.

On the other hand, the occurrence of condensation on top of the potassium layer, in spite of the heat of adsorption being lower than the heat of condensation, requires further clarification.

In a total equilibrium situation appreciable adsorption and subsequent condensation, as observed, are conceivable, if the pressure of xenon gas is raised above its saturation value at  $77^{\circ}\text{K}$  when the level of the liquid nitrogen in the Dewar is sinking, the temperature at the light spot still being fixed at  $77^{\circ}\text{K}$ . One tentative explanation could be, that the temperature of the outer atomic layer of the solid xenon agglomerate on the lower side of the Dewar wall increases when the thickness of the xenon layer reaches high values. As the outer layer is in contact with xenon gas at much higher temperature the heat transfer from this outer layer to the Dewar may become insufficient to keep the temperature low. By consequence the vapour pressure of xenon would increase.

It is also possible that non-equilibrium processes are involved. Thus, when the glass wall is heated some xenon atoms may jump directly to the gas phase while others first diffuse over the potassium film before they jump off. Consequently, the potassium film is covered to a finite degree during the steady state of this process.

Summarizing our present results we arrive at the following statements:

- (i) The heat of adsorption of xenon on alkali metals and alloys is lower than the heat of sublimation ( $= 3.79 \text{ kcal/mole}$ ).
- (ii) After condensation of xenon on top of potassium the work function does not change within  $0.01 \text{ eV}$ , but the emission constant decreases.
- (iii) Films contaminated with oxygen do not adsorb xenon either. (This appeared from some of the films studied in photocell No. 3 which got contaminated

during the xenon experiments: while pumping off xenon no change in the yield could be observed).

These results are in line with those of Pierotti and Halsey,<sup>90</sup> who found no adsorption of krypton on sodium films at 77°K. Sodium oxide films did not adsorb krypton either. On the basis of our results we conclude that no appreciable adsorption of xenon on potassium took place in Mignolet's experiments.<sup>81, 83</sup> The fact that Germer and Mayer<sup>46</sup> observed no change in the surface tension of alkali metals at their melting points under an argon pressure of  $10^{-1}$  Torr is also easily understood as adsorption is precluded under the conditions of their measurements.

According to Podgurski and Davis<sup>92</sup> the vapour pressure of xenon is given by:  $\log p_{\text{Xe}} = \frac{-833.33}{T} + 8.044$ . At the temperature of liquid nitrogen (77.3°K) the calculated vapour pressure is  $1.84 \times 10^{-3}$  Torr. The difference between the behaviour of potassium (no detectable adsorption at this temperature and xenon pressure) and various other substrates (e. g. tungsten,<sup>96</sup> molybdenum,<sup>96</sup> nickel<sup>55</sup> and glass<sup>6, 96</sup> for which adsorption isotherms were determined in the pressure range of  $10^{-10}$  -  $10^{-5}$  Torr at 77°K) appears to be a major one, for it requires a revision or extension of the hypotheses by which physical adsorption is accounted for.

All theoretical calculations of heats of adsorption are based on dispersion forces (see e. g. ref. 90) where only very quickly fluctuating dipoles are taken into account so that no net dipole moment results. After the discovery of high dipole moments in physically adsorbed noble gas atoms and the unusual high heats of adsorption (6.5 - 8.5 kcal/mole) one recognized that other types of binding must also be involved in physical adsorption.

Two possible contributions are mainly considered: first, induction forces brought about by a surface electric field acting on the induced dipoles of the adsorbed layer and, second, charge-transfer forces between the adsorbed species and the surface, resulting in a no-bond resonance state, according to the proposal of Mulliken.<sup>86</sup>

Gundry and Tompkins<sup>48</sup> made a more or less quantitative analysis of the merits of the two concepts for the case of xenon on graphite. They showed that the heats of adsorption and the surface potentials could be rationalized in terms of both polarization and charge-transfer no-bond theory. They concluded that it was difficult to decide which of the two theories was more applicable.

Mignolet<sup>81a</sup> originally attributed the surface potentials to polarization of the adsorbate, but later he suggested<sup>81b, 83</sup> that charge-transfer no-bond inter-

action was more feasible. On the other hand, de Boer<sup>13</sup> has maintained that polarization is the more important factor. Recently, Hall<sup>50</sup> analyzed a number of experimental data on surface potentials and showed that, with some exceptions, they satisfied a certain correlation expected on the basis of polarizability and field strength, the latter being related to the heat of sublimation of the metal.

A first remark concerns the physical meaning of the surface field. Gundry and Tompkins calculated the surface field for graphite from the contribution of the polarization energy and obtained a value of  $1 \times 10^8$  V/cm. This value already led to a too large dipole moment of the adsorbed xenon atoms. On another basis Ross and Olivier<sup>99</sup> derived a surface field of  $3.6 \times 10^7$  V/cm. Hall reported that values of the field strength were about  $10^7$  V/cm.

However, in field emission of electrons the imaging field at the tip surface also amounts to about  $4 \times 10^7$  V/cm. In the presence of xenon atoms, which lower the work function, nothing like a depolarization effect has ever been observed.<sup>38, 98</sup> On the contrary, the surface potentials obtained by this method were usually somewhat higher.

The second remark concerns the concept of a linear relationship between the surface potentials and the polarizability of the adsorbate. In those cases where such a relationship is found (e.g. when comparing different noble gases on one and the same metal) the polarizability as a variable can be replaced by other properties, for example, the ionization potential,<sup>116</sup> because these quantities show a simple interrelationship for similar (e.g. noble gas) atoms. This means that a good correlation between polarizability and surface potentials for a group of gases cannot provide a proof for a particular model, if the other model makes use of a related quantity (ionization potential). Moreover, closer inspection of all data reveals that the correlation proposed by Hall is less well obeyed than he presumed. This is more serious because there is no place for refinements in the polarization theory, extremely simple as it is, which can allow for these deviations (see e.g. data for different, also not noble, gases on the same metal).

The third remark concerns the sign of the dipole moment being related to the direction of the surface field. It is not entirely clear why the dipole moment should have the observed sign with the positive pole pointing outwards, or, why the surface electric field should have the proper direction from positive outside towards negative inside the metal.

In the case of potassium and sodium the binding forces are exclusively of

a dispersion character\*. This is verified by the absence of a dipole moment in adsorbed, or condensed, atoms. In terms of the polarization theory this would imply that what is normally described as the surface field is not present at all or very weak in the case of alkali metals. This seems difficult to understand.

Therefore, we feel that other factors are also involved in the interactions occurring in physical adsorption. As was demonstrated by Gundry and Tompkins, the charge-transfer no-bond theory, too, can account for the high heats of adsorption and for the high dipole moments observed in the case of transition metals. In principle this theory will be capable to stress more the particular chemical properties of the surface atoms of the substrate as embodied in the orbitals emerging outside the microscopic surface. Parameters like intermetallic bond strength (latent heat of sublimation) and polarizability of adsorbate atoms are included in a more subtle way. On the other hand a simple scheme of physical adsorption in general is not attainable any more. Calculation of heats of adsorption and surface potentials for distinct combinations of gases and metals meets with the same difficulties as encountered in chemisorption.

The fact that alkali metals cannot build up charge-transfer complexes with xenon is quite intelligible as these metals do not possess appropriate orbitals for overlap. In this way the zero surface potential and the very low heat of adsorption can be qualitatively explained.

The present conclusions are also of special interest in view of some peculiar results reported in recent years. Ponec<sup>93</sup> observed a change in the resistance of nickel and other transition metal films after physical adsorption of xenon which pointed to a "chemisorption-like" interaction between the substrate and the adsorbate. Moreover, Ponec and Knor<sup>94</sup> found that a higher number of xenon atoms can be accommodated in one adsorbed monolayer compared to krypton. This result has been confirmed by other workers.<sup>17</sup> These facts also support the assumption that other than dispersion and polarization forces must be involved in physical adsorption and that bonding by charge-transfer complexes offers possibilities for explanation of experimental data on transition metals.

\* For the system Xe-K the dispersion interaction energy appears to be lower than for the system Xe-Xe. For the krypton-sodium system Pierotti and Halsey<sup>90</sup> showed that the Kirkwood-Muller equation of dispersion forces correctly predicts the energetic incompatibility which they found to exist also for that system.

#### REFERENCES

1. ADAWI, I., Phys. Rev. 134, A 788, A 1649 (1964).
2. APPELBAUM, J. A., Phys. Rev. 154, 435 (1966).
3. ANDERSON, J. R. and N. J. CLARK, J. Phys. Chem. 67, 2135 (1963).
4. ANDERSON, J. R., E. A. FAULKNER and D. F. KLEMPERER, Australian J. Phys. 12, 469 (1959).
5. AXELROD, N. N., J. Opt. Soc. Am. 56, 203 (1966).
6. BAKER, B. G. and P. G. FOX, Trans. Faraday Soc. 61, 2001 (1965).
7. BARDEEN, J., Phys. Rev. 49, 653 (1936).
8. BARR, L. W., J. N. MUNDY and F. A. SMITH, Phil. Mag. 15, 1139 (1967).
9. BAUMANN, F., Z. Physik 158, 607 (1960).
10. BERGLUND, C. N. and W. E. SPICER, Phys. Rev. 136, A 1030, A 1044 (1964).
11. BLODGETT, Jr., A. and W. E. SPICER, Phys. Rev. 146, 390 (1966).
12. BOER, J. H. de, *Electron Emission and Adsorption Phenomena*, Cambridge, At the University Press, 1935.
13. BOER, J. H. de, in *Chemisorption*, (W. E. Garner, ed.) p. 171, Butterworths, London, 1957.
14. BOSWORTH, R. C. L., Proc. Roy. Soc. (London) Ser. A 150, 58 (1935) and Ser. A 154, 112 (1936).
15. BOUTRY, G., R. ÉVRARD and J. RICHARD, C. R. Acad. Sc. (Paris) 258B, 143 (1964).
16. BOUTRY, G., H. DORMONT, R. ÉVRARD and R. PERRIN, C. R. Acad. Sc. (Paris) 261B, 383 (1965).
17. BOUWMAN, R., to be published.
18. BRADY, J. J., Phys. Rev. 41, 613 (1932).
19. BRADY, J. J. and V. P. JACOBSMEYER, S. J., Phys. Rev. 49, 670 (1936).
20. BRAUER, M., Phys. Stat. Sol. 14, 413 (1966).
21. BREEN, W. M., F. WOOTEN and T. HUEN, Phys. Rev. 159, 475 (1967).
22. BUCK, U. and H. PAULY, Z. Physik. Chem. N.F. 44, 345 (1965).
23. BUCKEL, W., Z. Physik 138, 136 (1954).
24. BUCKINGHAM, M. J., Phys. Rev. 80, 704 (1950).

25. CAFASSO, F. A., V. M. KHANNA and H. M. FEDER, *Advan. Phys.* 16, 535 (1967).
26. CHRISTMAN, J. R., *Phys. Rev.* 153, 217 (1967).
27. COPLEY, M. J. and T. E. PHIPPS, *Phys. Rev.* 48, 960 (1935).
28. COTTON, D. J., *J. Phys. Chem.* 73, 270 (1969).
29. *Crystal Data, Determinative Tables*, 2nd Ed., J. D. H. Donnay, ed. (American Crystallographic Association, 1963).
30. CULVER, R. V. and F. C. TOMPKINS, *Advan. Catalysis* 11, 67-131 (1959).
31. DATZ, S. and E. H. TAYLOR, *J. Chem. Phys.* 25, 391 (1956).
32. DEMCHENKO, V. V., *Fiz. Metal. Metalloved.* 21, 634 (1966).
33. DICKEY, J., *Phys. Rev.* 81, 612 (1951).
34. DYUBUA, B. Ch., O. K. KULTASHEV and L. V. GORSHKOVA, *Fiz. Tverd. Tela* 8, 1105 (1966).
35. DYUBUA, B. Ch., O. K. KULTASHEV and I. A. TSYGANOVA, *Radiotekhn. i Elektron.* 9, 2061 (1964).
36. DUWEZ, P., R. H. WILLENS and W. KLEMENT, *J. Appl. Phys.* 31, 1136 (1960).
37. EBERHAGEN, A., *Fortschr. Physik* 8, 245 (1960).
38. EHRLICH, G. and F. G. HUDDA, *J. Chem. Phys.* 30, 493 (1959).
39. ELSTER, J. and H. GEITEL, *Wied. Ann.* 43, 225 (1891); *Ann. Physik* 52, 433 (1894).
40. FAN, H. Y., *Phys. Rev.* 68, 43 (1945).
41. FARNSWORTH, H. E., *Proc. Phys. Soc. (London)* 71, 703 (1958).
42. FOWLER, R. H., *Phys. Rev.* 38, 45 (1931).
43. FRÖHLICH, H., *Ann. Physik* 7, 103 (1930).
44. FUJIME, S., *Japan. J. Appl. Phys.* 6, 305 (1967).
45. GARRON, R., L. GAUDART and R. PAYAN, *C. R. Acad. Sc. (Paris)* 268B, 266 (1969).
46. GERMER, D. and H. MAYER, *Z. Physik* 210, 391 (1966).
47. GÖRLICH, P., *Photoeffekte I*, Geest & Portig K-G, Leipzig, 1962.
48. GUNDRY, P. M. and F. C. TOMPKINS, *Trans. Faraday Soc.* 56, 846 (1960).
49. GUROV, K. P. and A. I. PEKAREV, *Fiz. Metal. Metalloved.* 17, 500 (1964).
50. HALL, P. G., *Chem. Commun.* 1966, 877.
51. *Handbook of Chemistry and Physics*, 48th ed., Chemical Rubber Co., Cleveland, Ohio, 1967-1968.
52. HENNINGER, E. H., R. C. BUSCHERT and L. HEATON, *J. Chem. Phys.* 44, 1758 (1966).
53. HERMANN, H., Thesis, Braunschweig, Germany, 1955.
54. HERRING, C. and M. H. NICHOLS, *Rev. Mod. Phys.* 21, 185 (1949).
55. HOBSON, J. P. and R. A. ARMSTRONG, *J. Phys. Chem.* 67, 2000 (1963).
56. HUNTINGTON, H. B., *Phys. Rev.* 89, 357 (1953).
57. HUSMANN, O. K., *J. Appl. Phys.* 37, 4662 (1966).
58. IVES, H. E. and A. L. JOHNSRUD, *Astrophys. J.* 60, 231 (1924).
59. IVES, H. E. and G. R. STILWELL, *Phys. Rev.* 29, 252 (1927).

60. IVES, H.E. and H.B. BRIGGS, J. Opt. Soc. Am. 26, 238 (1936); 27, 181 (1937).
61. JAMISON, N.C. and R.J. CASHMAN, Phys. Rev. 50, 624 (1936).
62. KEYES, F.E., J. Am. Chem. Soc. 34, 782 (1912).
63. KURNAKOW, N.S. and N.A. PUSHIN, Z. Anorg. Allgem. Chem. 30, 109 (1910).
64. LAAR, J. van, private communication.
65. LANGMUIR, I. and K.H. KINGDON, Proc. Roy. Soc. (London) Ser. A 107, 61 (1925).
66. LAPEYRE, G.J. and K.A. KRESS, Phys. Rev. 166, 589 (1968).
67. LAPP, O. and K. NEUMANN, Z. Naturforsch. 24a, 596 (1969).
68. LAZAREV, V.B. and Yu.I. MALOV, Élektrokhimiya 3, 294 (1967); Izv. Akad. Nauk SSSR 1967, 2091.
69. LAZAREV, V.B., Yu.I. MALOV and G.A. SHARPATAYA, Dokl. Akad. Nauk SSSR 178, 355 (1968).
70. MADER, S., A.S. NOWICK and H. WIDMER, Acta Met. 15, 203, 215 (1967).
71. MADER, S., J. Vac. Sci. Tech. 2, 35 (1965).
72. MAKINSON, R.E.B., Proc. Roy. Soc. (London) Ser. A 162, 367 (1937).
73. MANN, Jr., M.M. and L.A. DuBRIDGE, Phys. Rev. 51, 120 (1937).
74. MAURER, R.J., Phys. Rev. 57, 653 (1940).
75. MAYER, H., Ann. Physik 29, 129 (1937); 33, 419 (1938); Z. Physik 124, 326 (1948).
76. MAYER, H. and H. THOMAS, Z. Physik 147, 419 (1957).
77. MAYER, H. and M.H. EL NABY, Z. Physik 174, 289 (1963).
78. Mc KNIGHT, L.B. and L.O. BROCKWAY, Inorg. Chem. 5, 1556 (1966).
79. MEESSEN, A., J. Phys. Rad. 22, 135, 308 (1961).
80. MEESSEN, A., Phys. Stat. Sol. 26, 125 (1968).
81. MIGNOLET, J.C.P., a) Discussions Faraday Soc. 8, 105 (1950); b) J. Chem. Phys. 21, 1298 (1953).
82. MIGNOLET, J.C.P., Rec. Trav. Chim. 74, 685 (1955).
83. MIGNOLET, J.C.P., in *Chemisorption* (W.E. Garner, ed.) p. 118, Butterworths, London, 1957.
84. MITCHELL, K., Proc. Roy. Soc. (London) Ser. A 146, 442 (1934); Ser. A 153, 513 (1936).
85. MOESTA, H., *Chemisorption und Ionisation in Metall-Metall Systemen*, Springer-Verlag, Berlin, 1968, p. 128-140.
86. MULLIKEN, R.S., J. Am. Chem. Soc. 74, 811 (1952).
87. OVERHAUSER, A., Phys. Rev. 156, 844 (1967).
88. PHILLIPS, J.C., in *Optical Properties and Electronic Structure of Metals and Alloys* (F. Abelès, ed.), North-Holland Publishing Co., Amsterdam, 1966, p. 22.
89. PIEPENBRING, F.J., in *Optical Properties and Electronic Structure of Metals and Alloys* (F. Abelès, ed.), North-Holland Publishing Co., Amsterdam, 1966, p. 316.
90. PIEROTTI, R.A. and G.D. HALSEY, Jr., J. Phys. Chem. 63, 680 (1959).
91. PLANK, P. van der, Thesis, Leiden, 1968.
92. PODGURSKI, H.H. and F.N. DAVIS, J. Phys. Chem. 65, 1343 (1961).

93. PONEC, V., private communication.
94. PONEC, V. and Z. KNOR, Coll. Czech. Chem. Comm. 27, 1091 (1962).
95. QUINN, J.J., Phys. Rev. 126, 1453 (1962).
96. RICCA, F. and A. BELLARDO, Z. Physik. Chem. N.F. 52, 276, 318 (1967).
97. ROBERTS, R.W. and Th. A. VANDERSLICE, *Ultra-high Vacuum and its Applications*, Prentice-Hall Inc., Englewood Cliffs, New York, 1963.
98. ROOTSAERT, W.J.M., L.L. van REIJEN and W.M.H. SACHTLER, J. Catalysis 1, 416 (1962).
99. ROSS, S. and J.P. OLIVIER, *On Physical Adsorption*, Interscience, New York, 1964.
100. SACHTLER, W.M.H., G.J.H. DORGELO and R. JONGEPIER, J. Catalysis 4, 654, 665 (1965).
101. SACHTLER, W.M.H., G.J.H. DORGELO and A.A. HOLSCHEER, Surface Sci. 5, 221 (1966).
102. SCHROEN, W., Z. Physik 176, 237 (1963).
103. SEIB, D.H. and W.E. SPICER, Phys. Rev. Letters 20, 1441 (1968).
104. SIMON, H. and R. SURHMANN, *Der lichtelektrische Effekt und seine Anwendungen*, Springer-Verlag, Berlin, 1958.
105. SMOLUCHOWSKI, R., Phys. Rev. 60, 661 (1941).
106. SPICER, W.E., in *Optical Properties and Electronic Structure of Metals and Alloys*, (F. Abelès, ed.), North-Holland Publishing Co., Amsterdam, 1966, p. 285.
107. STERN, O., Z. Physik 39, 754 (1926).
108. STUART, R.N., F. WOOTEN and W.E. SPICER, Phys. Rev. 135, A 495 (1964).
109. SUHRMANN, R., Z. Naturforsch. 9a, 968 (1954).
110. SUHRMANN, R., J. Chim. Phys. 54, 15 (1957).
111. SUHRMANN, R., G. KRÜGER and G. WEDLER, Z. Physik. Chem. N.F. 30, 1 (1961).
112. SUTHERLAND, J.C. and E.T. ARAKAWA, J. Opt. Soc. Am. 58, 1080 (1968).
113. TAMM, I. and S. SCHUBIN, Z. Physik 68, 97 (1931).
114. TAYLOR, J.B. and I. LANGMUIR, Phys. Rev. 44, 423 (1933).
115. THOMAS, H., Z. Physik 147, 419 (1957).
116. TUCK, D.G., J. Chem. Phys. 29, 724 (1958).
117. VERNIER, P., J. Phys. 26, 87 (1965).
118. WALLDÉN, L.E., D.H. SEIB and W.E. SPICER, J. Appl. Phys. 40, 1281 (1969).
119. WINTERBOTTOM, W.L., J. Chem. Phys. 47, 3546 (1967).
120. WOOTEN, F. and T. HUEN, J. Opt. Soc. Am. 57, 102 (1967).

## SUMMARY

It is the prime objective of the present investigation to gain a better insight into correlations between the surface and bulk properties of alloys and their photoelectric emission characteristics.

The photoelectric emission from sodium, potassium and Na-K alloy films has been measured for wave-lengths between 270 and 550 nm under ultra-high vacuum ( $10^{-10}$  Torr). The layers were prepared by means of "vapour quenching", i. e. vacuum evaporation from atomic beam ovens onto a (molybdenum) substrate held at low temperature ( $80^{\circ}\text{K}$ ). During deposition of the films the atoms were counted by directing part of the beam onto a hot platinum surface and measuring the ion current between this surface and a (negative) collector. Spectral sensitivity curves were obtained immediately after condensation and at different stages of subsequent annealing-cooling cycles. Photoelectric yields were recorded for the pure metals at 365, 405 and 436 nm and for the alloys at 436 nm during deposition and annealing to room temperature, where the alloys are, at least partially, liquid.

The Chapters II-IV of this thesis deal with the apparatus used and the general procedures followed (Ch. II), with the principles and techniques of photoelectric measurements (Ch. III) and with a detailed description of the purification of alkali metals and the *in situ* determination of film thickness and alloy composition (Ch. IV).

The experimental results of the pure alkali metals are reported in Chapter V. Vapour quenched films of sodium and potassium appeared to possess higher work functions (2.40 and 2.43 eV; cf. 2.36 and 2.30 eV), higher emission capacities (by about an order of magnitude) and spectral maxima at higher wave-lengths (300 and 430 nm; cf. 270 (hardly observable) and 400 nm, resp.) than the same films sintered at room temperature. Furthermore, the measured

photoelectric yields of vapour quenched films showed much scattering at the maxima, but after sintering the results were found fairly reproducible. The drastic changes caused by sintering were found to take place as a single irreversible step in a narrow temperature range at about  $130^{\circ}\text{K}$ . Only sodium films at room temperature gave a good fit to the Fowler plot. Results of deposition experiments are quantitatively, and for sodium even qualitatively, at variance with recent literature data; a correlation with escape depths of photoelectrons is proved to be unjustified. The changes in the yield during deposition and sintering can be rationalized, respectively, in terms of a prolonged increase of the concentration, or the precipitation of lattice defects. Recooling a potassium film results in minor and reversible changes; for sodium a spectral maximum clearly reappears at 315 nm. The work function of both metals slightly increases during this process (K: 2.36 eV, Na: 2.45 eV).

The experimental results of Na-K alloys are presented in Chapter VI. The photoelectric properties of vapour quenched alloys (high rates of simultaneous deposition, thick layers (about  $7000 \text{ \AA}$ ) were found to vary strongly with composition, but after annealing they were almost independent of composition. Quenched alloys with compositions between 20 and 85 at. % of potassium all possess similar distribution curves, about equal work functions (2.42 eV) and the same, strikingly low, yields and emission constants. Whereas diluted sodium alloys ( $> 85\% \text{ K}$ ) respond in a way intermediate between potassium and these "concentrated" alloys, an anomaly has been observed for diluted potassium alloys: the yields were very high over a broad spectral region and the work function was minimum (2.34 eV).

During deposition and sintering the change in the yield at 436 nm was, in particular for concentrated alloys, entirely different from that of pure metal films. For example, during the irreversible annealing stage of concentrated alloys the yield passes through a pronounced maximum at temperatures above  $130^{\circ}\text{K}$ . At higher temperatures (above  $180^{\circ}\text{K}$ ) phase separations and solid-liquid transitions occur, the latter producing sharp and small decrements of the photoyield. At room temperature the alloys do not exhibit a minimum in the work function pattern; all work functions and emission constants are approximately equal (2.36 eV). Some evidence was obtained for a preferential enrichment of potassium in the surface layer. After recooling the films are less uniform than at  $293^{\circ}\text{K}$ ; all work functions increase to 2.40 eV, but the emission constants differ, probably partly due to the occurrence of the compound  $\text{Na}_2\text{K}$ .

The results are discussed in Chapter VII. The changes in the work func-

tion during sintering of vapour quenched alkali metals and alloys cannot be ascribed to the disappearance of unstable crystal faces at the surface. The minimum found for vapour quenched alloys has been tentatively explained. The small difference between the work functions of sodium and potassium in spite of a large difference in chemical potential seems to reveal a compensating difference in the double layer potential.

Phenomena observed during deposition and sintering are interpreted in terms of structural properties by assuming that concentrated alloys condense in an amorphous state which anneals out via a single-phase crystalline metastable state (at about  $150^{\circ}\text{K}$ ) comparable to the state after rapid cooling a liquid alloy. While condensing, the pure metals and dilute alloys build up an at least partially crystalline state, containing many lattice imperfections. On the basis of the theory of the volume photoeffect, which is lent support by the present results, a qualitative discussion is given of the development of the yield during deposition and annealing of pure metals and alloys and for the striking differences in behaviour between the groups of dilute quenched alloys.

Chapter VIII deals with the photoelectric study of physical adsorption of xenon on potassium. Even at the saturation vapour pressure of solid xenon, no appreciable adsorption of xenon takes place on potassium (or on sodium or Na-K alloys). This implies that the heat of adsorption on alkali metals is lower than the heat of condensation and much lower than the heat of adsorption on numerous substrates (including glass) studied before. Under special experimental conditions a condensed layer of xenon could be obtained on potassium in a steady state, lowering the emission constant but not changing the work function within 0.01 eV. From these observations conclusions are drawn favouring the applicability of the charge-transfer no-bond theory in the theoretical treatment of physical adsorption of noble gases.

## SAMENVATTING

De belangrijkste doelstelling van dit onderzoek vormt het verkrijgen van een beter inzicht in correlaties tussen oppervlak- en volume-eigenschappen van legeringen en de karakteristieke hoedanigheden van hun fotoelektrische emissie.

De fotoelektrische emissie van films van natrium, kalium en Na-K-legeringen is gemeten voor golflengtes tussen 270 en 550 nm in ultra-hoogvacuüm ( $10^{-10}$  Torr). De laagjes werden bereid door middel van "afschrikken" uit de dampfase, d. w. z. verdampen in vacuüm vanuit atoomstraalovens op een (molybdeen) substraat, dat op lage temperatuur ( $80^{\circ}\text{K}$ ) gehouden wordt. Gedurende het opdampen van de films werden de atomen geteld door een gedeelte van de bundel op een gloeiend platina-oppervlak te richten en de ionenstroom tussen dit oppervlak en een collector te meten. Spectrale verdelingscurves van de gevoeligheid werden onmiddellijk na opdampen en in verschillende stadia van daarop volgende cycli van opwarmen en afkoelen verkregen. Op een recorder werd de fotoelektrische opbrengst voor de zuivere metalen bij 365, 405 en 436 nm en voor de legeringen bij 436 nm gevolgd gedurende opdampen, en bij verwarmen naar kamertemperatuur, waar de legeringen, althans gedeeltelijk, vloeibaar zijn.

In de Hoofdstukken II-IV van dit proefschrift worden achtereenvolgens behandeld: de gebruikte basisapparatuur en de in het algemeen gevolgde werkwijze (II), de principes en de technieken van fotoelektrische metingen (III) en, in detail, de zuivering van de alkalimetalen en de bepaling van de laagdikte en de samenstelling van legeringen *in situ* (IV).

De experimentele resultaten zijn voor de zuivere alkalimetalen beschreven in Hoofdstuk V. Door afschrikken uit de damp verkregen natrium- en kaliumfilms bleken een hogere uittreearbeid (2,40 en 2,43 eV; vgl. 2,36 en 2,30 eV, resp.), een verhoogd emissievermogen (met ongeveer één grootte-orde) en een naar hogere golflengtes verschoven spectraal maximum (300 en 430 nm; vgl. 270 (nauwelijks waarneembaar) en 400 nm, resp.) te bezitten, vergeleken met dezelfde films na sinteren bij kamertemperatuur. Bovendien vertoonden de ge-

meten fotoelektrische opbrengsten van afgeschrikte films veel strooing bij de maxima, maar werden de meetresultaten na sinteren tamelijk goed reproduceerbaar bevonden. De door sinteren veroorzaakte drastische veranderingen bleken zich te voltrekken in de vorm van een enkele, irreversibele stap in een nauw temperatuur-gebied in de buurt van  $130^{\circ}\text{K}$ . Alleen natriumfilms bij kamertemperatuur gaven een goede dekking met de Fowler-grafiek. De resultaten van de opdamp-experimenten wijken kwantitatief, en voor natrium zelfs ook kwalitatief af van recente literatuurgegevens; een correlatie met de uittreediepte van fotoelektronen blijkt ongerechtvaardigd. Het verloop van de opbrengst gedurende opdammen en sinteren kan respectievelijk verklaard worden uitgaande van een langdurige toename van de concentratie van roosterfouten, en het neerslaan daarvan. Opnieuw afkoelen van een kaliumfilm resulteert in kleine reversibele veranderingen; bij natrium verschijnt er dan weer duidelijk een spectraal maximum bij 315 nm. De uittreearbeid van beide metalen neemt in dit proces lichtelijk toe (K: 2,36 eV, Na: 2,45 eV).

De experimentele resultaten zijn voor de Na-K-legeringen vermeld in Hoofdstuk VI. De fotoelektrische eigenschappen van door gelijktijdig afschrikken uit de damp verkregen legeringen (hoge opdamsnelheden, dikke lagen (ongeveer  $7000 \text{ \AA}$ )) bleken sterk te variëren met de samenstelling, maar na sinteren waren ze daarvan bijna onafhankelijk. Afgeschrikte legeringen met een samenstelling tussen 20 en 85 at. % K vertonen alle op elkaar lijkende verdelingscurven, ongeveer dezelfde uittreearbeid (2,42 eV) en dezelfde, opvallend lage opbrengst en emissieconstante. Terwijl kaliumrijke legeringen ( $> 85\% \text{ K}$ ) zich op een manier gedragen die ligt tussen die van kalium en deze "geconcentreerde" legeringen is een anomalie waargenomen voor natriumrijke legeringen: de opbrengsten daarvan waren hoog in een breed spectraal gebied en de uittreearbeid vertoonde er een minimum (2,34 eV).

Gedurende opdammen en sinteren was het verloop van de opbrengst bij 436 nm, speciaal voor geconcentreerde legeringen, geheel anders dan dat voor de zuivere metalen. Als voorbeeld zij vermeld dat de opbrengst van geconcentreerde legeringen gedurende de irreversibele sinterstap een geprononceerd maximum doorloopt bij temperaturen boven  $130^{\circ}\text{K}$ . Bij nog hogere temperaturen (boven  $180^{\circ}\text{K}$ ) doen zich fasescheidingen en overgangen van vaste stof naar vloeistof voor, welke laatste scherpe en kleine dalingen in de fotostroom tweeebrengen. Bij kamertemperatuur vertonen de legeringen geen minimum in het patroon van de uittreearbeid; alle uittreearbeiden en emissieconstanten zijn dan ongeveer gelijk (2,36 eV). Enige aanwijzingen werden verkregen voor

een preferentiële verrijking van kalium in de oppervlakte-laag. Na opnieuw koelen van de films is er sprake van een minder uniform gedrag dan bij  $293^{\circ}\text{K}$ : alle uittreearbeiden nemen toe tot 2,40 eV, maar de emissieconstanten lopen uiteen, vermoedelijk mede veroorzaakt door de aanwezigheid van de verbinding  $\text{Na}_2\text{K}$ .

De resultaten worden besproken in Hoofdstuk VII. De veranderingen in de uittreearbeid gedurende sinteren van uit de damp afgeschrikt alkalimetalen en -legeringen kunnen niet toegeschreven worden aan het verdwijnen van instabiele kristalvlakken uit het oppervlak. Het kleine verschil tussen de uittreearbeid van natrium en kalium, dat optreedt ondanks een groot verschil in chemische potentiaal, lijkt een compenserend verschil in de potentiaal van de dubbellaag aan het licht te brengen. Voor het minimum in de uittreearbeid van afgeschrikte legeringen wordt een voorlopige verklaring gegeven.

De verschijnselen tijdens opdampen en sinteren worden geïnterpreteerd vanuit het oogpunt van structurele eigenschappen door aan te nemen dat geconcentreerde legeringen condenseren in een amorfe toestand, die naar de evenwichtstoestand sintert via een één-fase kristallijne metastabiele toestand (bij ongeveer  $180^{\circ}\text{K}$ ), welke vergelijkbaar is met de toestand na snel afkoelen van een vloeibare legering. Gedurende het afschrikken uit de damp groeien de zuivere metalen en verdunde legeringen in een, tenminste gedeeltelijk, kristallijne toestand, die veel rooster-onvolkomenheden bevat. Op basis van de theorie van het volume fotoeffect, die door onze resultaten zeer gesteund wordt, worden het verloop van de opbrengst tijdens opdampen en sinteren van metalen en legeringen alsmede de frappante verschillen in gedrag tussen de groepen van verdunde afgeschrikte legeringen kwalitatief bediscussieerd.

Hoofdstuk VIII beschrijft het fotoelektrische onderzoek naar de fysische adsorptie van xenon op kalium. Zelfs bij de verzadigde dampspanning van vast xenon vindt geen merkbare adsorptie van xenon op kalium (en op natrium en Na-K legeringen) plaats. Dit houdt in dat de adsorptiewarmte op alkalimetalen lager is dan de condensatiewarmte en veel lager dan de adsorptiewarmte op de talrijke substraten (glas inbegrepen), die eerder onderzocht werden. Onder bijzondere experimentele omstandigheden kon een op kalium gecondenseerde laag xenon verkregen worden in een stationaire toestand, waarbij de emissieconstante verlaagd werd, maar de uittreearbeid tot op 0,01 eV niet veranderde. Uit deze waarnemingen worden conclusies getrokken ten gunste van de toepasbaarheid van de "charge-transfer no-bond" theorie voor de theoretische benadering van de fysische adsorptie van edelgassen.

Op verzoek van de Faculteit der Wiskunde en Natuurwetenschappen volgt hier een overzicht van mijn academische studie.

Na het behalen van het eindexamen HBS-B aan de St. Paulus HBS (thans St. Paulus Lyceum) te Tilburg begon ik in oktober 1960 met mijn studie in de scheikunde aan de Rijksuniversiteit te Leiden.

In mei 1963 legde ik het kandidaatsexamen, letter F, af. Onder leiding van de hoogleraren Prof. Dr. M. Mandel en Prof. Dr. A. J. Staverman (fysische chemie), Prof. Dr. W. M. H. Sachtler (heterogene katalyse) en Prof. Dr. L. J. Oosterhoff (theoretische organische chemie) bereidde ik mij voor op het doctoraalexamen met als hoofdvak fysische chemie, dat ik op 15 februari 1966 cum laude aflegde.

Van september 1962 tot september 1965 vervulde ik een assistentschap op de afdeling fysische chemie bij het pré-kandidatenpracticum, vanaf juni 1963 als kandidaatassistent. Daarna was ik als kandidaatassistent (vanaf september 1965), als doctoraalassistent (vanaf maart 1966) en als wetenschappelijk medewerker (van 15 augustus 1968 tot 12 november 1969) verbonden aan de afdeling heterogene katalyse. Het was op deze afdeling waar de in dit proefschrift beschreven onderzoekingen werden gedaan.

Vanaf augustus 1966 tot augustus 1968 was ik voor een beperkt aantal uren werkzaam als leraar natuur- en scheikunde bij het St. Agnes Lyceum te Leiden, van augustus 1968 tot augustus 1969 als leraar scheikunde bij het St. Bonaventura College aldaar. Vanaf december 1969 ben ik als gedetacheerde tewerkgesteld op het Chemisch Laboratorium van de Rijksverdedigingsorganisatie TNO.

Een woord van dank aan allen, die meegewerkt hebben aan het tot stand komen van dit proefschrift, mag bij het gereedkomen ervan niet ontbreken. Deze dank geldt in de eerste plaats de heren F. C. Kauffeld en B. J. Erades voor de vakkundige constructie van de fotocellen en de realisatie van de glazen componenten van de vacuümsystemen. De overige apparatuur werd in de instrumentmakerij vervaardigd, merendeels onder leiding van de heer G. Selier, of was welwillend ter beschikking gesteld door het Koninklijke/Shell Laboratorium te Amsterdam.

De vlamfotometrische analyses werden verricht door Dr. D. P. den Os, terwijl M. van den Brink (chem. kand.) bekwaam assisteerde bij het uitvoeren van een gedeelte der metingen.

Mijn bijzondere erkentelijkheid gaat uit naar Dr. V. Ponec voor de vele

waardevolle discussies, en voor het kritisch doorlezen van de oorspronkelijke tekst.

Veel dank ben ik verschuldigd aan mevrouw I. E. Muller-Hordijk voor het uittypen van een groot deel van het manuscript, en aan wijlen de heer W. F. Tegelaar en de heren M. Pison en J. J. Pot, die gezamenlijk de figuren hebben verzorgd.

